Redox potential controls electron transfer through the inner membrane of *Geobacter sulfurreducens*

A DISSERTATION

SUBMITTED TO THE FACULTY OF THE

UNIVERSITY OF MINNESOTA

BY

Komal Joshi

IN PARTIAL FULFILLMENT OF THE REQUIREMENTS

FOR THE DEGREE OF

DOCTOR OF PHILOSOPHY

Dr. Daniel R. Bond

August 2021

Acknowledgements

Pursuing a PhD degree would not have been possible if it was not for grandpa H. M. Joshi's belief in me. Thank you for instilling the importance of listening and observation in life, and in science. I am so fortunate to have shared the last five years with a group of highly motivated individuals and experts.

I am very grateful to a number of people who have been instrumental in getting this thesis to completion. Rebecca Calvo and Chi Ho Chan taught me the basics of molecular biology, and answered all my questions with so much patience. Thank you Rebecca for not let me quit graduate school, and for your constant support throughout these years. Kelly Wallin, Zach Schreiber, and Freddie Miller helped me get through the prelims. This dissertation work is built upon the tremendous work done by former lab members, Caleb Levar and Lori Zacharoff on the electron transfer through the inner membrane in *Geobacter sulfurreducens.*

I would not have come this far in graduate school, if Bridget Conley was not there by my side from day one in the lab. Bridget has given me confidence to ask questions, and lead by example what it means to get things done with all the heart. I will always cherish the fun and chaotic days of fixing equipments and instruments in the lab, and all our shenanigans. I am grateful for the friends I have gained in last few years- Bridget, Ruth Lee, David Hsu, Leslie Day, Dallas Fonseca,

and many more people who have been a part of the Bond lab in the past. I am really fortunate to have met you, and learn from you. You all made the lab environment fun and exciting, and overall a happy place for me.

I couldn't have wished for a better chair on my committee than Michael Freeman. Thank you for your constant support throughout, for making time to listen to my issues, and for not letting me quit graduate school in 2017. If it was not for you and Rebecca, I would not have made it to see the end of this degree. Cara Santelli has been very encouraging and compassionate through the challenging days in graduate school, I am really thankful to have you in my committee, and to know that I could always reach out to you. Lab meetings of Bond-Gralnick labs have taught me to always have a critical eye in learning new things, importance of small details in a project. Thank you to Jeff Gralnick for always expecting better, and pointing out my mistakes. It is because of your questions, I was able to measure the yields of *G. sulfurreducens* on Fe(III) citrate, a key result to answer the question of growth *vs.* reduction on Fe(III) citrate.

I will forever be grateful to my advisor, Daniel Bond for letting me a part of his lab, allowing me the freedom and flexibility of developing my research project. Thank you for letting me fail countless number of times, and supporting me through every hurdle life threw at me in the last five years. There is no match to your patient mentoring, never ending enthusiasm for science and excitement for Nernst equation, and all things electrons. You have taught me the value of being a good human in science, and led by example. You have never said no to learning new skills, and showed the importance of quality over quantity of Science. Thank you for believing in me when I doubted myself, and for allowing me the space and time to grow as a scientist at a slow pace. I will

forever cherish the time spent learning from you.

Outside the science family, I am grateful to my family back home- my grandparents, my parents, guruji for always being there, supporting me through all the difficulties in graduate school. Thank you for listening to my frustrations over failed experiments, and making sure that I am doing okay from across the globe.

Finally, I would not have survived 2020 without the support of Leslie, Lola Rubens, Bridget, Kelly and Ally. Special thank you to my furry friends- Frances, Harriet, Angelwings, Oscar, and Terra. Your unconditional love has been a huge support throughout the pandemic.

Abstract

Harnessing energy for growth and survival is universal to all living forms. Bacteria are constantly faced with changing environment forcing them to quickly adapt to the conditions to gain maximum energy available. Acquisition of energy involves transfer of electrons from substrate that gets oxidized to the reduction of electron acceptors. Microorganisms performing extracellular electron transfer have evolved to couple oxidation of electron donors to the reduction of electron acceptors present outside the cell using a chain of redox active proteins. *Geobacter sulfurreducens* is one such model organism for studying extracellular electron transfer, providing unique opportunities for the development of bioelectronic devices and sensors. Despite the usefulness of *G. sulfurreducens* extracellular electron transfer ability in biotechnological applications, the complete electron transfer pathway still remains unknown. The factors regulating the electron transfer between different cytochromes, as well as the specific utilization of different cytochromes in energy conservation is one of the lesser studied aspects of *G. sulfurreducens* physiology. The work presented in this thesis includes discovery and characterization of an inner membrane cytochrome complex, CbcBA essential for respiration of electron acceptors near the thermodynamic limit of acetate respiration (< -0.21 V *vs.* Standard Hydrogen Electrode (SHE)). A σ^{54}–dependent transcription factor, BccR controlling the expression of CbcBA was also characterized. Other

inner membrane cytochromes involved in redox dependent electron transfer, ImcH, and CbcL are constitutively expressed. Using genetic and electrochemical approaches, CbcL was found to function as a redox dependent switch showing oxidative inactivation above redox potentials of −0.1 V *vs.* SHE. Using specific mutants lacking one or more inner membrane cytochromes, cellular yields were measured corroborating earlier reported data that the ImcH-dependent electron transfer pathway supported the highest cellular yield, while the CbcL-dependent pathway supported much lower cell yields. The CbcBA-dependent pathway could not support growth under conditions tested, but was found to be needed for survival under low electron acceptor conditions. Expressing fluorescent proteins in specific inner membrane cytochrome mutants allowed studying metabolic heterogeneity of *G. sulfurreducens* biofilms visualized using confocal microscopy. At high redox potentials (+0.24 V *vs.* SHE), *G. sulfurreducens* utilizes ImcH-dependent pathway in cells closest to the electrode, and CbcL-dependent pathway in cells beyond 10 μm from the electrode surface. At low redox potentials (−0.13 V *vs.* SHE), only the CbcL-dependent pathway is utilized. The findings reported in this thesis, suggests a route for building biosensors for redox sensing.

Table of Contents

List of Tables

List of Figures

Chapter 1

Extracellular respiration in *Geobacter sulfurreducens*: A review of the evolutionary relationship between inner membrane cytochromes

Komal Joshi

1.1 Modes of energy conservation

Redox reactions are vital to all life forms. Microbial life has evolved to thrive in different environments by utilizing multiple strategies to gain energy across all possible combinations of thermodynamic reactions. The type of reaction involved depends on the availability and concentration of substrates, and environmental conditions like pH, temperature. The energy metabolism for microorganisms involves either a linear electron transport chain or branched electron transport chains as is the case in many anaerobic bacteria. Electrons generated from oxidation of carbon sources and electron donors are transferred along an electron transport chain to a terminal electron acceptor in turn generating ATP. Each electron transport chain has a different thermodynamic efficiency, resulting in different overall ATP gain [1]. Despite this complexity, the basic principles of ATP generation are simple, following the thermodynamic principles [2]. Modes of energy conservation in all life forms follows a simple theme, and can be categorized into three classes: (i) redox reactions that drive chemiosmotic ATP synthesis, (ii) substrate level phosphorylation, and (iii) flavin-based electron bifurcation.

1.1.1 Chemiosmotic process of ATP generation

Peter Mitchell first proposed the chemiosmotic hypothesis in 1961 [3, 4] explaining energy conservation during respiration and photosynthesis occur by generation of an electrochemical gradient across the membrane driving the generation of ATP. According to the chemiosmotic theory, protons are translocated across the cytoplasmic, anammoxosome, inner mitochondrial membrane, or

thylakoid membrane of chloroplast generating a proton gradient or chemiosmotic potential. When the protons return to the inside of the membrane via transmembrane proteins, this translocation can be coupled to ATP generation.

Chemiosmotic theory is central to energy generation through electron transfer chains associated with respiratory lifestyle using oxidative phosphorylation or phototrophic lifestyles using photophosphorylation to generate a proton motive force (PMF), and ultimately ATP synthesis. The amount of ATP generated depends on the redox potentials of electron donors and electron acceptors following the rules of thermodynamics ($\Delta G = -nF\Delta E$). For example– energy available from oxidation of a substrate like glucose or glycerol coupled to reduction of oxygen is higher than the energy available from reduction of nitrate or nitrite [2, 5].

1.1.2 Substrate level phosphorylation

Substrate level phosphorylation is the mechanism which involves synthesis of ATP in the cytoplasm through transfer of phosphate (Pi) from a donor molecule with high group transfer potential to ADP (adenosine diphosphate). The enzyme catalyzing the transfer is a kinase, and only certain phosphorylation reactions have high group transfer potentials to generate an ATP. For example– formation of pyruvate from phosphoenolpyruvate (PEP) catalyzed by pyruvate kinase results in generation of an ATP, thus conserving energy and forming a high-energy intermediate (pyruvate) [6].

Substrate level phosphorylation is observed in metabolic pathways involving net electron transfer through glycolysis, or release of acetate through acetate kinase. *Shewanella*

oneidensis MR–1, a non-fermentative facultative anaerobe able to respire a lot of terminal electron acceptors ranging from oxygen to soluble electron acceptors (nitrate, fumarate, TMAO, DMSO) and insoluble metals (Fe(III), Mn(IV)) [7] utilizes substrate level phosphorylation as the primary source of ATP generation under anaerobic conditions [8].

1.1.3 Flavin-based electron bifurcation

Electron bifurcation is the recently discovered third mechanism of biological energy conservation in which an endergonic reaction and an exergonic reaction are coupled to generate a net exergonic electron transfer reaction, without ATP hydrolysis, thus minimizing free energy loss. The significance of electron bifurcation is that low potential acceptors, such as ferredoxin, can be reduced even when only higher potential electron donors are available. The reduced ferredoxin can then function to drive essential cellular reactions such as carbon fixation, or disposal of reducing equivalents via hydrogen production [9, 10].

Electron bifurcation was first proposed in 1975 by Peter Mitchell to explain the behavior of ubiquinol in the bc_1 complex of mitochondria using a process called the "Q–cycle" [11]. He hypothesized that quinone oxidation (reduction potential, E_o' = +100 mV) could be coupled to reduction of a high potential Rieske iron-sulfur cluster (E_o' = +300 mV) and reduction of low potential *b*–type cytochrome (E_o' = −100 mV), generating a net exergonic reaction, and allowing additional proton translocation via recycling of the low potential electron to the quinone pool. This remained the only example of bifurcation until Wolfgang Buckel and Rudolf Thauer, discovered "flavin-based electron bifurcation" in 2008 [12]. Flavin-based systems differ from quinone-based

electron bifurcation at both the biochemical, and energetic level. Flavin-based bifurcation proteins share no sequence similarity with Q–cycle complex enzymes. The electron bifurcation process occurs at much more negative redox potentials (−300 mV to −500 mV) than Q–cycling, and involves soluble and membrane bound redox proteins. Generation of ATP from electron bifurcation is commonly observed in archaea, and some anaerobic bacteria [10].

1.2 Anaerobic respiration

Majority of life exists under reduced environments where oxygen is absent. Ancient bioenergetic respiratory chains are thought to have evolved under anoxic environments before branching to using oxygen as a terminal electron acceptor after the Great Oxidation Event [2]. Many different organic and inorganic compounds like nitrate, nitrite, DMSO, arsenate, fumarate, sulfate, chelated metal oxides as well as insoluble mineral oxyhydroxides serve as terminal electron acceptors in anaerobic respiration [1]. The respiratory chain of anaerobic prokaryotes is diverse, functionally organized in the cytoplasmic membrane to maximize thermodynamic energy gain from utilization of a variety of combination of electron donors and acceptors.

Electrons generated from the oxidation of carbon sources and electron donors in the form of reducing equivalents (NADH, NAD(P)H) are delivered to the enzyme complexes (NADH dehydrogenase) where NADH gets oxidized with simultaneous reduction of quinones. Redox reactions involving membrane-bound quinone molecules are key steps in cellular bioenergetics. Each branch in bioenergetic chain of electron transfer leads to a different ATP generation and thermodynamics efficiency of ATP synthesis. The ability to tune thermodynamic efficiency has

allowed these organisms to grow respiring a variety of soluble and insoluble electron acceptors.

1.3 Case of insoluble electron acceptors: Extracellular electron transfer

Microorganisms are able to couple oxidation of an electron donor such as hydrogen or small chain fatty acids like acetate or lactate to the reduction of insoluble electron acceptors such as Fe(III) oxides, and Mn(IV) oxides [13–15]. Organisms performing dissimilatory metal reduction have evolved strategies to transfer electrons generated from oxidation to carbon sources and electron donors to an acceptor present outside the cell crossing one or two insulating lipid bilayers. Microorganisms can perform extracellular electron transfer using one or more of three strategies– direct electron transfer, electron transfer using appendages, and reduction of electron acceptors using redox active mediators. Some bacteria such as *Geothrix fermentans, Pseudomonas aeruginosa, Shewanella oneidensis,* and the recently discovered mechanism in Gram–positive, *Listeria monocytogenes* are well known examples of electron transfer using redox active mediators like riboflavin, FMN, or phenazines [16–20]. Members of *Geobacter* and *Shewanella* utilizes electrically conductive nanowires or appendages in the form of outer membrane extensions in *S. oneidensis*, or multiheme cytochrome wires in *G. sulfurreducens* [21–24]. Direct electron transfer is the most well-studied of the three mechanisms of electron transfer in *Geobacter* and *Shewanella,* where outer membrane conduits are involved in direct electron transfer to electron acceptors [25–30]. While *S. oneidensis* utilizes only one inner membrane cytochrome, CymA, containing four heme binding domains (CXXCH) for electron transfer across the inner membrane [31, 32], *G. sulfurreducens* utilizes at least three pathways for electron transfer through the inner membrane

[33–35]. Despite the interest in using extracellular electron transfer ability of *G. sulfurreducens* in developing biotechnologies, the molecular mechanism of complete electron transfer remains unknown.

1.4 Cytochromes involved in extracellular electron transfer in *G. sulfurreducens*

G. sulfurreducens genome encodes for over 70 multiheme cytochromes [36] that are expressed under various growth conditions [30, 37, 38], providing a remarkable versatility to gain energy from reduction of a range of Fe(III) oxides, Mn(IV) oxides, poised electrodes, or syntrophic partners [38–43]. The multiheme cytochromes are localized in the inner membrane, periplasm, and outer membrane. With the abundance of multiheme cytochromes, there are multiple pathways for electron transfer across each location within the *G. sulfurreducens* cell. Redundancy of electron transfer pathways complicates determining the complete pathway of extracellular electron transfer. However, through genetic mutational analysis, cytochromes involved in electron transfer have been identified.

Outer membrane cytochromes interact with the electron acceptors directly, and at least five outer membrane electron conduits have been characterized in *G. sulfurreducens* [28, 30, 44, 45]. These electron conduits are composed of a periplasmic cytochrome, an outer membrane integral membrane protein, and one or more lipoprotein cytochromes predicted to transfer electrons from periplasmic partners to the electron acceptor. The electron conduits include OmcB (GSU2737–2739), OmcC (GSU2733–2731), ExtABCD (GGSU2645–2642), ExtEFG (GSU2724–2726), and ExtHIJKL (GSU2940–2936). None of the components in each of the electron

conduits share any homology. Reduction studies under different electron acceptors involving combination of mutants lacking one or more electron conduit complexes, exhibited only partial defects, requiring deletion of all five conduit complex encoding genes to eliminate electron transfer under most electron acceptors tested [30, 46]. These conduits show some level of substrate specificity, since each of the conduits is essential for reduction of at least one of the electron acceptors– Fe(III) citrate, Fe(III) oxide, Mn(IV) oxide, and poised electrodes. Homology searches revealed that these gene clusters are not conserved [30]. Substrate specificity of the conduits, and the fact that outer membrane is not involved in energy conservation with no electrochemical gradients coupled to energy generation, may provide an explanation for variability among outer membrane cytochromes.

Many **extracellular cytochromes** are reported to be involved in electron transfer, out of which only a few have been biochemically and electrochemically characterized including OmcS, OmcZ, OmcE, and PgcA [23, 24, 47–51]. CryoEM analysis of filaments produced by *G. sulfurreducens* showed that these filaments are made up of the hexaheme *c*–type cytochrome, OmcS present as polymerized chains. The structure revealed that the OmcS nanowires has closely stacked hemes for efficient transfer of electrons [23]. Despite conductivity values of Δ*omcS* being diminished by over 100 fold as compared to WT, there is no concrete evidence linking the presence of OmcS to an electron transfer deficient phenotype. There are at two OmcS homologs (GSU2503, GSU2501) present downstream of OmcS (GSU2504). Transcriptional analysis suggested that *omcST* are part of an operon, however only OmcS was found to be present as filaments [47, 50]. OmcZ, an octaheme cytochrome is shown to exist in a large 50 kDa form and a small 30 kDa

form [49]. Electrochemical analysis of mutants lacking OmcZ showed a growth defect on electrodes, and is thought to be involved in electron transfer in multi-cell layered biofilms. Recently published spectroscopic and conductivity studies on OmcZ predicted a model structure for OmcZ nanowires, with a tighter stacking of hemes resulting in higher conductivity of OmcZ [24].

Periplasmic cytochromes transfers electrons from inner membrane cytochromes, to the outer membrane conduits. *G. sulfurreducens* encodes five triheme periplasmic *c*–type cytochromes– PpcA, PpcB, PpcC, PpcD, and PpcE. Out of these, only PpcA has been extensively studied for its role in electron transfer [52]. Despite the abundance of biochemical information, the physiological role of PpcA in electron transfer is still lacking. Transcriptional and proteomic analysis showed that *ppcA* is one of the most highly expressed and abundant cytochromes, whereas others are differentially expressed under specific growth conditions [30, 37, 38].

Inner membrane cytochromes transfer electrons from the quinone pool to the periplasmic cytochromes, conserving energy. The respiratory chain in *Geobacter* is branched at the quinone level– two previously characterized multiheme *c*–type cytochromes, ImcH, a seven heme containing *c*–type cytochrome is essential for respiration of electron acceptors above -0.1 V *vs.* SHE, and CbcL, a *bc*–cytochrome containing domains for diheme *b*–type cytochrome, and nine heme *c*–type cytochrome is required for respiration of electron acceptors below -0.1 V *vs.* SHE [33, 34], and a third *bc*–type cytochrome complex characterized in chapter 2 of this thesis is required for reduction of electron acceptors below -0.21 V *vs.* SHE. Three more *bc*–type cytochrome complexes are encoded in *G. sulfurreducens* genome, but have not been characterized yet. Inner membrane cytochromes show the highest level of conservation as compared to periplasmic or outer membrane

cytochromes. Of all the inner membrane cytochromes, CbcBA (GSU0593–0594) is reported to be the most conserved among *Geobacteraceae* [53].

1.5 Conservation of inner membrane cytochromes: CbcBA, a *bc*–cytochrome complex

Cytochrome *bc* complexes represent enzymes found in almost all respiratory electron transfer chains. Cytochrome *b* complexes, also referred to as Rieske complexes, are associated with energy conserving membrane oxidizing quinone and reducing associated electron carriers like *c*–type cytochrome, iron-sulfur proteins or plastocyanin [54, 55]. Peter Mitchell in 1976 first described the electron transfer in bc_1–cytochrome complex linked to proton transfer, defined as Q–cycle [56]. Cytochrome *bc* complexes are widely distributed among different phyla. Crystallographic studies of cytochrome *b* from mitochondria, cyanobacteria, proteobacteria show remarkable similarity in their architecture [57, 58]. While cytochrome *b* in *bc* complexes is mostly conserved, cytochrome *c* *is* variable, adding structural and functional diversity to the family of *bc* complexes. Cytochrome *bc* complexes function to translocate electrons and protons from quinone pool to the electron accepting partner present outside the membrane, generating a proton motive force (*pmf*). The *pmf* generated could be utilized for ATP synthesis [54, 59]. Structural information of cytochrome *bc* complexes provided evidence for conformational changes in cytochrome *b* as electrons are transferred from cytoplasmic side to periplasmic side of the membrane, suggesting a route for gated electron transfer [58, 60].

Cytochrome *b* in cytochrome *bc* complexes is well conserved, and makes a good candidate for phylogenetic analyses. Cytochrome *b* domain containing proteins belong to

[NiFe]–hydrogenases, formate dehydrogenases, nitrate reductase, or heterodisulfide reductases classes of enzymes [61]. To gather more information on the properties of cytochrome *bc* complexes of *G. sulfurreducens,* phylogenetic analyses of cytochrome *b* (CbcB) of *G. sulfurreducens* were conducted. CbcB is a 218 amino acid long, diheme containing *b*–type cytochrome domain with four transmembrane domains [62, 63]. CbcB belongs to the cytochrome b^I family characterized by the conservation of histidines involved in *b*–heme coordination within the predicted transmembrane domains. The cytochrome b^I family encodes two histidines within one transmembrane domain, and one each in two out of three transmembrane domains. Sequence homology searches revealed *cbcB* encoded in all of *Geobacteraceae* with the exception of *G. lovleyi.* Psi–BLAST was utilized to search for homologs with a cut off value of 50% of sequence similarity, and genomic neighborhood of each candidate was studied; only genomes containing genes encoding cytochrome *b,* and cytochrome *c* were selected for alignment. Multiple sequence alignment was performed using mafft_linsi option, and maximum likelihood tree was constructed using raxml option provided in ETE toolkit [64] (Figure 1.1).

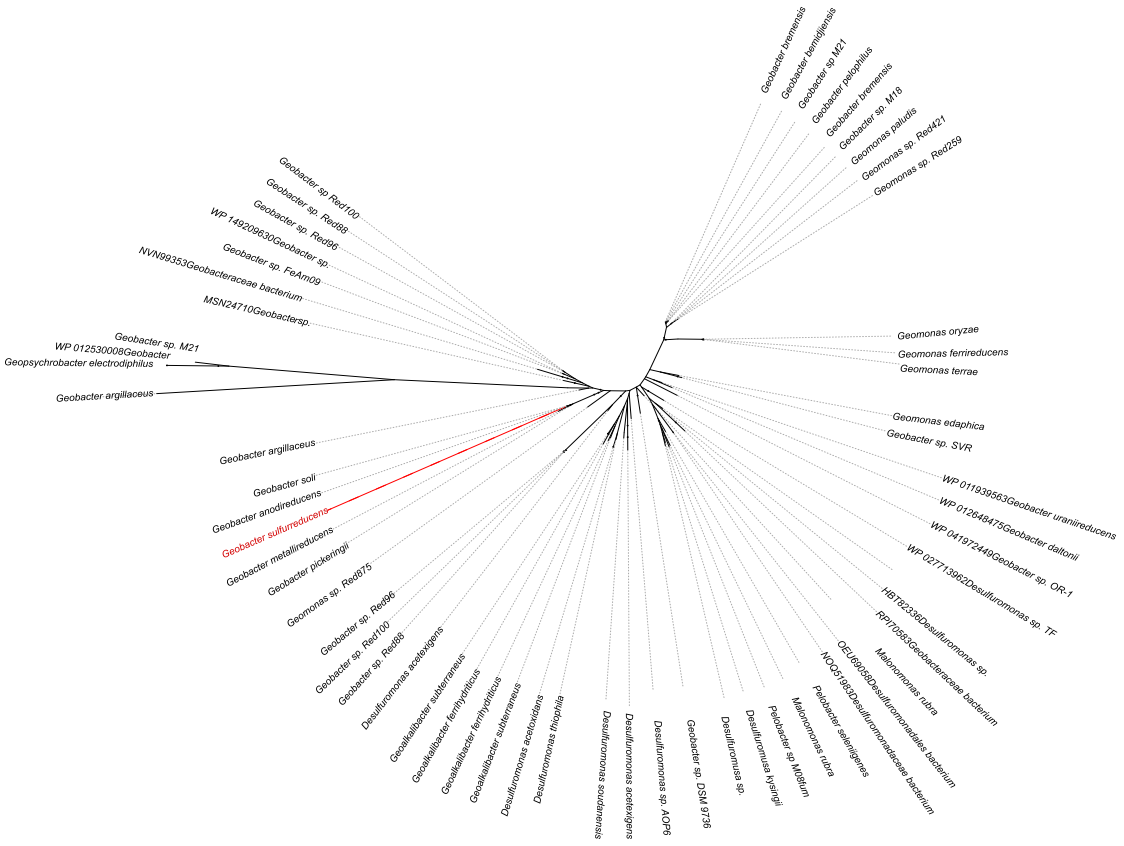

Figure 1.1: **CbcB homologs are conserved among Desulfuromonadales.** CbcB homologs with 80% sequence length of *G. sulfurreducens'* CbcB, and sequences with greater than 50% sequence similarity were included in phylogenetic analysis. Multiple sequence alignment using mafft, and tree building using raxml method was performed using ETE toolkit [64]. Strains represented here also contain a *c*–type cytochrome encoding gene next to *cbcB* homologs.

Another interesting feature of CbcBA is that the four transmembrane (TM) domains of CbcB have only three histidine residues for *b*–heme coordination present in TM1 and TM4, whereas CbcA also contains a transmembrane domain in addition to a *c*–type cytochrome domain. The TM domain of CbcA contains one histidine residue, possibly involved in *b*–heme coordination. This feature of transmembrane domain sharing has been characterized in *Wollinella succinogenes* [65,66]. Further studies involving site directed mutagenesis of different histidine residues present in CbcB and CbcA would provide information on key residues involved in heme ligation and subsequent

electron transfer.

To study evolutionary relationships between the three inner membrane cytochromes of *G. sulfurreducens* (ImcH, CbcL, and CbcBA), the stringent constraint of sequence similarity was lowered to 30%, and the top five hundred genomes containing homologs of any length were selected. Sequences containing partial sequence information from metagenomic bins were excluded. Cytochrome *b* domain containing proteins are often annotated as hydrogenases, formate dehydrogenases, or heterodisulfide reductases, but only a few have been functionally characterized [61]. For example– CbcL, the *bc*–cytochrome complex from *G. sulfurreducens,* contains a formate dehydrogenase domain along with six transmembrane domains, and five potential histidine coordination sites for *b*–heme binding. The results from phylogenetic analysis of CbcB homologs are explained in this review. Some CbcB homologs were found to be fused to a *c*–type cytochrome domain containing seven heme binding domains (Figure 1.2).

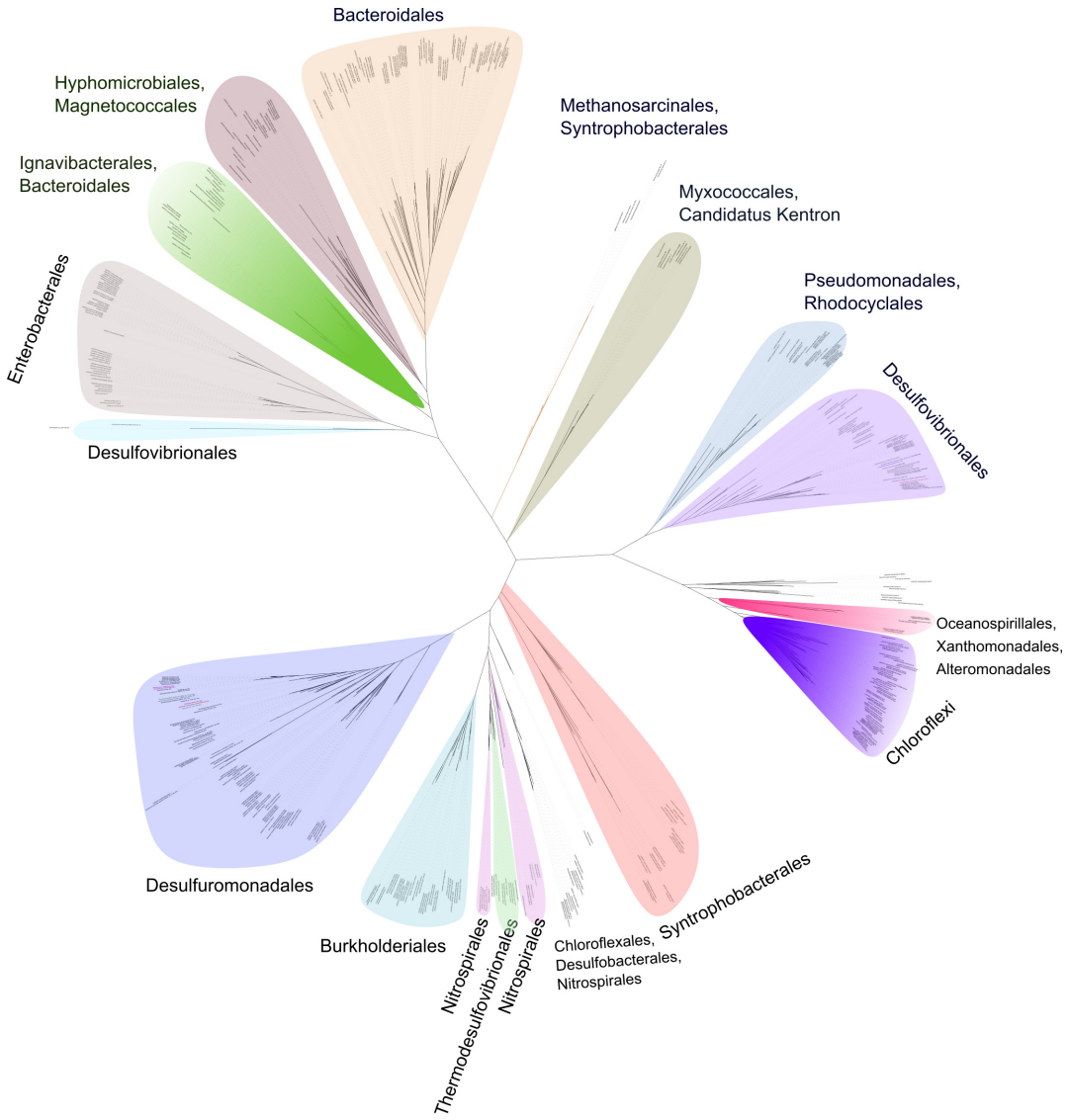

Figure 1.2: **Phylogenetic analysis of the cytochrome *b* domain of CbcB shows evolutionary conservation, with evidence for diversification from Ni–dependent hydrogenases.** A maximum likelihood tree was generated using ETE toolkit like mentioned in figure 1.1. Sequences with greater than 80% sequence identity were collapsed, and the unrooted tree containing clades of single order is colored. Color gradients represent clades containing sequences with fused *b*– and *c*–type cytochromes.

Members of the order Desulfuromonadales contained at least four transmembrane domains with upto five histidine residues that could be involved in *b*–heme coordination. Members of deltaporoteobacteria– Desulfuromonadales, Desulfovibrionales, Syntrophobacterales were found to be present in many divergent clades. Interestingly, few members of Syntrophobacterales clustered

with Methanosarcinales archaea, known to contain multiheme cytochromes [67]. Members of Ignavibacteriales, some Bacteroidales, members from Chloroflexi phyla, and Xanthomonadales, Oceanospirillales, and Altermonadales orders were found to have fused *bc*–cytochrome (Figure 1.2). Sequence homology of *c*–type domain placed these *c*–type cytochromes in bins with ImcH homologs. These results reflect an evolutionary relationship between ImcH and CbcBA, but requires further genetic and phenotypic characterization. Both ImcH, and CbcBA are required for respiration of electron acceptors on two sides of the redox potential spectrum. Structural information from these cytochromes might shed light on the architectures of extracellular electron transferring proteins.

The data presented in this thesis generates hypotheses for the potential mechanism of electron transfer through these inner membrane cytochromes. Future experiments might reflect strategies for fine-tuning of protein structure to maximize thermodynamic energy conservation.

Chapter 2

Geobacter sulfurreducens inner membrane cytochrome CbcBA controls electron transfer and growth yield near the energetic limit of respiration.

Komal Joshi, Chi Ho Chan, Daniel R. Bond

(modified from Joshi *et al.,* 2021, submitted)

2.1 Summary

Geobacter sulfurreducens utilizes extracellular electron acceptors such as Mn(IV), Fe(III), syntrophic partners, and electrodes that vary from +0.4 to −0.3 V *vs.* Standard Hydrogen Electrode (SHE), representing a potential energy span that should require a highly branched electron transfer chain. Here we describe CbcBA, a *bc*–type cytochrome essential near the thermodynamic limit of respiration when acetate is the electron donor. Mutants lacking *cbcBA* ceased Fe(III) reduction at −0.21 V *vs.* SHE, could not transfer electrons to electrodes between −0.21 and −0.28 V, and could not reduce the final 10% – 35% of Fe(III) minerals. As redox potential decreased during Fe(III) reduction, *cbcBA* was induced with the aid of the regulator BccR to become one of the most highly expressed genes in *G. sulfurreducens*. Growth yield (CFU/mM Fe(II)) was 112% of WT in Δ*cbcBA*, and deletion of *cbcL* (a *bc*–cytochrome essential near −0.15 V) with *cbcBA* increased yield 220%. Together with ImcH, which is required at high redox potential, CbcBA represents a third cytoplasmic membrane oxidoreductase in *G. sulfurreducens*. This expanding list implies metal-reducing bacteria can constantly sense redox potential to adjust growth efficiency in changing environments.

2.2 Introduction

Life generates cellular energy by linking electron donor oxidation to acceptor reduction. Each electron source and sink has an inherent affinity for electrons, or redox potential, which defines the maximum amount of energy available in such coupled reactions. For example, the redox potentials of NO_3^- and Fe(III) differ by more than half a volt, representing an opportunity to generate an additional ATP per electron when acetate is the donor ($E^{\circ\prime}$ of NO_3/NO_2 = +0.43 V *vs.* $E^{\circ\prime}$ of Fe(III) (oxyhydr)oxides ~ −0.2 V *vs.* SHE) [1,68,69]. As the redox potential of soils and sediments can vary widely [70–72], adjusting electron transfer chains to use acceptors with more favorable potentials allows anaerobes to maximize growth in response to environmental conditions [1, 10, 73, 74].

The respiration of Fe(III) and Mn(IV) poses unique challenges. These elements exist as insoluble (oxyhydr)oxides near neutral pH, requiring metal-reducing bacteria to divert inner membrane respiratory chains to electron-accepting surfaces outside the cell [14, 15]. Additional complexity arises from the number of metal oxide polymorphs that exist in nature, with nearly 30 Mn oxides and 15 Fe oxides described, each with its own characteristic redox potential [75–78]. While all of these could appear to the cell as similar extracellular electron sinks, the higher redox potential of Mn(IV) compared to Fe(III) oxides ($E^{\circ\prime}$ ~ +0.5 to +0.3 V *vs.* +0.1 to −0.3 V *vs.* SHE) predicts that bacteria should be able to recognize and prefer specific metal forms. Sequential reduction of Mn(IV) before Fe(III) was observed in sediments as early as 1966 [71] and in pure cultures of *Geobacter metallireducens* in 1988 [79], suggesting that biological mechanisms exist to differentiate between higher *vs.* lower potential materials outside the cell.

Geobacter spp. can utilize multiple oxidized metals, directly transfer electrons to methanogens, and utilize electrode surfaces as electron acceptors [13, 39, 40, 80–82]. The genomes of *Geobacter spp.* reflect this flexibility, with multiheme *c*–type cytochromes and extracellular appendages identified that facilitate reduction of extracellular compounds. In *G. sulfurreducens*, at least five triheme cytochromes are linked to periplasmic electron transfer, five multi-protein cytochrome complexes aid electron transfer through the outer membrane, and two multiheme cytochrome nanowires and extracellular pili extend beyond the cell to facilitate contact with acceptors [23, 24, 30, 52, 83, 84]. Some outer membrane cytochromes are necessary for reduction of specific oxyanions such as SeO_3 [85], or use of Fe(III) *vs*. electrode surfaces, but none explain how *Geobacter* might adapt its energy generation strategy to changes in redox potential [30,33,34,36,86].

The inner membrane cytochromes ImcH and CbcL provide a possible mechanism for potential-dependent electron transfer [33, 34]. *G. sulfurreducens* requires the seven-heme *c*–type cytochrome ImcH to respire above redox potentials of -0.1 V *vs.* SHE, but requires CbcL, a fusion of a diheme *b*–type cytochrome and a nine-heme *c*–type cytochrome, to use electron acceptors below -0.1 V *vs.* SHE. As *imcH* and *cbcL* are constitutively expressed [30, 34], the requirement for each protein appears to be controlled by ambient redox potential, switching from ImcH to CbcL as conditions change [33, 34].

Multiple lines of evidence suggest that ImcH and CbcL are not the only *G. sulfurreducens* quinone oxidoreductases capable of routing electrons into the periplasm. The redox potentials of subsurface environments and microbial fuel cell anodes where *Geobacter* typically dominate can be as low as -0.3 V vs. SHE, below the range where ImcH or CbcL are essential

[87, 88]. Incubations of Δ*cbcL* with low-potential Fe(III) oxides produces unexplained Fe(II) [41], and Δ*cbcL* attached to electrodes still shows electron transfer below −0.2 V *vs.* SHE [34]. In addition, *Geobacter* genomes contain many uncharacterized gene clusters where a quinone oxidase–like *b*–type diheme is adjacent to a periplasmic multiheme *c*–type cytochrome, reminiscent of the two domains fused together in CbcL.

In this report, we identify CbcBA, a *bc*–type quinone oxidoreductase necessary for respiration near the thermodynamic limit of acetate oxidation. CbcBA is essential for extracellular metal and electrode reduction below −0.21 V *vs.* SHE, and is found within every sequenced *Geobacter* genome [53]. We also provide evidence that use of CbcBA leads to lower growth yields, may primarily act as a non energy-conserving route allowing electron disposal. Unique from *imcH* and *cbcL*, *cbcBA* requires a σ^{54}–dependent transcriptional activator for expression, and *cbcBA* is one of the most highly expressed genes during reduction of low potential Fe(III). Taken together, ImcH, CbcL, and CbcBA are part of a branched electron transfer pathway that allows *Geobacter* to adjust its energy conservation in response to the redox potential of a given extracellular electron acceptor, and compete where the energy available is near the threshold able to support microbial life.

2.3 Materials and Methods

2.3.1 Bacterial strains and culture conditions

All strains and plasmids used in this study are listed in Table 2.1. *Geobacter sulfurreducens* strains and mutants were grown in NB minimal medium containing 0.38 $g.L^{-1}$ KCl, 0.2 $g.L^{-1}$ NH_4Cl, 0.069 $g.L^{-1}NaH_2PO_4.H_2O$, 0.04 $g.L^{-1}$ $CaCl_2.2H_2O$, 0.2 $g.L^{-1}$ $MgSO_4.7H_2O$, 10 mL of trace mineral mix, and buffered with 2 $g.L^{-1}$ of $NaHCO_3$ purged with N_2:CO_2 (80:20) atmosphere, incubated at 30 ºC. Trace mineral mix was composed of 1.5 $g.L^{-1}$ of nitrilotriacetic acid as a chelator for growth in all medium (except when Fe(III) was provided as the terminal electron acceptor, in which case minerals were prepared in 12.5 $mL.L^{-1}$ of 7.7 M HCl to final concentration of 0.1 M HCl), 0.1 $g.L^{-1}$ $MnCl_2.4H_2O$, 0.5 $g.L^{-1}$ $FeSO_4.7H_2O$, 0.17 $g.L^{-1}$ $CoCl_2.6H_2O$, 0.10 $g.L^{-1}$ $ZnCl_2$ 0.03 $g.L^{-1}$ $CuSO_4.5H_2O$, 0.005 $g.L^{-1}$ $AlK(SO_4)_2.12H_2O$, 0.005 $g.L^{-1}$ H_3BO_3, 0.09 $g.L^{-1}$ Na_2MoO_4, 0.05 $g.L^{-1}$ $NiCl_2$, 0.02 $g.L^{-1}$ $Na_2WO_4.2H_2O$, 0.10 $g.L^{-1}$ Na_2SeO_4. Routine growth was performed in acetate-fumarate NB medium (NBFA) containing 20 mM acetate as the carbon source and electron donor and 40 mM fumarate as the electron acceptor. For solid medium, 1.5% agar was added to acetate-fumarate medium for growth on plates in an anaerobic workstation (Microbiology International, Maryland) under N_2:CO_2:H_2 (75:20:5) atmosphere at 30 ºC. Every experiment was initiated by streaking fresh strains of *G. sulfurreducens* from −80 ºC culture stocks. 200 $\mu g.mL^{-1}$ kanamycin was used for *G. sulfurreducens*, 100 $\mu g.mL^{-1}$ ampicillin and 50 $\mu g.mL^{-1}$ kanamycin for *E. coli* as indicated.

Strains or Plasmids	Description or relevant genotype	Reference or source

***G. sulfurreducens* strains**		
	Wildtype *G. sulfurreducens*	Lab culture collection
DB789	Δ*imcH*	[89]
DB868	Δ*cbcL*	[34]
DB790	Δ*imcH* Δ*cbcL*	This study
DB1674	Δ*bccR*	This study
DB1717	Δ*cbcBA*	This study
DB1718	Δ*imcH* Δ*cbcBA*	This study
DB1719	Δ*cbcL* Δ*cbcBA*	This study
DB1720	Δ*imcH* Δ*cbcL* Δ*cbcBA*	This study
DB1721	Δ*cbcBA* Tn7::p0597*cbcBA*-Kan	This study
DB1725	Δ*cbcBA* Tn7::p0597*cbcB*-Kan	This study
DB1729	Δ*cbcBA* Tn7::p0597*cbcA*-Kan	This study
***E. coli* strains**		
UQ950	Cloning strain of *E. coli*	
S17-1	Conjugation donor strain	
MFDpir	Conjugation donor strain	
DB2068	S17-1 strain containing pk18mobsacBDGSU0593-94 for *cbcBA* deletion	This study
DB1658	S17-1 strain containing pk18mobsacBDGSU0598 for *bccR* deletion	This study
DB1325	MFDpir conjugation donor strain containing helper plasmid pmobile-CRISPRi	[90]
DB2075	UQ950 strain containing pGeo2::p0597*cbcBA*	This study
DB2076	UQ950 strain containing pGeo2::p0597*cbcB*	This study
DB2077	UQ950 strain containing pGeo2::p0597*cbcA*	This study
DB2079	UQ950 strain containing pTn7c147::p0597*cbcBA*	This study

DB2081	UQ950 strain containing pTn7c147::p0597*cbcB*	This study
DB2083	UQ950 strain containing pTn7c147::p0597*cbcA*	This study
Plasmids		
pk18mobsacB		[89]
prk2Geo2		[89]
pTn7C147		[91]
pmobile-CRISPRi		[90]
pDGSU0593-94	Flanking regions of GSU0593-GSU0594 in pk18mobsacB	This study
pDGSU0598	pk18mobsacB deletion vector containing flanking regions of GSU0598.	This study
prk2Geo2::0597 p*cbcBA*	Complementation vector of GSU0593-0594 with its predicted native promoter	This study
prk2Geo2::0597 p*cbcB*	Complementation vector of GSU0593 with its predicted native promoter	This study
prk2Geo2::0597 p*cbcA*	Complementation vector of GSU0594 with its predicted native promoter	This study
pTn7C147::p0597 *cbcBA*-Kan	Complementation vector subcloned from pGeo2 expressing *cbcBA* under the control of native promoter.	This study
pTn7C147::p0597 *cbcB*-Kan	Complementation vector subcloned from pGeo2 expressing *cbcB* under the control of native promoter.	This study
pTn7C147::p0597 *cbcA*-Kan	Complementation vector subcloned from pGeo2 expressing *cbcA* under the control of native promoter.	This study

Table 2.1: List of strains and plasmids used in this study

2.3.2 Strain construction and complementation

Deletion constructs were designed based on strategy previously described [89]. Briefly, ~1 kb upstream and downstream region of *cbcBA* (GSU0593–0594), and *bccR* (GSU0598) were amplified using primers listed in Table 2. Amplified upstream and downstream DNA fragments were fused using overlap extension PCR. Amplified fused DNA fragments were digested with restriction enzymes HindIII and EcoRI, and ligated into digested and gel purified pk18mobsacB. The ligation product was transformed into UQ950 chemically competent cells. The resulting plasmid was sequence verified before transformation into S17–1 conjugation donor cells. Overnight grown S17–1 donor strain containing the plasmid was conjugated with *G. sulfurreducens* acceptor strain inside an anaerobic chamber on a sterile filter paper placed on an NBFA agar plate. After ~4 h, cells scraped from filters were streaked on NBFA agar plates containing kanamycin. After positive integrants were identified, *sacB* counter selection was performed by growing positive integrants on NBFA + 10% sucrose plates. Colonies from NBFA + 10% sucrose plates were patched on NBFA and NBFA + 200 $\mu g.mL^{-1}$ to select for antibiotic sensitive, markerless deletion strains. The strains were verified by PCR for the gene deletion, and final strains were checked for off-site mutations via Illumina re-sequencing.

Deletion	**Sequence (5'-3')**	**Restriction enzyme**
GSU0593-94 U1F KJ112	CTAATAAGCTTGGACCGGCTCCCTT GACCTT	HindIII
GSU0593-94 U2R KJ105	GTGCTGTCGCTCCTCGCGCCCATGT GGGATGGCTGGGAA	
GSU0593-94 D3F KJ106	TTCCCAGCCATCCCACATGGGCGCG AGGAGCGACAGCAC	

GSU0593-94 D4R KJ107	GCTACGAATTCGGCCGGCGAAAGAT ATCGCCA	EcoRI
GSU0598 U1F CHC652	AGTCGTCTAGACAGTCCCTTGACCA TCGCTGC	XbaI
GSU0598 U2R CHC653	GCAATGCCTGAAAGTTGGGACGCTC CCGGATAATCGCTTCATCGTC	
GSU0598 D3F CHC654	GACGATGAAGCGATTATCCGGGAGC GTCCCAACTTTCAGGCATTGC	
GSU0598 D4R CHC655	AGACTAAGCTTGATCGTCAAAGAGA CCCAGCGC	HindIII
Confirmation of gene deletion		
GSU0593-94 Uflank F KJ110	CACGTGTACATGGAGAGGTGCA	
GSU0593-94 Dflank R KJ111	GCTCATGCTCTTCGCAGCGA	
GSU0598 Uflank CHC656	CGTTTCGTTGCCCGATGTTCC	
GSU0598 Dflank CHC657	CTTGCCTCTCTGGGCGAACTG	
Complementation		
GSU0593-94 comp 3 F KJ129	CCAAGCATATGGGCCGGCCCCGAC ATCACTT	NdeI
GSU0593-94 comp 4 R KJ130	CCAAGGAGCTCTTTCCGGTCTGGC AGGCGGTGG	SacI
GSU0593 comp 5 F KJ131	CCAAGCATATGACGGGACCTTCAGA TTCCTGAC	NdeI
GSU0594 comp 6 R KJ132	CCAATGCTAGCTCGGCATGCTCGTT ATGGGCG	NheI
GSU0597 promoter F KJ133	CTTGAGGCGCGCCAGGGGAAGTCA AACCCATTGAC	SgsI
GSU0597 promoter R KJ134	CCAAGCATATGATCCGGAGATGTGAG CCTTTT	NdeI

Table 2.2: Primers used in this study.

Complementation was performed using the method described in Hallberg *et. al* [91]. Complement strains were constructed by first cloning *cbcBA* (GSU0593–94), *cbcB* (GSU0593), or *cbcA* (GSU0594) gene into the pRK2Geo2 vector. The *cbcBA* cluster with native ribosomal binding sites was cloned under the control of its native promoter (GSU0597). The resulting vectors were sequence verified, then subcloned into pTn7c147 between the n7L and n7R regions. Newly subcloned pTn7 vectors were transformed in MFDpir chemically competent cells [92]. Any DNA between n7L and n7R regions is integrated downstream of the *glmS* (GSU0270) site, surrounded by strong terminators [93]. A helper plasmid pmobile-CRSPRi expressing recombinase TnsABCD in MFDpir cells was utilized to recognize n7L and n7R regions in pTn7 vectors, and integrate DNA onto *G. sulfurreducens* chromosome downstream of *glmS.* A triparental mating strategy was used to create complement strains. Integrating genes onto the genome minimizes growth-rate and biofilm defects encountered when using most plasmids in *Geobacter*.

2.3.3 Cyclic voltammetry

Three electrode bioreactors were setup with a 3 cm^2 1500-grit polished polycrystalline graphite (POCO AXF–5Q, TriGemini LLC, Illinois) attached to a platinum loop serving as a working electrode, platinum wire as a counter electrode, Ag/AgCl as a reference electrode [94]. The assembled bioreactors were autoclaved at 121 ºC for 20 min. Anoxic conditions were maintained by constantly flushing reactors with anoxic humidified N_2:CO_2 (80:20) gas. 40 mM acetate served as an electron donor and carbon source, and poised electrodes (+0.24 V *vs.* SHE) served as the

sole electron acceptor. NBFA grown cells ($OD_{600} \simeq 0.5$) were inoculated into the reactors at 25% inoculation. Reactors were housed in a water bath maintained at 30 ºC, and stirred constantly. A 16-channel potentiostat (Biologic Science Instruments) was used to constantly monitor and record current generated over time using chronoamperometry technique. After all the strains reached a current density between 350–400 $\mu A.cm^{-2}$, cyclic voltammetry technique was applied by forward scanning the working electrode reduction potential from -0.55 V *vs.* SHE to +0.24 V *vs.* SHE, and reverse scan back to -0.55 V *vs.* SHE at 1 mV/s for two scans [95]. Current generated over this potential window was recorded. Second scan was used for data analysis.

2.3.4 Growth with Fe(III) citrate

Minimal medium containing 20 mM acetate and 55 mM Fe(III) citrate was used in anaerobic balch tubes, or in bioreactors when redox potential was measured over time [41, 94]. Media were autoclaved at 121 ºC on a gravity cycle and were immediately removed to cool at room temperature in the dark. For measuring growth in Fe(III) citrate containing medium, anaerobic tubes containing Fe(III) citrate medium with 55 mM Fe(III) citrate and 20 mM acetate were inoculated at 1:100 v/v from the acetate-fumarate grown ($OD_{600} \simeq 0.5$) culture. To measure Fe(III) reduction, 0.1 mL of sample was taken at regular intervals and dissolved in 0.9 mL of 0.5 N HCl. Fe(II) concentrations were measured using a modified Ferrozine assay [96].

2.3.5 Redox potential measurement

For monitoring continuous change in redox potential as cells grow in Fe(III) citrate medium, three-electrode bioreactors were used with two platinum wire electrodes of approximately 1 cm in length as working and counter electrodes, and Ag/AgCl electrode (+0.21 V *vs.* SHE) was used as a reference electrode. Cells were inoculated into bioreactors after the baseline redox potential is equilibrated. Redox potential was measured by applying open circuit potential (OCP) method using a 16-channel potentiostat. Reactors were constantly flushed with N_2:CO_2 (80:20) gas to prevent Fe(II) reoxidation. Platinum electrodes were routinely cleaned in 0.5 M H_2SO_4 in a three-electrode cell set-up connected to a potentiostat using the following technique: holding working electrode at +2.24 V *vs.* SHE, then cycling the electrode potential between +0.01 V *vs.* SHE and +1.34 V *vs.* SHE for 20 cycles with scanning stopped at +1.34 V *vs.* SHE. Electrodes were then rinsed with DI water, and dried before using in any experiment.

2.3.6 Fe(III) oxide reduction

NB medium containing 20 mM acetate as the electron donor and carbon source was used and either ∼60 mM akaganeite or ∼30 mM XRD–amorphous Fe(III) (oxyhydr)oxide was used as an electron acceptor. NB medium was supplemented with 0.69 $g.L^{-1}$ $NaH_2PO_4.H_2O$ to prevent formation of crystalline forms of Fe(III) (oxyhydr)oxide while autoclaving [77]. Fresh akaganeite was synthesized by adding 25% NaOH dropwise to a stirring solution of 0.4 M $FeCl_3$ until the pH was 7. The suspension was aged for at least one hour, bringing the pH to 7 and washed with one volume of DI H_2O. 1 mL of the resulting mineral identified as akaganeite (β–FeOOH) was added to 9 mL

NB medium before autoclaving [41, 77]. XRD–amorphous Fe(III) (oxyhydr)oxide was synthesized first as schwertmannite ($Fe_8O_8(OH)_6(SO_4).nH_2O$) by adding 5.5 mL of 30 % hydrogen peroxide to a solution of 10 g.L^{-1} $FeSO_4$, stirred overnight to stabilize pH. Schwertmannite solids collected were washed with DI H_2O thrice by centrifugation at 3700$\times$g. After final wash, the resulting mineral was added to NB medium with 20 mM acetate as the carbon source and adjusted to a final pH of 6.8 before autoclaving. Bringing the pH of the medium to neutral pH and autoclaving thereafter altered the Fe(III) (oxyhydr)oxide mineral into an amorphous mineral form called XRD–amorphous Fe(III) (oxyhydr)oxide [41, 77, 91]. Iron oxide medium was inoculated with 1:100 v/v of stationary phase cells ($OD_{600}\simeq0.5$) grown in NBFA medium. 0.1 mL samples were taken periodically and dissolved in 0.9 mL 0.5N HCl, and stored in the dark. Fe(III) reduction was calculated as increase in Fe(II) concentrations measured by a modified ferrozine assay.

2.3.7 Transcriptomic analysis using RNA-seq

Total RNA was extracted from *G. sulfurreducens* fumarate-grown cultures in exponential phase. For cells grown with Fe(III) citrate, RNA was extracted from cultures at exponential growth phase when ~30% or ~70% of Fe(III) citrate was reduced. Cells were collected using vacuum filtration to minimize inhibition from Fe(III)/Fe(II) in the medium. Electrode biofilms were scraped from electrodes immediately after disconnecting them from the potentiostat. All cell pellets were washed in RNAprotect reagent (Qiagen) and stored at -80 ºC before extraction using RNeasy with on column DNase treatment (Qiagen). Ribosomal RNA was depleted using Ribozero (Illumina) before sequencing on the Illumina Hiseq 2500 platform in 125 bp pair-ended mode.

Residual ribosomal RNA sequences were removed using Bowtie2 [97] before analysis. Duplicate rRNA-depleted biological samples were analyzed for each strain and condition using Rockhopper [98], using our re-sequenced *G. sulfurreducens* genome [89]. Expression was normalized by reads mapped by the upper quartile of gene expression values, and full RNA-seq data are in Supplementary table 1.

2.3.8 CFU and yield measurements

Growth of different *G. sulfurreducens* strains in NB medium with 20 mM acetate as the carbon source and electron donor and either 40mM fumarate or 55 mM Fe(III) citrate as an electron acceptor was measured by counting colony-forming units (CFUs) at regular intervals. Drop plate method adapted from Herigstad *et al*., 2001 [99] was used to plate cells on NBFA agar medium. Briefly, 100 μL of samples were taken periodically, serially diluted 1:10 in NBFA liquid medium, and 10 μL of each dilution was plated on NBFA agar plates. Sampling, dilution and plating were performed inside an anaerobic chamber (Coy laboratory products) with N_2:CO_2:H_2 (75:20:5) atmosphere. Total Fe(III) reduced was measured using ferrozine assay. Total CFUs were counted after 5 days of incubation. Cellular yield was calculated as CFU per mM Fe(III) citrate reduced when cells were actively growing between 14–36 h.

2.4 Results

2.4.1 The *cbcBA* gene cluster encodes a *b*– and *c*–type cytochrome expressed late in Fe(III) reduction.

The *G. sulfurreducens* genome contains at least six putative inner membrane quinone oxidoreductase gene clusters. Five encode both *b*– and *c*–type cytochrome domains: Cbc1 (GSU0274, *cbcL*), Cbc3 (GSU1648–GSU1650, *cbcVWX*), Cbc4 (GSU0068–GSU0070, *cbcSTU*), Cbc5 (GSU0590–GSU0594, *cbcEDCBA*), Cbc6 (GSU2930–GSU2935, *cbcMNOPQR*) [36], and one that contains only a multiheme *c*–type cytochrome (GSU3259, *imcH*) [33]. The *b*– and *c*–type cytochrome CbcL (Cbc1) is essential for growth below redox potentials of −0.1 V *vs.* SHE [34], while the *c*–type cytochrome ImcH is essential for respiration above these redox potentials [33]. Among these *b*– and *c*–type cytochrome gene clusters, Cbc5 is the most conserved cytochrome-containing gene cluster among *Geobacter* species [53].

Bioinformatic [100–102] and transcriptomic analyses [30, 103] place *cbcBA* in an operon with a σ^{54}–dependent promoter upstream of GSU0597 and a transcriptional terminator downstream of *cbcB* (Figure 2.1A). This operon encodes two hypothetical proteins (GSU0597 and GSU3489), a RpoN–dependent response regulator (GSU0596), a quinone oxidoreductase-like diheme *b*–type cytochrome (CbcB) [63], and a seven-heme *c*–type cytochrome (CbcA) (Figure 2.1C). Inner membrane localization of CbcBA is predicted by PSORT [104], with CbcB integrated into the inner membrane and CbcA exposed in the periplasm anchored by a C–terminal transmembrane domain. Cell fractionation studies also report a cytoplasmic membrane association

of CbcA [37], implying that CbcBA is localized to the inner membrane.

A

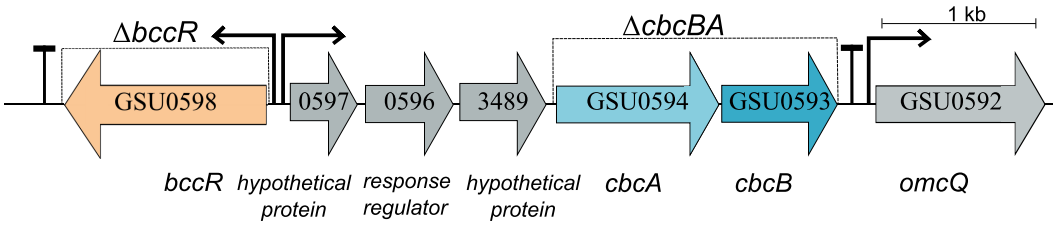

B

Electron acceptor	Expression level (RPKM)						
Fumarate	145	26	10	7	4	4	145
Electrode	178	95	105	237	217	258	293
Fe(III) citrate *30% reduced*	213	3	3	4	4	3	359
Fe(III) citrate *70% reduced*	2508	8451	12201	16596	9611	15565	125

C

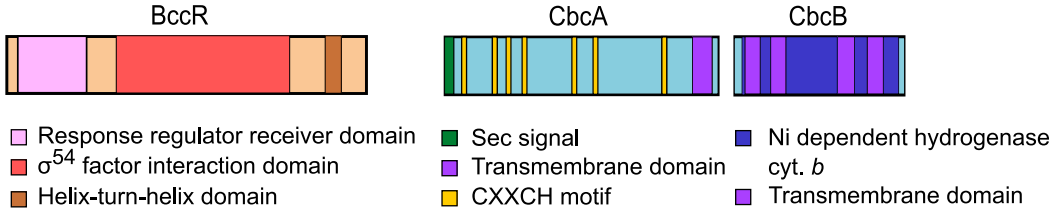

Figure 2.1: **Genetic organization, expression, and domain structure of the *cbcBA* region.** A. *cbcBA* is part of a five-gene operon divergently transcribed from a σ^{54}–dependent transcriptional regulator (*bccR*). B. Expression levels, as reads per kilobase mapped (RPKM), when growing exponentially with different electron acceptors: fumarate, electrodes, or Fe(III) citrate (30% *vs.* 70% Fe(III) reduced). The expression values correspond to the gene labels in panel A. See Supplementary Table 1 for full RNA-seq data. C. Predicted features and domain structure of BccR, CbcB, and CbcA.

Divergently transcribed from this operon is GSU0598, a putative σ^{54}–dependent transcriptional regulator, which we have named *bccR* (for *bc*–type cytochrome regulator) (Figure 1A). BccR belongs to the RpoN–dependent family of regulators that bind −12 /−24 elements [105]. BccR contains a response receiver domain, a σ^{54} factor interaction domain, and a C–terminal helix-turn-helix domain [106] (Figure 2.1C).

The *cbcBA* operon (GSU0597–GSU0593) had near zero expression when fumarate was

the electron acceptor, but low expression was detected in electrode-grown biofilms [30] (Figure 2.1B). When growing with Fe(III) citrate as the electron acceptor, expression of the *cbcBA* operon remained low during the first 20 h of growth (Figure 2.1B), or as the first ~30% Fe(III) was reduced (Figure 2.3A). However, *cbcBA* was dramatically upregulated after 30 h of growth (Figure 2.1B), as ~70% of Fe(III) became reduced (Figure 2.3A). The level of *cbcBA* expression (>12 000 RPKM) was higher than 99% of *G. sulfurreducens* genes at this stage (Figure 2.2).

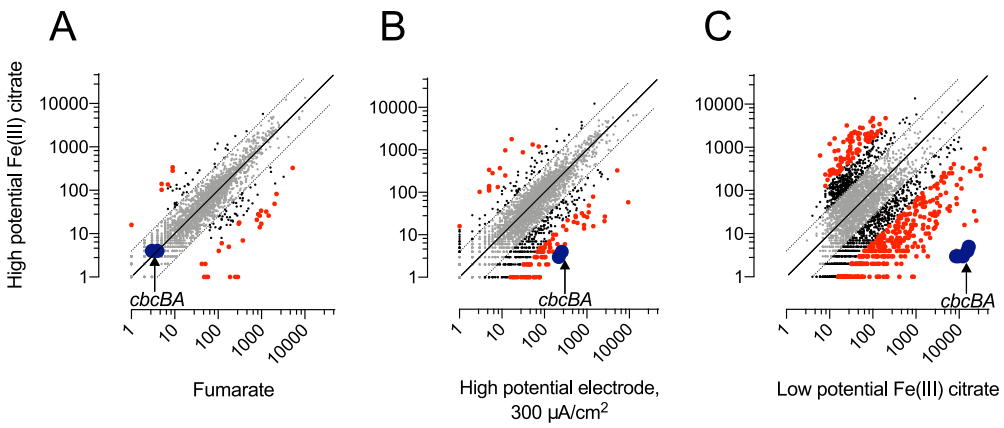

Figure 2.2: **RNA-Seq of WT *G. sulfurreducens* grown with different electron acceptors compared to early exponential growth in Fe(III) citrate (30% reduced).** A. Expression of *cbcBA* is barely detectable when both fumarate and high redox potential Fe(III) citrate are the electron acceptor. B. Expression of *cbcBA* increases in electrode-grown biofilms compared to fresh Fe(III) citrate, and C. Expression of *cbcBA* increases to over more than 10,000 RPKM (reads per kilobase mapped) in low potential Fe(III) citrate (70% reduced). Each comparison is the average of two biological replicates. Significant differences greater than 2-fold (black) or 4-fold (red) are highlighted. X and Y axes represent expression values.

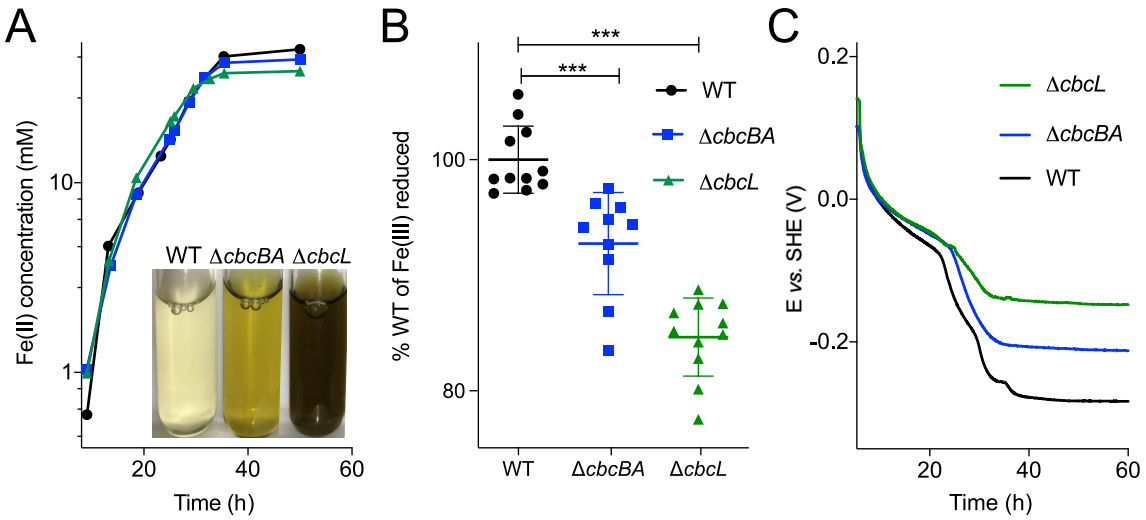

Figure 2.3: **Mutants lacking *cbcBA* or *cbcL* cannot reduce all available Fe(III) citrate, and *cbcBA* is required for reduction below −0.21 V *vs.* SHE.** A. Fe(III) citrate reduction over time. Inset image shows the difference in endpoint Fe(III) citrate reduction by different strains. B. Δ*cbcBA* reduces ~93% of Fe(III) citrate compared to WT, whereas Δ*cbcL* reduces ~85% of Fe(III) citrate compared to WT. C. Redox potential recorded over time in the same medium, as cells reduce Fe(III) citrate. The Δ*cbcL* mutant fails to lower redox potential below −0.15 V *vs.* SHE whereas the Δ*cbcBA* mutant fails to lower redox potential below −0.21 V *vs.* SHE. All experiments were conducted in triplicate, and representative curves are shown in A and C ($N \geq 5$). B shows end point values from individual experiments averaged with standard deviation reported as error bars ($n \geq 10$). Two-tailed t-test was performed to calculate p-values.

2.4.2 CbcBA is essential for complete reduction of Fe(III) citrate.

To determine if CbcBA was involved in extracellular electron transfer, a markerless deletion of GSU0593–94 (Δ*cbcBA*) was created. The Δ*cbcBA* mutant did not show any defect with fumarate as the electron acceptor (Figure 2.4). However, the extent of Fe(III) reduction by Δ*cbcBA* was lower. Mutants lacking *cbcBA* reduced up to 90% Fe(III) citrate (Figure 2.3A), regardless of the amount of electron donor provided or length of incubation.

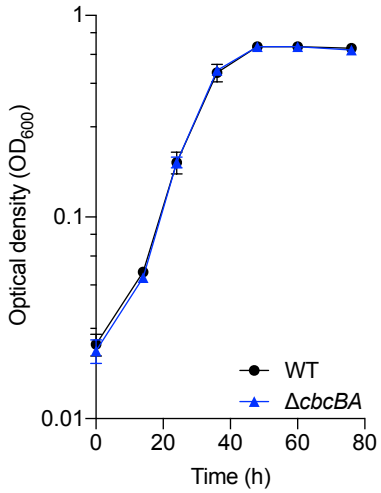

Figure 2.4: **Growth of Δ*cbcBA* compared to WT in NB fumarate-acetate (NBFA) medium.** Fully grown cultures of WT and Δ*cbcBA* in medium containing 40 mM fumarate and 20 mM acetate were inoculated 1:100 v/v, and optical density measured at 600 nm over time. Δ*cbcBA* did not show any growth defects as compared to WT when fumarate was the terminal electron acceptor (mean of three biological replicates, and error is reported as standard error of mean (SEM)).

The putative quinone oxidoreductase ImcH is essential for reduction of high potential electron acceptors such as freshly prepared Fe(III) citrate [33], while the *bc*–cytochrome CbcL becomes essential as Fe(III) is reduced and redox potential drops [34, 41]. As the type of Fe(III) reduction defect observed for Δ*cbcBA* was similar to Δ*cbcL*, mutants lacking *cbcL* and *cbcBA* were directly compared. The Δ*cbcBA* strain ceased reduction of Fe(III) after 92.7 ± 1.4% (n=10) of Fe(III) citrate was reduced, whereas Δ*cbcL* only reduced 84.6 ± 1.0% (n=11) of Fe(III) citrate (Figure 2.3A, 2.3B). This suggested that CbcBA became necessary in the final stages of Fe(III) reduction.

2.4.3 CbcBA is required for reduction of Fe(III) citrate below −0.21 V *vs.* SHE.

Because the 3000–fold up-regulation of *cbcBA* occurred later in incubations with Fe(III) (Figure 2.2) induction of *cbcBA* did not appear to be due to the presence of Fe(III) *per se*. To more accurately determine the energy available during each stage of Fe(III) reduction, we measured redox potential continuously during growth [41, 107]. Redox potential titrations and voltammetry determined the midpoint potential of the Fe(II) citrate/Fe(III) citrate half-reaction in our medium to be −0.043 V *vs.* SHE (Figure 2.5). This is lower than values calculated in literature, likely due to high levels of chelating carboxylic acids in commercial Fe(III) citrate combined with electron donors, creating bi– or tri–dentate complexes with lower redox potential than the 1:1 ratios assumed in standard calculations [108–110].

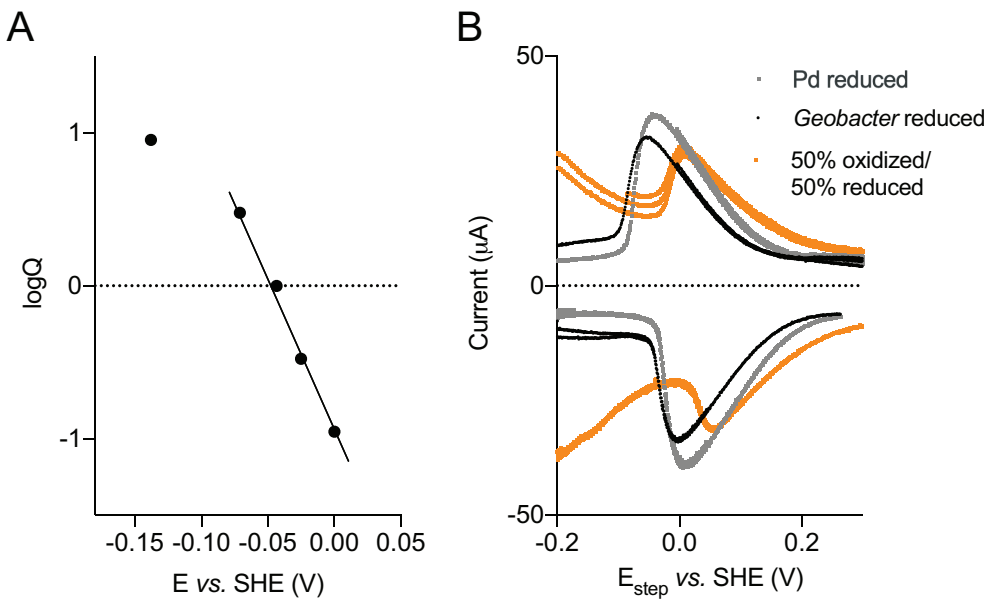

Figure 2.5: **Calculating midpoint potential of Fe(III) citrate prepared in our laboratory.** A. Calculation of midpoint potential of Fe(III) citrate using open circuit potential (OCP) method. Log(Fe(II)/Fe(III)) ratio of Fe(III) citrate follows Nernstian behavior only in a narrow potential window of about 0.1 V. Midpoint potential of Fe(III) citrate is −0.043 V *vs.* SHE. B. Comparing redox potential of Fe(III) citrate reduced by *G. sulfurreducens* or reduced by palladium (Pd) using differential pulse voltammetry method. These results show a much lower value of midpoint potential of Fe(III) citrate as previously reported [41] compared to the published values of +0.37 V *vs.* SHE [76].

When wildtype (WT) cells were inoculated into freshly prepared Fe(III) citrate (>99% oxidized), redox potential dropped rapidly from +0.15 V, and stabilized at −0.27 V *vs.* SHE when nearly 100% of Fe(III) was reduced. Considering the formal redox potential of CO_2/acetate is −0.28 V, cells utilized nearly all the free energy available. In contrast, Δ*cbcL* ceased Fe(III) reduction near −0.15 V *vs.* SHE (equivalent to 38 mM Fe(III) reduced) [41]. Under the same conditions, Δ*cbcBA* stabilized at −0.21 V *vs.* SHE (equivalent to 45 mM Fe(III) reduced). Each mutant produced these same endpoint potentials independent of inoculation size or incubation time (Figure 2.6), or when the concentration of Fe(III) citrate was increased to 80 mM [41].

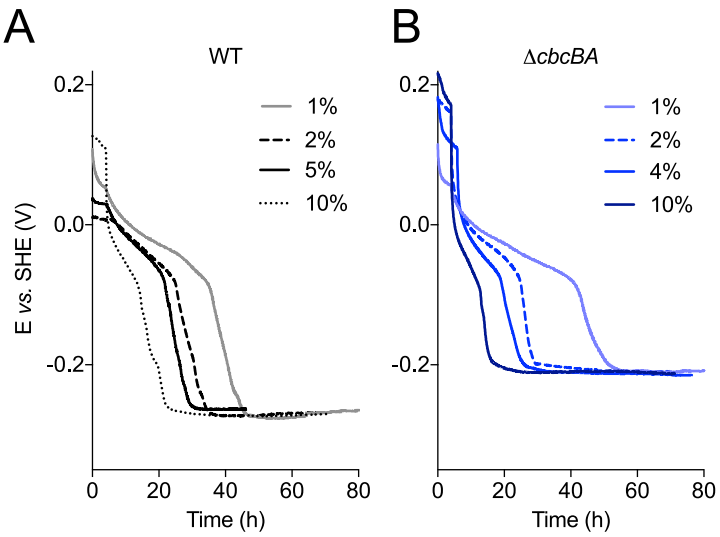

Figure 2.6: **The extent of Fe(III) reduction does not change with the percentage of inoculation or the time of incubation.** A. Redox potential of WT cultures reducing Fe(III) citrate when the percentage of inoculation was varied from 1% v/v to 10% v/v. The redox potential always stabilized at the same value. B. Redox potential of Δ*cbcBA* when inoculation was varied from 1% v/v to 10% v/v. Δ*cbcBA* always ceased reduction at a higher redox potential of −0.21 V *vs.* SHE, regardless of the percentage of inoculation. Redox potential was monitored for up to 80 h to test if Δ*cbcBA* cultures would lower the redox potential with longer incubation times. In similar experiments, the concentration of Fe(III) citrate was increased to 80 mM, and redox potential profiles followed similar trends, ending at the same final values [41].

2.4.4 Complementation of Δ*cbcBA* requires both *cbcB* and *cbcA*.

To test if *cbcB* or *cbcA* alone were responsible for the inability to reduce Fe(III) below −0.21 V *vs.* SHE, single genes were integrated into the chromosome under control of the *cbcBA* operon's promoter [91]. When Δ*cbcBA*::*cbcB* or Δ*cbcBA*::*cbcA* strains were grown with Fe(III) citrate, reduction still ceased at the same redox potential (Figure 2.7A). However, when both *cbcBA* genes were integrated and expressed in the Δ*cbcBA* strain, the extent of Fe(III) reduction was restored to WT levels (Figure 2.7A). Based on these results, all subsequent experiments were conducted with mutants lacking both genes.

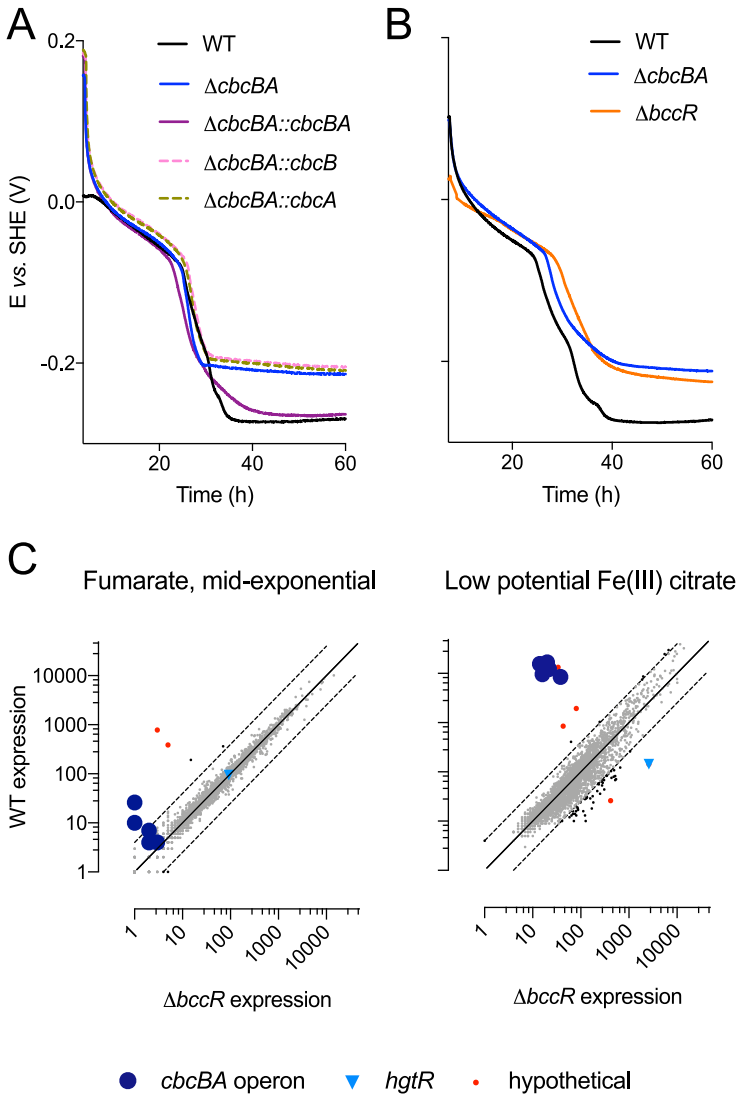

Figure 2.7: **Complementation of Δ*cbcBA* requires expression of both *cbcB* and *cbcA*, and *bccR* is essential for induction of *cbcBA*.** A. Complementation with both *cbcB* and *cbcA* are required to fully restore Fe(III) reduction in Δ*cbcBA*. B. Deletion of *bccR*, a σ^{54}–dependent transcriptional response regulator upstream of the *cbcBA* operon and comparison with Δ*cbcBA*. C. Transcriptomic analysis of WT *G. sulfurreducens vs.* Δ*bccR* grown with fumarate or Fe(III) citrate. Points above the 1:1 line indicate reduced expression due to deletion of *bccR*, points below the line had increased expression when *bccR* was deleted.

2.4.5 BccR is necessary for expression of *cbcBA*.

A response regulator is divergently transcribed upstream of *cbcBA bc*–type cytochrome operons in all examined *Geobacter* genomes [30, 111]. When *bccR* (GSU0598) was deleted, Δ*bccR*

ceased reduction of Fe(III) at −0.21 V *vs.* SHE, the same potential as Δ*cbcBA* (Figure 2.7B). RNAseq revealed that expression of *cbcBA* was no longer upregulated in Δ*bccR* during Fe(III) citrate reduction (Figure 2.7C) consistent with BccR being an activator of the *cbcBA* operon. Deletion of *bccR* did not affect other putative quinone oxidoreductases, in particular *imcH* or *cbcL*, which were constitutively expressed at much more moderate (~500 RPKM) levels.

While the largest effect of *bccR* deletion was downregulation of *cbcBA* operon (Figure 2.7C), Δ*bccR* showed upregulation of *hgtR* (GSU3364) when Fe(III) was the electron acceptor. HgtR is a RpoN–dependent repressor involved in downregulating acetate oxidation when hydrogen is the electron donor [105, 112]. The increase in *hgtR* expression by more than 1,000× in Δ*bccR* implies a possible role for HgtR in down-regulating the TCA cycle during reduction of Fe(III) as acetate oxidation becomes thermodynamically limited.

2.4.6 Double mutants show that *imcH*, *cbcL*, and *cbcBA* are required within different redox potential windows.

If only one inner membrane cytochrome is able to lower redox potential enough to activate the next, then double and triple markerless deletion mutant strains should show the phenotype of their dominant missing pathway. All single, double, and triple mutant strains lacking *imcH* failed to initiate Fe(III) citrate reduction when inoculated into fresh >+0.1 V *vs.* SHE medium, and did not lower the redox potential more than 20 mV over the following 60 h (Figure 2.8). The dominance of Δ*imcH* in all backgrounds corroborates data showing ImcH to be essential for electron transfer in fresh Fe(III) citrate, Mn(IV) oxide, and electrodes at redox potentials above 0 V [33, 41].

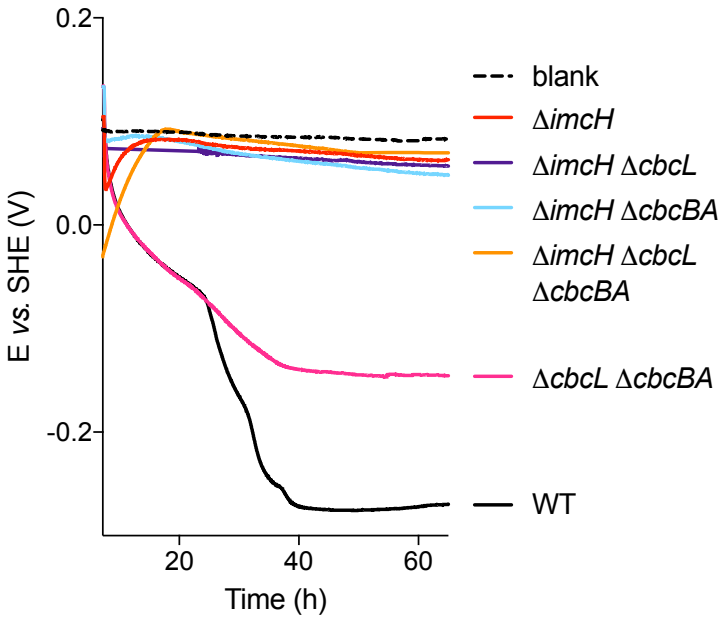

Figure 2.8: **Deletion of *imcH* prevents reduction of high potential Fe(III) citrate in all mutant backgrounds, while deletion of *cbcL* always prevents reduction beyond −0.15 V *vs.* SHE.** Mutants lacking *imcH* (Δ*imcH*, Δ*imcH* Δ*cbcL*, Δ*imcH* Δ*cbcBA*, Δ*imcH* Δ*cbcL* Δ*cbcBA*) fail to reduce fresh Fe(III) citrate and cannot lower redox potential. The double mutant lacking *cbcL* and *cbcBA* (Δ*cbcL* Δ*cbcBA*) fails to lower redox potential below −0.15 V *vs.* SHE, similar to the Δ*cbcL* single mutant. Representative curves from experiments conducted in triplicates are shown here.

Like the single Δ*cbcL* mutant, the Δ*cbcL* Δ*cbcBA* double mutant ($ImcH^+$) initially reduced Fe(III), then ceased reduction at −0.15 V *vs.* SHE. This provides additional evidence that ImcH can function down to a redox potential of −0.15 V, and that only CbcL can lower redox potential beyond this point, regardless of whether CbcBA is present (Figure 2.8). The phenotype of Δ*cbcBA* (Figure 2.3) similarly implies that CbcL is essential until −0.21 V *vs.* SHE, at which point CbcBA is required for electron transfer (Figure 2.7).

2.4.7 Cyclic voltammetry detects a CbcBA-dependent electron transfer process with a midpoint potential of −0.24 V *vs.* SHE.

All evidence that *cbcBA* was required at specific redox potentials was derived from soluble Fe(III) incubations, which could be non-physiological compared to environments where *G. sulfurreducens* uses a partner in syntrophy, or a solid electrode as the electron acceptor. To examine electron transfer in the absence of Fe(III), we grew *G. sulfurreducens* on graphite electrodes, and subjected the biofilms to cyclic voltammetry. During cyclic voltammetry, redox potential can be brought to a value too low to support acetate oxidation (−0.4 V *vs.* SHE) to obtain a baseline. As electrode potential is slowly increased, electron transfer from adherent cells is observed at a key onset potential as it becomes thermodynamically favorable, accelerates until a maximum electron transfer rate is reached, and follows the reverse trend as potential is decreased.

In theory, when a single event is rate-limiting, a Nernstian sigmoidal rise in current occurs over a ~100 mV window, rising most steeply at the potential that most strongly affects the oxidation state of a key redox center. The potential-dependent responses of *G. sulfurreducens* cells during voltammetry are more complex than one-event models, and instead display at least three overlapping processes [34, 48, 95, 113, 114]. The maximal rate of current increase defines these three features, which can be highlighted by the derivative of current increase as a function of applied potential.

Prior work described a change in voltammetry centered at −0.10 V *vs.* SHE when *cbcL* was deleted, which could be restored by *cbcL* complementation [34]. These experiments

also detected a lower potential process independent of CbcL that increased with each subsequent voltammetry sweep. Impedance measurements by Yoho *et al.* [113] reported a similar low potential electron transfer process detectable within minutes of applying reducing electrode potentials. Based on our data, these unexplained features [34, 113] could be due to *cbcBA* activation during exposure to low potential electrodes.

To test this hypothesis, we first grew WT and Δ*cbcL* biofilms on electrodes as electron acceptors at $+0.24$ V *vs.* SHE, then subjected biofilms to voltammetry sweeps to reveal the low potential response below -0.2 V, and confirm the loss of the middle -0.15 V process attributed to CbcL (Figure 2.9A). When *cbcBA* was deleted in the Δ*cbcL* background, the low potential electron transfer event disappeared, and all electron transfer below -0.15 V was eliminated. In the single Δ*cbcBA* mutant, only current below -0.2 V was eliminated, further linking *cbcBA* to activity in this low potential range (Figure 2.9A). By plotting the first derivative of voltammetry data, regions where changes in potential caused the steepest response(s) could be identified. According to these data, deletion of *cbcBA* eliminated an electron transfer process between -0.28 and -0.21 V, with a midpoint potential of -0.24 V *vs.* SHE (Figure 2.9B).

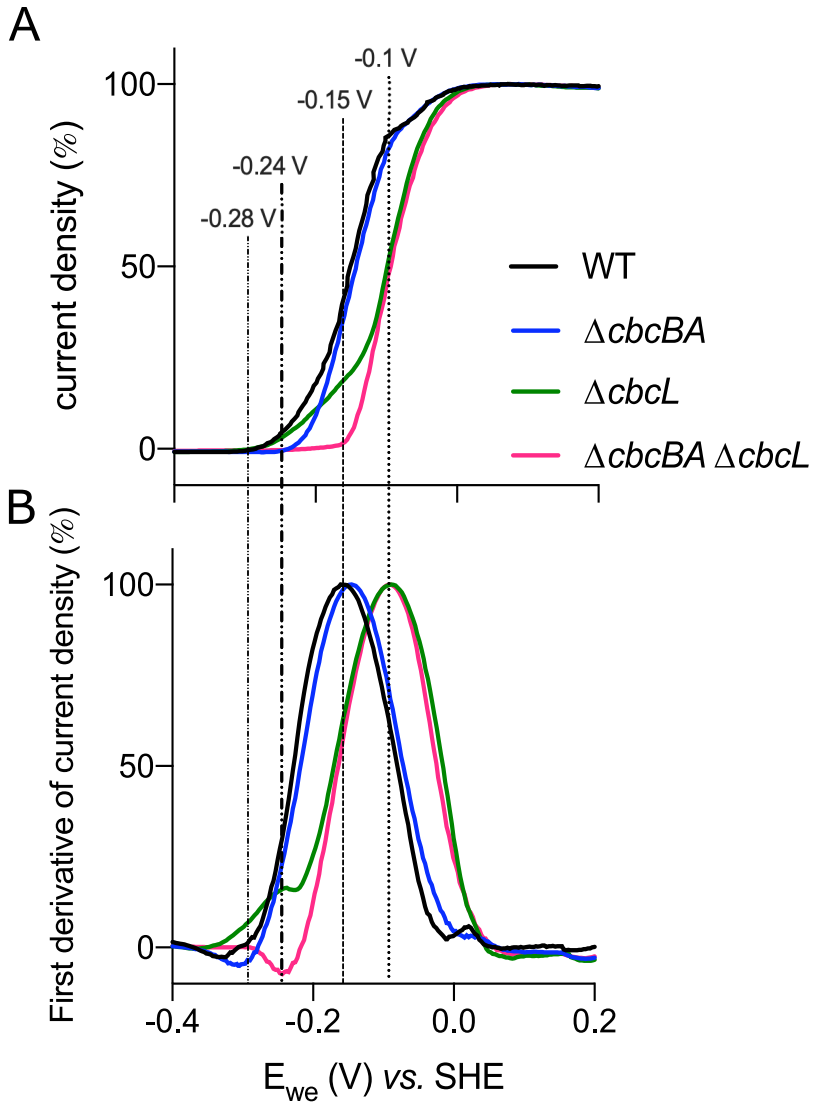

Figure 2.9: **Activation of a CbcBA-dependent electron transfer pathway at redox potentials below −0.21 V *vs.* SHE.** A. *G. sulfurreducens* mutants grown on poised electrodes (+0.24 V *vs.* SHE) to 300–400 μA.cm^{-2} subjected to cyclic voltammetry at 1 mV/s scan rate in the presence of acetate. The Δ*cbcL* mutant still showed a WT-like onset potential at −0.28 V *vs.* SHE, and retained electron transfer at potentials below −0.2 V. The Δ*cbcBA* mutant lost this low potential ability and shifted to a more positive onset potential. B. First derivative of cyclic voltammetry data of mutant strains revealed clear differences in the potential where maximal rate of reduction occurs. The Δ*cbcL* strain lacked the WT response at −0.15 V *vs.* SHE, corresponding to reduction defect of low potential electron acceptors. The Δ*cbcBA* Δ*cbcL* double mutant lacked another low potential response at −0.24 V *vs.* SHE. All experiments were conducted in duplicate, two scans were performed, and data from the reverse second scan was used for analysis.

2.4.8 CbcBA is essential for complete reduction of different Fe(III) (oxyhydr)oxides.

With the evidence that *G. sulfurreducens* not only required *cbcBA* for electron transfer to soluble metals, but also to electrode surfaces, we then asked if *cbcBA* was involved in reduction of insoluble Fe(III) (oxyhydr)oxide particles found in the environment [76]. While common forms such as ferrihydrite, akaganeite, goethite, and hematite all have the same chemical formula (FeOOH), these minerals differ greatly in calculated redox potentials [115]. For example, freshly synthesized hydrous ferric oxide possesses a relatively high estimated redox potential (+0.1 to 0 V) [78, 116], while more crystalline hematite can be as low as −0.2 to −0.3 V [117]. These differences could affect the relative importance of *cbcBA*, especially if a lower-potential form is used.

To compare insoluble Fe(III) minerals, two different forms representing progressively lower redox potential acceptors compared to Fe(III) citrate were synthesized. First, single mutants were incubated with a freshly precipitated hydrous ferric oxide, which has an estimated redox potential of ~0 V *vs.* SHE. Consistent with this acceptor having a potential near where both ImcH and CbcL have both been shown to operate, Δ*imcH* initially reduced Fe(III) slowly until Fe(II) accumulated to 1–2 mM, then accelerated to reduce nearly the same total Fe(III) as reduced by WT cells (Figure 2.10A). In a pattern similar to soluble Fe(III), Δ*cbcL* reduced only 50% of Fe(III), and Δ*cbcBA* reduced 90% of total Fe(III) compared to WT (Figure 2.10A).

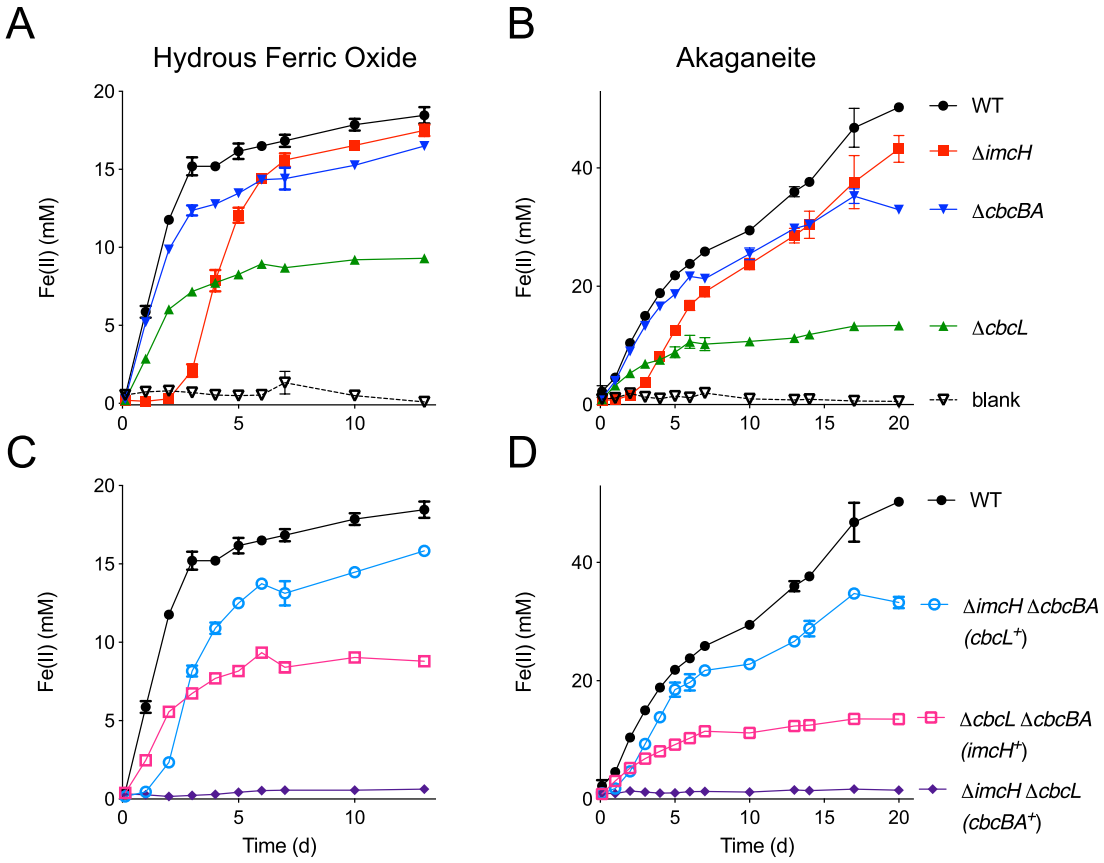

Figure 2.10: **Complete reduction of Fe(III) oxides also requires *cbcBA*, regardless of Fe(III) (oxyhydr)oxide mineral preparation method.** A and C. Reduction of hydrous Fe(III) oxide, which has a formal redox potential lower than Fe(III) citrate, by single and double mutants lacking inner membrane cytochromes (Δ*imcH*, Δ*cbcL*, Δ*cbcBA*, Δ*imcH* Δ*cbcL*, Δ*cbcBA* Δ*cbcL*, and Δ*cbcBA* Δ*imcH*). A lag is observed by the Δ*imcH* mutant, but up to 95% of ferric oxide is eventually reduced. All mutants lacking Δ*cbcL* reduce 50% of Fe(III) oxide, and the Δ*cbcBA* mutant reduced only 90%. B and D. Reduction of akaganeite, which has a lower formal redox potential than hydrous ferric oxide, showed shorter lag for Δ*imcH*, and a larger defect for Δ*cbcL* mutants who could reduce only 26% of the Fe(III). Similarly, a larger defect was observed for the Δ*cbcBA* mutants in akaganeite. All experiments were conducted in triplicate, and the results are reported as mean values ± standard deviation.

The double deletion mutant Δ*imcH* Δ*cbcBA* ($CbcL^+$) displayed the same lag as seen in Δ*imcH* but then also failed to reduce the last 10–15% of Fe(III) as seen for Δ*cbcBA* (Figure 2.10A, 2.10C). The double mutant Δ*cbcL* Δ*cbcBA* ($ImcH^+$) ceased reduction similar to Δ*cbcL*, reducing 50% as much Fe(III) as WT (Figure 2.10C). Fe(III) reduction by double mutants aligned with the abilities of single mutants. Notably, even though concentrations of Fe(II) were much lower in

hydrous ferric oxide incubations than in Fe(III) citrate, each cytochrome was necessary at the same phase of reduction, supporting the hypothesis that phenotypes were linked to the effective redox potential, not absolute Fe(III) or Fe(II) concentrations.

When a lower potential Fe(III) mineral (akaganeite) was used, the lag by Δ*imcH* was shorter (Figure 2.10B), consistent with less Fe(II) needing to accumulate to reduce redox potential and activate CbcL. Mutants lacking *cbcL* initiated growth, but only reduced 26% of Fe(III) compared to WT. Cells lacking *cbcBA* only reduced 65% of WT Fe(III) (Figure 2.10B). The extent of Fe(III) reduction by the double mutant Δ*cbcL* Δ*cbcBA* ($ImcH^+$) was the same as Fe(III) reduction by Δ*cbcL*, and reduction by Δ*imcH* Δ*cbcBA* ($CbcL^+$) was equivalent to reduction by the single mutant Δ*cbcBA* (Figure 2.10D).

These results across different electron acceptors, Fe(III) forms, and Fe(II) concentrations were consistent with ImcH, CbcL, and CbcBA each having a role at a different redox potential. In all cases, ImcH was essential when redox potential was above ~0 V, CbcL was needed for reduction of moderately low potential acceptors (to about −0.2 V), and CbcBA was necessary for reduction closest to the thermodynamic limit. As lower potential electron acceptors such as akaganeite were used, *cbcBA* became more important for complete reduction.

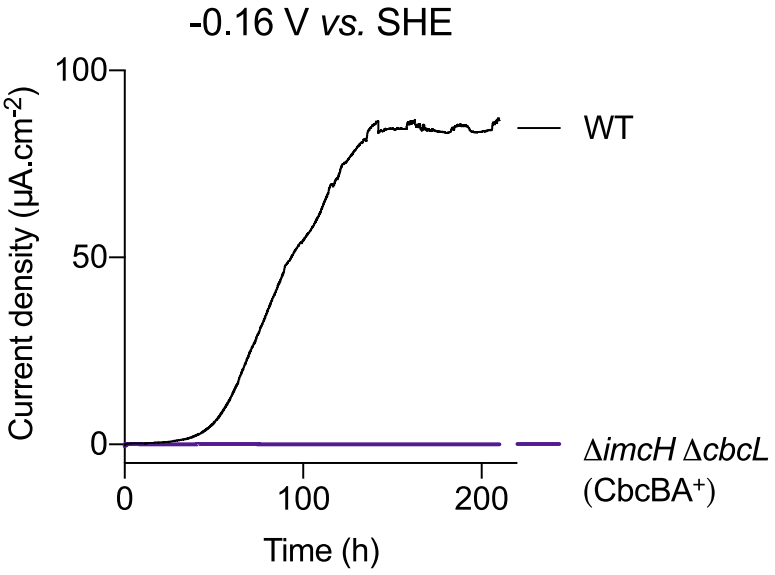

Figure 2.11: **The Δ*imcH* Δ*cbcL* (CbcBA$^+$) strain is unable to support growth on electrodes, even at lower potentials.** When growth of Δ*imcH* Δ*cbcL* (CbcBA$^+$) was tested with electrodes, shown here poised at −0.16 V *vs.* SHE as the terminal electron acceptor and acetate as the electron donor, CbcBA$^+$ cells failed to produce any current as compared to WT. Experiments at −0.2 V also failed to produce current.

While double mutants containing either *imcH* or *cbcL* demonstrated growth under at least one condition, double mutants containing only *cbcBA* failed to reduce any Fe(III) (Figure 2.10C, 2.10D), and the same Δ*imcH* Δ*cbcL* mutant also failed to grow at any potential on electrodes (Figure 2.11). The inability of cells containing only *cbcBA* to grow raised the possibility that CbcBA-dependent electron transfer conserves much less energy than when ImcH or CbcL is involved, possibly to the point where it can not produce enough energy to support growth by *G. sulfurreducens* (Figure 2.12). It also suggested that these are the only three options supporting Fe(III) reduction in this organism.

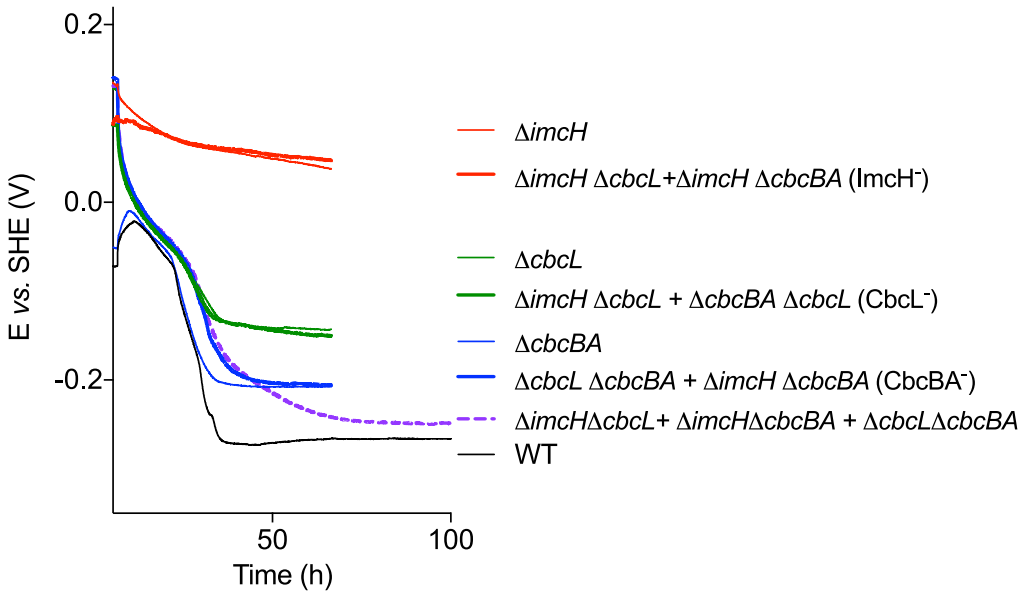

Figure 2.12: **Combinations of mutants can 'work together', and produce the same final redox potential as mutants lacking the dominant inner membrane cytochrome.** When reactors were inoculated with mixtures of double mutants, such as a mixture of cells lacking ImcH (Δ*imcH* Δ*cbcL* + Δ*imcH* Δ*cbcBA*), mixtures still failed to reduce any Fe(III) citrate, just as seen with Δ*imcH*.
When mixtures of cells lacking CbcL (Δ*imcH* Δ*cbcL* + Δ*cbcL* Δ*cbcBA*) were inoculated, as one functional copy of *imcH* was present, together the mixture lowered redox potential to −0.15 V as observed with Δ*cbcL*. A combination of mutants, each lacking CbcBA (Δ*cbcL* Δ*cbcBA* + Δ*imcH* Δ*cbcBA*) together were able to reduce Fe(III) until redox potential reached −0.21 V *vs.* SHE, identical to the Δ*cbcBA* phenotype.
When a mixture of all three double mutants (Δ*imcH* Δ*cbcL* + Δ*imcH* Δ*cbcBA* + Δ*cbcL* Δ*cbcBA*) was inoculated, redox potential went below the −0.21 V *vs.* SHE threshold common to all Δ*cbcBA* mutants, but showed a slower rate of redox potential drop near the end of the incubation. A hypothesis for this behavior is the Δ*imcH* Δ*cbcL* cells which should induce *cbcBA* and finish reduction were unable to generate enough energy to fully produce enough *cbcBA*. Representative curves are shown from experiments (N=2) performed in duplicates.

2.4.9 Inner membrane cytochrome background affects growth yield.

Similar to how oxygen-limited *E. coli* induces separate terminal oxidases with a lower proton pumping stoichiometry, an explanation for different quinone oxidoreductase-like genes in *Geobacter* could be generation of variable amounts of proton motive force in response to environmental conditions [5, 118]. Support for this hypothesis can be found in slower growth rates of electrode-reducing Δ*imcH* cells [33] and higher cell counts per mol Fe(II) in Δ*cbcL* cells

[41]. However, strains in these prior experiments still contained *cbcBA*, which could have been contributing to phenotypes.

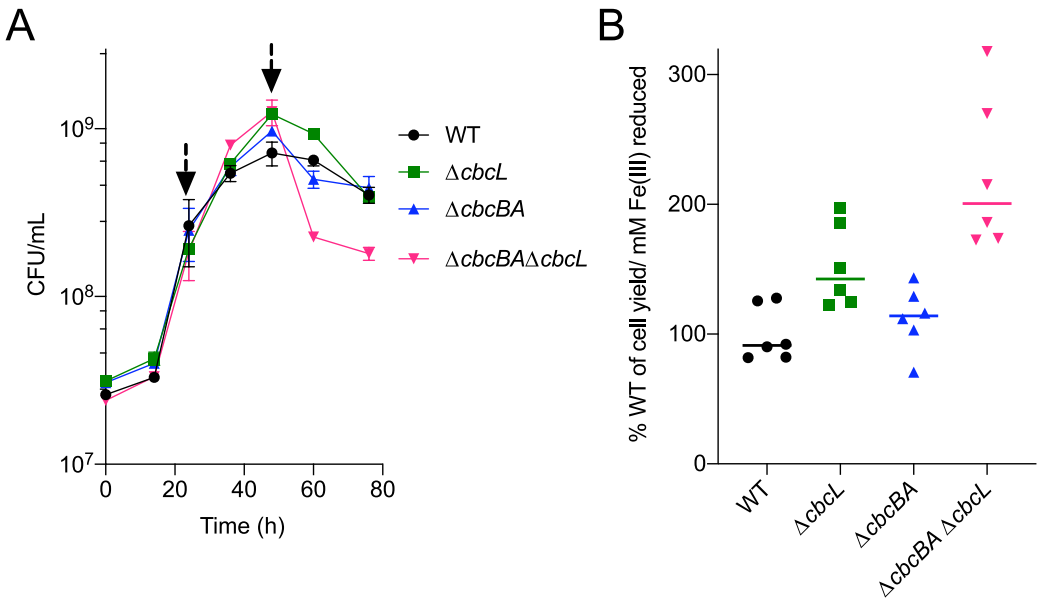

Figure 2.13: **Cell yield (cells per mol Fe(III) reduced) increases in mutants lacking CbcL and CbcBA.** A. Colony forming units (CFU/mL) measured from Fe(III) citrate-grown cultures. All mutants had similar initial growth rates, but mutants lacking *cbcBA* (Δ*cbcBA*, and Δ*cbcBA* Δ*cbcL*) showed a sharp decrease in viability compared to WT or Δ*cbcL*. Arrows represent the time interval used to calculate yield. B. Mutants lacking *cbcL*, *cbcBA*, or both had higher cellular yield per unit Fe(III) reduced. The ImcH-only strain (Δ*cbcBA* Δ*cbcL*) had the highest cellular yield, or 223% compared to WT, suggesting higher H^+/e^- compared cultures where CbcL or CbcBA-dependent electron transfer initiated later in the growth curve. All experiments were conducted in triplicate (N=4), and data shown is represented as mean ± standard error of mean (SEM).

If cells containing ImcH translocate more protons than when a CbcL or CbcBA-dependent pathway is in use, then forcing cells to only use ImcH and not transition to use of the other pathways should increase ATP production and growth yield. In agreement with this prediction, *cbcL* deletion led to higher cell numbers at the end of Fe(III) reduction (Figure 2.13A). Cell counts increased further when both *cbcL* and *cbcBA* were deleted. When accounting for how much Fe(III) was reduced, these differences were even more pronounced (Figure 2.13B). Growth yield of Δ*cbcBA* increased 112 ± 25% compared to WT, yield of Δ*cbcL* increased 152 ± 32%, and

yield of Δ*cbcBA* Δ*cbcL* ($ImcH^+$) more than doubled, to 223 ± 59% (Figure 2.13B). This supported higher net ATP generation by ImcH-utilizing cells compared to those using CbcL or CbcBA.

While *cbcL* and *cbcBA* negatively affected yield, viability data showed that these genes positively affect viability as Fe(III) became limiting. Near the end of Fe(III) reduction, viability of Δ*cbcBA* dropped over 50%, and Δ*cbcL* dropped by 68%. Cells lacking both *cbcL* and *cbcBA* had the worst survival, losing over 85% of cell viability within 24 h. A decrease in proton translocation stoichiometry would not only lower growth yield, but would also allow *G. sulfurreducens* to continue conserving energy as Fe(III) reduction becomes less favorable. Because we have been unable to demonstrate growth with extracellular electron acceptors by *cbcBA*-only strains, and CbcBA is necessary when less than 0.07 V/electron is available (7 kJ/e^-), we hypothesize that CbcBA participates in an electron disposal route that primarily meets maintenance requirements when conditions are near thermodynamic limits.

2.5 Discussion

Long before the isolation of metal-reducing bacteria, higher potential Mn(IV) in sediments was shown to be reduced before lower potential Fe(III) [71]. In this report, we provide a molecular explanation for how a microorganism can choose the most thermodynamically beneficial acceptor amid a collection of minerals that lie beyond the cell membrane. Our data supports a model where redox potential controls which of three different inner membrane cytochromes are used, removing the need to sense the solubility or chemistry of complex extracellular metal oxides in a changing environment.

Data from this study, combined with prior genetic observations [33, 34, 41] are consistent with *G. sulfurreducens* utilizing ImcH to achieve high growth rates and yields when redox potential is above -0.1 V. As redox potential decreases below this level, cells are increasingly dependent on CbcL, which lowers growth rate and yield but continues generating energy. As both of these cytochromes are constitutively expressed, this model predicts that CbcL should have a mechanism which prevents it from functioning at higher potentials. When redox potential approaches -0.2 V *vs.* SHE, induction of *cbcBA* provides a means for cells to respire if CbcL cannot function, and the energy available to the organism approaches zero (Figure 2.8). The fact that *cbcBA* is not expressed until it is needed is consistent with it supporting the lowest growth yields.

Although CbcBA and CbcL both have type I *b*–type diheme quinone oxidoreductase domains, they share no sequence homology, and have a different number of transmembrane helices predicted to coordinate their hemes. CbcB has four transmembrane domains, with 3 conserved

histidines linked to *b* heme coordination, based on alignments with characterized diheme proteins. While CbcA is a separate protein, a fourth histidine for binding a *b*–type heme appears to be located in its C–terminal domain. This pattern, where a *b*–type cytochrome is coordinated by a domain from a periplasmic enzyme is also seen in [NiFe] hydrogenases related to CbcB [65, 66].

CbcL has a different domain structure, with six transmembrane helices. One histidine capable of *b*–heme coordination is found in each of the first three transmembrane domains, but an additional two histidines arranged similar to those in formate dehydrogenase are in the fifth transmembrane domain [119]. The presence of five heme-coordinating residues could enable more than one *b*–heme binding configuration in CbcL, and provide a mechanism for preventing electron transfer until a key redox potential is reached. This hypothesis lacks precedent in other model systems, and illustrates the need to biochemically characterize these putative quinone oxidoreductases.

Another feature of CbcBA is its consistent location in a regulated operon that is amongst one the most conserved cytochrome-encoding regions in *Geobacter*, occurring in 93 out of 96 *Geobacteraceae*, and 119 out of 134 Desulfuromonadales. Unlike *imcH* and *cbcL*, *cbcBA* is expressed only under low potential conditions (Figure 2.7). Our data here help explain studies that detected *cbcBA* expression in cells harvested after Fe(III) oxide reduction, but not higher-potential Mn(IV) oxide reduction [27]. Upregulation of *cbcBA* in electrode-grown biofilms is also consistent with *G. sulfurreducens* biofilms having low-potential regions farther from electrodes [30, 120, 121]. We predict that moderate *cbcBA* expression in electrode biofilms is an average of high expression in upper leaflets of biofilms with low levels in the rest of the biofilm [121, 122]. Considering all of

these studies, the radical change in *cbcBA* expression during growth with the same electron acceptor highlights how redox potential should be considered when cells are harvested for RNA extraction (Figure 2.2).

Such fine-tuning of respiration is not found in all metal reducing organisms. *Shewanella oneidensis* uses one inner membrane quinone dehydrogenase, the tetraheme *c*–type cytochrome CymA [31] for reduction of acceptors that differ in redox potential by over 0.6 V, including fumarate, nitrate, DMSO, Fe(III), and Mn(IV) [32]. This may be explained by the fact that *Shewanella* partially oxidizes organic compounds to derive most of its ATP via substrate-level phosphorylation, using extracellular electron transfer primarily for electron disposal [8]. In contrast, *Geobacter* completely oxidizes substrates and requires chemiosmosis for ATP generation. Having multiple options for coupling electron flow to proton extrusion may allow *Geobacter* to utilize all available electrons and compete under such varied conditions as laboratory enrichments selecting for rapid growth, energy-limited aquifers selecting for persistence, and electrodes that create redox-stratified biofilms [120, 123, 124].

Nearly every important biological respiration can be easily identified by a highly conserved functional gene, such as *mcr* for methanogenesis, *dsr* for sulfate reduction, or *amo* for ammonia oxidation. No such tools enabling molecular detection of metal-reducing bacteria or prediction of extracellular electron transfer in uncultivated organisms exist, due to poor sequence similarity between multiheme cytochromes and poor conservation of cytochrome content between organisms [30, 53, 125, 126]. Unlike most *Geobacter c*–type cytochromes, the sequence of the *b*–type cytochrome CbcB is highly conserved, possibly because its donor (menaquinone)

and acceptor (CbcA) remains more constant. This reduced rate of genetic drift allows CbcBA homologs near BccR–like regulators to be easily identified in other Deltaproteobacteria (such as metal-reducing *Anaeromyxobacteria*) where the *b*–heme protein is typically annotated as 'thiosulfate reductase'–like. Homologous *cbcBA* clusters annotated as hypothetical proteins are present in metal-reducing genera within the *Calditrichaeota* (*Caldithrix*) and *Bacteroidetes* (*Prolixibacter*, *Marinilabilales*, *Labilibaculum*), making *cbcBA* a possible marker for extracellular electron transfer in more distant phyla. Based on the presence of *cbcBA* homologs in genomes from uncultivated organisms within the *Verrucomicrobia*, and a family of *cbcB–cbcA* gene fusions within *Chloroflexi* genomes, undiscovered organisms capable of extracellular respiration still remain buried deep within anoxic sediments and metagenomic bins.

Chapter 3

CbcL, a *bc*–type inner membrane cytochrome functions as a redox gating protein in *Geobacter sulfurreducens*

Komal Joshi, Chi Ho Chan, Caleb E. Levar, Daniel R. Bond

(manuscript in preparation for submission)

3.1 Summary

The *Geobacter sulfurreducens* genome encodes multiple cytoplasmic membrane electron transfer pathways to maximize thermodynamic energy conservation. *G. sulfurreducens* utilizes an ImcH-dependent pathway for respiration of electron acceptors above the redox potential of −0.1 V *vs*. SHE, CbcL-dependent pathway for respiration of electron acceptors between −0.1 to −0.21 V, and CbcBA-dependent pathway for respiration of electron acceptors below −0.21 V, representing a branched electron transfer chain. In this report, we provide evidence that CbcL is regulated by redox potential. Suppressor enrichment analysis in Δ*imcH* identified three point mutations in CbcL allowing the CbcL-dependent pathway to also function above redox potentials of −0.1 V *vs.* SHE. Two mutations replaced valine at 205th residue with alanine or glycine, whereas one mutation replaced phenylalanine at 525th residue with tyrosine. $CbcL^{V205A+}$, $CbcL^{V205G+}$, and $CbcL^{F525Y+}$ strains supported growth on high potential electron acceptors including Fe(III) citrate, Mn(IV) oxides, electrodes poised at 0 V *vs.* SHE. Electrochemical characterization of $CbcL^{+}$ strain showed an oxidative inactivation of CbcL-dependent electron transfer whereas $CbcL^{V205A+}$, $CbcL^{V205G+}$, and $CbcL^{F525Y+}$ strains did not show inactivation at high redox potentials suggesting that the CbcL-dependent electron transfer pathway is gated. Growth yields of these strains measured around 50% of WT, supporting earlier evidence that CbcL-dependent electron transfer pathway conserves less energy as compared to ImcH-dependent pathway (160% of WT).

3.2 Introduction

Electron transfer is the universal currency of biological energy transformation. Living systems display remarkable ability to organize and regulate electron transport chain in a way that maximizes optimal growth and energy conservation. The diversity and variability of respiratory chains allow organisms to thrive under various environments from aerobic to facultative to strict anaerobic conditions, under different temperatures, and light conditions. For example, *Escherichia coli* encodes 15 dehydrogenases, and ten terminal reductases [5], with three oxidases only for respiration of oxygen (cytochrome *bo,* cytochrome *bd–I,* and cytochrome *bd–II*). This redundancy in electron transport chains to respire a single electron acceptor equips *E. coli* with the ability to maximize efficiency of energy conservation under all concentrations of oxygen. A sulfate reducing anaerobic bacterium, *Desulfovibrio vulgaris* also encodes multiple electron transfer components like quinone-interacting membrane-bound oxidoreductase (Qmo) complex, tetraheme cytochrome c_3, CO-induced membrane bound hydrogenase, and dissimilatory bisulfite reductase, enabling electron transfer flexibility under different growth conditions [127].

Similarly, a model organism for studying dissimilatory metal reduction, *Geobacter sulfurreducens,* utilizes three specific inner membrane cytochrome (ImcH-, CbcL-, and CbcBA-) dependent electron transfer pathways based on the redox potential of the electron acceptors [33–35]. ImcH (GSU3259), a seven heme cytochrome *c* containing NapC/NirT domain is essential for respiration of high potential electron acceptors [33], CbcL (GSU0274), a *bc*–type cytochrome containing nine hemes, and a diheme cytochrome *b* with six transmembrane domains is required

for respiration of low potential electron acceptors below −0.1 V *vs.* SHE, whereas CbcBA (GSU0593–0594), another *bc*–type cytochrome complex is required for reduction of electron acceptors below −0.21 V *vs.* SHE to the thermodynamic limit of acetate respiration. Utilization of multiple pathways for electron transfer through inner membrane across different redox potential windows may provide competitive advantage to *G. sulfurreducens* for survival under environmental conditions spanning over half a volt. Likewise in *E. coli,* the three terminal oxidases allows it to respire under all oxygen concentrations. The efficiency of respiration is maintained by regulating the expression of genes required, or by post-translational modification of proteins essential for that specific condition [5, 128]. However, in *G. sulfurreducens,* of the three inner membrane cytochromes, only *cbcBA* is induced by the BccR (GSU0598) transcriptional regulator in a redox dependent process, whereas both *imcH* and *cbcL* are constitutively expressed [30, 34, 35].

Peptides from CbcL (GSU0274) have been detected in proteome analysis of *G. sulfurreducens* under different electron acceptors, and different growth conditions [37, 38]. The inactivity of CbcL-dependent electron transfer pathway at higher available thermodynamic energies (high redox potential) has remained a mystery. CbcL belongs to the family of *bc*–cytochromes, widely distributed across all three domains of life [55, 129]. Cytochrome *bc*–complexes function in electron transfer, for example– complex III in mitochondrial respiration chain, hydrogenases, and formate dehydrogenases [130, 131]. These enzymes' activity is dependent on the concentration of substrate, product, and presence of inhibitor. Some hydrogenases, like [NiFe]–hydrogenase from *Ralstonia eutropha* show reductive activation at −0.558 V *vs.* SHE, and oxidative inactivation above redox potentials of 0 V [132], and [FeFe]–hydrogenases from *Desulfovibrio desulfuricans*

also show inactivation of the enzyme at high redox potentials and rapid activation when the redox potentials are low [132]. [NiFe]–hydrogenases from *D. gigas* also show reduction in enzyme activity as the redox potential is increased from −0.4 to −0.2 V [133]. The reversible activation/inactivation of these enzymes results in quick structural changes allowing them to switch on and off rapidly. Since CbcL-dependent electron transfer also show inactivation at high redox potentials, and share homology to hydrogenases and some formate dehydrogenases, we hypothesize that CbcL activity is activated and inactivated by redox potential.

To identify regulatory strategies governing the utilization of the CbcL-dependent electron transfer pathway, we utilized suppressor enrichment analysis in strains lacking ImcH with high redox potential electron acceptors (Fe(III) citrate, and poised electrodes). Extended incubation times and repeated transfers enriched strains able to reduce these high potential electron acceptors. Through short read sequencing, we identified point mutations in two amino acid residues (V205A, V205G, and F525Y) in CbcL that allow Δ*imcH* to respire at high redox potentials. Point mutations were created in strains lacking ImcH (Δ*imcH,* and Δ*imcH* Δ*cbcBA*) to directly answer if CbcL-dependent electron transfer can function at high redox potentials. Electrochemical analysis showed redox potential dependent activity of $CbcL^{+}$ biofilms. We also provide evidence that use of CbcL supports lower growth yields. Although, the variants in CbcL can support growth on high redox potential complementing the lack of Δ*imcH,* they do not support higher yields like ImcH suggesting the proton to electron ratio remains the same and amino acids at 205 or 525th position only changed the conformation of CbcL allowing it to function at high redox potentials. Redox gating behavior of CbcL suggests *G. sulfurreducens* possesses a regulated respiratory chain across

the inner membrane like complex electron transfer chains found in other microorganisms.

3.3 Materials and Methods

3.3.1 Bacterial strains and culture conditions

All strains used in this study, including Δ*imcH* suppressor strains, are listed in Table 3.1. Every experiment was initiated by streaking strains from −80 ºC frozen culture stocks. All *G. sulfurreducens* strains were cultured in minimal medium (NB) consisting of 0.38 $g.L^{-1}$ KCl, 0.2 $g.L^{-1}$ NH_4Cl, 0.069 $g.L^{-1}$ $NaH_2PO_4.H_2O$, 0.04 $g.L^{-1}$ $CaCl_2.2H_2O$, and 0.2 $g.L^{-1}$ $MgSO_4.7H_2O$, 10 mL of trace mineral mix containing 1.5 g nitrilotriacetic acid (NTA), 0.1 $g.L^{-1}$ $MnCl_2.4H_2O$, 0.5 $g.L^{-1}$ $FeSO_4.7H_2O$, 0.17 $g.L^{-1}$ $CoCl_2.6H_2O$, 0.1 $g.L^{-1}$ $ZnCl_2$, 0.03 $g.L^{-1}$ $CuSO_4.5H_2O$, 0.005 $g.L^{-1}$ $AlK(SO_4)_2.12H_2O$, 0.005$g.L^{-1}$ H_3BO_3, 0.09 $g.L^{-1}$ Na_2MoO_4, 0.05 $g.L^{-1}$ $NiCl_2$, 0.02 $g.L^{-1}$ $NaWO_4.2H_2O$, and 0.10 $g.L^{-1}$ Na_2SeO_4, and buffered with 2 $g.L^{-1}$ $NaHCO_3$ to a final pH of 6.8 purged with N_2:CO_2 (80:20) gas passed over heated copper column to remove trace oxygen. Nitrilotriacetic acid in trace mineral mix was replaced with HCl to a final concentration of 0.1 M HCl when Fe(III) served as the electron acceptor. For growth on solid medium, 15 $g.L^{-1}$ agar was added to minimal medium containing acetate and fumarate. 20 mM acetate served as the carbon source and electron donor, and 40 mM fumarate as the electron acceptor for routine growth in an anaerobic workstation maintained at 30 ºC under N_2:CO_2:H_2 (75:20:5) atmosphere. *Escherichia coli* strains were grown aerobically in lysogeny broth (LB) at 37 ºC. 200 $\mu g.mL^{-1}$ kanamycin was supplemented to *G. sulfurreducens* growth medium, 50 $\mu g.mL^{-1}$ kanamycin was supplemented to *E. coli* growth medium as necessary. For *G. sulfurreducens*, sucrose to a final concentration of 10%

was added to NB fumarate acetate (NBFA) medium during mutant construction counter-selection step. 55 mM Fe(III) citrate, ~30 mM amorphous Fe(III) oxide, and ~30 mM Mn(IV) oxide was used as electron acceptor with 20 mM acetate serving as electron donor for growth with acceptors other than fumarate.

Strains or Plasmids	**Description or relevant genotype**	**Reference or source**
***Geobacter sulfurreducens* strains**		
	Wildtype *G. sulfurreducens* MN-1	Lab culture collection
DB789	Δ*imcH*	[89]
	Δ*imcH::kan*^{R}	[33]
5A5	Δ*imcH::kan*^{R} CbcL(V205G) ΔGSU2737 ΔGSU0279, Fe(III) citrate suppressor strain	[134]
5B2	Δ*imcH* CbcL(V205A) GSU0758(R133W), Fe(III) citrate suppressor strain	[134]
Electrode C	Δ*imcH::kan*^{R} CbcL(F525Y), electrode suppressor strain	[134]
DB1718	Δ*imcH* Δ*cbcBA*	[35]
DB1088	Δ*imcH* CbcL(V205A)	This study
DB1089	Δ*imcH* CbcL(V205G)	This study
DB1090	Δ*cbcBA* CbcL(F525Y)	This study
DB1752	Δ*cbcBA* Δ*imcH* CbcL(V205A)	This study
DB1753	Δ*cbcBA* Δ*imcH* CbcL(V205G)	This study
DB1748	Δ*cbcBA* Δ*imcH* CbcL(F525Y)	This study
***E. coli* strains**		
UQ950	Cloning strain of *E. coli*	
S17-1	Conjugation donor strain	

DB1053	UQ950 pk18cbcLV205A	This study
DB1054	UQ950 pk18cbcLV205G	This study
DB1055	UQ950 pk18cbcLF525Y	This study
DB1065	S17-1 pk18cbcLV205A	This study
DB1066	S17-1 pk18cbcLV205G	This study
DB1067	S17-1 pk18cbcLF525Y	This study
Plasmids		
pk18mobsacB		[89]
pDGSU0593-94	Flanking regions of GSU0593-GSU0594 in pk18mobsacB	[35]
pk18cbcLV205A	~750 bp flanking regions to GSU0274(T614C) in pk18mobsacB	This study
pk18cbcLV205G	~750 bp flanking regions of GSU0593-GSU0594 in pk18mobsacB	This study
pk18cbcLF525Y	Flanking regions of GSU0593-GSU0594 in pk18mobsacB	This study

Table 3.1: List of strains and plasmids used in this study

3.3.2 Mutant construction

Scarless genome modification constructs were designed based on strategy as previously described [89]. Briefly, ~750 bp flanking *cbcL* (GSU0274) point mutation regions (T614C encoding V205A, T614G encoding V205G, and T1574A encoding F525Y) were amplified using primers listed in Table 3.2. DNA fragments were amplified from genomic DNA extracted from Δ*imcH* suppressor strains 5B2, 5A5, and electrode C respectively. Amplified DNA fragment was digested with XbaI and HindIII, and ligated into the same restriction sites in pk18mobsacB. The ligation

product was transformed into UQ950 chemically competent cells. The resulting plasmids were sequence verified before transformation into S17–1 conjugation donor cells. Overnight grown S17-1 donor strain containing the plasmid was conjugated with *G. sulfurreducens* acceptor strain inside an anaerobic chamber on a sterile filter paper placed on an NBFA agar plate. After ~4 h, cells were scraped from filters, and streaked on NBFA agar plates containing kanamycin. After positive integrants were identified by sequencing, *sacB* counter selection was performed by growing positive integrants on NB fumarate acetate + 10% sucrose plates. Colonies from sucrose plates were patched on NBFA and NBFA + kanamycin plates to select for antibiotic sensitive, markerless point mutation strains. The mutants were verified by PCR, and Sanger sequencing, and final strains were re-sequenced for off-site mutations via Illumina short read sequencing.

Deletion	**Sequence (5'-3')**	**Restriction enzyme**
GSU0274_CbcLV205_F	GACTTCTAGA TGGCTGTCAATAATGCGCCCTGA	XbaI
GSU0274_CbcLV205_R	GACTACAAGCTT GGAACAGGAACCAGCGGACCAT	HindIII
GSU0274_CbcLF525_F	GACTTCTAGA CCAAGTTCTACTCCCACGGTGAGC	XbaI
GSU0274_CbcLF525_R	GACTACAAGCTT GCGACGGCATAAGGCTAAACGCA	HindIII
Confirmation of gene deletion		
GSU0274_V205	TGCAACGACTGCCACAACCTG	
GSU0274_F525	GTATGTTTGCCATCGGCGGCT	

Table 3.2: Primers used in this study.

3.3.3 Suppressor enrichment on Fe(III) citrate and poised electrode

For enrichments on Fe(III) citrate, late exponential phase NBFA grown Δ*imcH* or Δ*imcH::kan*^{R}cultures were inoculated at 1:10 v/v to NB medium containing 55 mM Fe(III) citrate as the sole electron acceptor and 20 mM acetate as the carbon and electron donor. High initial inoculum was used to increase the chances of permissive mutations leading to the enrichment of suppressors. After complete reduction of Fe(III) citrate containing medium, cultures were transferred to fresh Fe(III) citrate containing medium up to five transfers. After the fifth transfer, cultures were streaked for isolation on NB acetate fumarate agar plates. Isolated colonies were picked into 96-well plates with wells containing NBFA medium. Fully grown cultures were transferred by stamping into Fe(III) citrate containing medium. Isolates that cleared Fe(III) citrate medium significantly faster than than of the parent mutant were chosen for further studies [134].

For electrochemical enrichment, three electrode bioreactors were assembled containing 3 cm^2 1500 grit polished graphite working electrode, platinum wire as counter electrode, and saturated calomel electrode as reference electrode [134]. 40 mM acetate served as the electron donor, and 50 mM NaCl was added to maintain osmolarity when fumarate was omitted, and working electrode poised at +0.24 V *vs.* SHE served as the sole electron acceptor. Late exponential phase cells ($OD_{600} \simeq 0.5$) grown in NBFA medium were used to inoculate bioreactors with 50% v/v inoculum size. After current densities of over 50 $\mu A.cm^{-2}$ were achieved, bioreactors were taken into an anaerobic chamber, and electrodes were harvested, rinsed once with NBFA medium to remove loosely attached cells, and placed in 10 mL of NBFA medium, then vortexed vigorously

to remove attached cells, and were allowed to grow until an $OD_{600} \simeq 0.5$ was reached. The electrode enrichment was repeated a total of three times, after which cells from the final electrode were streaked on NBFA agar medium for isolation in anaerobic chamber at 30 ºC maintained under N_2:CO_2:H_2 (75:20:5) atmosphere. Five individual colonies were inoculated into NBFA medium. Bioreactors with working electrode poised at +0.24 V *vs.* SHE were inoculated with these cultures after reaching an $OD_{600} \simeq 0.5$. Current production was monitored, and strains producing current densities comparable to WT *G. sulfurreducens* were selected for further studies [134].

Mutations in selected isolates were identified by sequencing genomic DNA using 50bp single read or 250bp paired end reads using the Illumina platform (University of Minnesota Genomics Center). Reads were aligned using breseq (version 0.24rc6) [135] with *G. sulfurreducens* MN1 as the reference [89].

3.3.4 Fe(III) citrate reduction by redox potential measurement

Three electrode bioreactors were assembled with two 1 cm long platinum wire electrodes as working and counter electrodes, and Ag/AgCl electrode (+0.21 V *vs.* SHE) served as a reference electrode. The bioreactors containing 10 mL of Fe(III) citrate containing medium with 20 mM acetate and 55 mM Fe(III) citrate were continuously flushed with humidified N_2:CO_2 (80:20) gas mix to maintain anaerobic conditions. Redox potential was monitored continuously as Fe(III) citrate was reduced using open circuit potential (OCP) method using a 16-channel potentiostat (VMP3, Biologic). Bioreactors were inoculated from NBFA grown cultures when OD_{600} reached ~0.5 to 1:100 v/v ratio. Before every experiment, platinum electrodes were cleaned

electrochemically following the protocol as previously described [35]. 0.1 mL of samples were taken at regular intervals for Fe(II) concentration measurement using modified ferrozine assay [96].

3.3.5 Electrochemical analysis

Three electrode bioreactors were assembled using method as described previously [94,95]. Briefly, 3 cm^2 1500-grit polished polycrystalline graphite served as the working electrode. 2 cm long platinum wire and Ag/AgCl (+0.21 V *vs.* SHE) served as the counter and reference electrode respectively. To maintain anaerobic conditions, reactors were constantly flushed with humidified N_2:CO_2 (80:20) gas passed over a heated copper column to remove trace amounts of oxygen. Working electrode was poised at 0 V *vs.* SHE using a VMP3 multichannel potentiostat (Biologic), and a 25% v/v inoculum of fumarate acetate grown cultures with $OD_{600} \simeq 0.5$ was used to initiate the experiments. 40 mM acetate served as the carbon source and electron donor, and poised electrodes served as the sole electron acceptor. Current production was recorded averaged every 120 sec using EC–Lab (Biologic) software.

3.3.6 Fe(III) oxide reduction

Hydrous ferric oxide, a poorly crystalline form of Fe(III) oxide was synthesized as schwertmannite ($Fe_8O_8(OH)_6(SO_4).nH_2O$) using a rapid precipitation method [136] by adding 5.5 mL of 30% hydrogen peroxide to a 10 $g.L^{-1}$ solution of $FeSO_4$. Addition of hydrogen peroxide results in precipitation of red-orange schwertmannite mineral. After overnight stabilization of mineral by continuous stirring, schwertmannite solids were washed with DI H_2O thrice by

centrifugation to remove any unreacted $FeSO_4$. The washed solids were added to basal medium containing 20 mM acetate supplemented with 0.69 g.L^{-1} $NaH_2PO_4.H_2O$ to prevent crystallization of iron mineral while autoclaving [77]. Schwertmannite mineral is stable in acidic pH but transforms into ferrihydrite mineral with an amorphous XRD–signature at neutral pH [77, 136]. Autoclaving the mineral also changes the properties of the mineral, and has a relatively low redox potential as compared to fresh non-autoclaved mineral [41, 77, 116]. For iron reduction assays, both autoclaved and non-autoclaved forms of hydrous ferric oxide minerals were used. Iron oxide medium was purged with N_2:CO_2 (80:20) gas and buffered with $NaHCO_3$ to maintain pH at 6.8. Medium containing iron oxide was inoculated with cultures grown in acetate fumarate medium when OD_{600} $\simeq$ 0.5 at 1:100 v/v. 0.1 mL samples were taken at regular intervals, dissolved in 0.9 mL 0.5 N HCl, and stored in the dark to prevent photo-oxidation of Fe(II). Fe(II) concentrations were measured using a modified Ferrozine assay [96].

3.3.7 Mn(IV) oxide reduction

Mn(IV) oxide was synthesized by mixing 20 mM $KMnO_4$ and 3.2 g.L^{-1} NaOH. To it, a 1000 mL solution of 30 mM $MnCl_2.4H_2O$ was added [137]. The mix was continuously stirred at room temperature for at least two hours, and then moved to 4 ºC with continuous stirring overnight. The continuous stirring, and long incubation helped with mineral formation. The $MnCl_2$ and NaOH served to stabilize the pH. The resulting amorphous mineral was washed with DI H_2O thrice by centrifugation to remove any unreacted $KMnO_4$. The Mn(IV) oxide yield was measured by drying out the mineral, and measuring weight. The yield of Mn(IV) oxide mineral used in the experiments

was calculated to be ~0.5 M. The MnO_2 was diluted to a final concentration of ~0.3 Mn(IV) oxide in basal medium lacking carbon source. This diluted Mn(IV) oxide containing medium was purged with argon gas passed over a heated copper column to make Mn(IV) oxide medium anaerobic. To bring the final concentration of Mn(IV) oxide to ~30 mM,1 mL of Mn(IV) oxide stock solution was added to autoclaved 9 mL *Geobacter* basal growth medium lacking electron acceptor supplemented with 10 mM acetate as carbon source and electron donor. 1 mL of Mn(IV) oxide was added to the tubes immediately before inoculation. Fumarate acetate grown cultures at $OD_{600} \simeq 0.5$ were inoculated at 1:100 v/v, and 0.1 mL samples were taken at regular intervals and dissolved in 0.9 mL of freshly prepared 2N HCl with 4 mM $FeSO_4$ for Mn(IV) reduction measurements. The samples were stored in dark before measurement via a modified Ferrozine assay [96]. As the reduction of Mn(IV) by Fe(II) is thermodynamically favorable, the measured Fe(II) concentration can be used to calculate the Mn(II) present in a given sample. Mn(II) concentrations were measured indirectly by measuring Fe(II) concentration by ferrozine assay.

3.3.8 Flow cytometry analysis and yield calculation

Double filtered medium containing 55 mM Fe(III) citrate and 20 mM acetate was used to count total cells using flow cytometry. Filtered acetate fumarate medium grown cultures ($OD_{600} \simeq 0.5$) at 1:100 v/v were used to inoculate Fe(III) citrate containing medium. All the glass wares used in this experiment were rinsed thrice with 0.45 μm filtered DI H_2O. Samples were taken at regular intervals for cell counting, and for Fe(III) reduction measurement via ferrozine assay. Cell counting measurements were conducted using a FACSCalibur flow cytometer (BD Biosciences) equipped

with 488 nm and 640 nm lasers through a 530/30 filter. Photodiode setting on E00 with Amp Gain of 1 was applied to forward scatter detector, photomultiplier tube (PMT) setting at 415 was applied to collect side scatter data. A threshold value of 90 was set for all measurements. All dilutions were made in filtered NB non-growth medium lacking any carbon sources. Sample flow rate used was 35 $\pm$5 $\mu L.min^{-1}$(medium flow), and samples were taken in 51 s passes. All events were recorded. Population counting was performed using FlowJo software (BD Biosciences). Fe(III) reduction was measured using ferrozine assay, and yield was calculated as total increase in cell counts per mM Fe(III) reduced.

3.4 Results

3.4.1 Enrichment of suppressor strains in Δ*imcH* revealed point mutations in *cbcL*

Strains lacking inner membrane multiheme cytochrome ImcH fail to respire high potential electron acceptors such as Fe(III) citrate, Mn(IV) oxide, and electrodes poised at high redox potentials above +0.1 V *vs.* SHE [33]. Two other inner membrane cytochromes, CbcL and CbcBA, are required for respiration of electron acceptors below −0.1 V and −0.21 V, respectively [34, 35]. Of these two cytochromes involved in electron transfer across the inner membrane, *cbcBA* is regulated at the transcriptional level, and expressed only under low redox potential conditions [35], whereas *cbcL* is constitutively expressed [30, 34]. At higher redox potentials, CbcL is not functional even when the conditions are thermodynamically favorable. One possible hypothesis could be the post-translational regulation of CbcL, or other protein-protein interactions.

Suppressor analysis was used to isolate, and identify candidates with alternative high potential electron transfer pathways from the inner membrane through enrichment of suppressors under high redox potential growth conditions. When Δ*imcH* strains were inoculated in Fe(III) citrate containing medium, high initial inoculum and extended incubation times yielded some replicates that fully reduced Fe(III) citrate. Fully reduced cultures were selected for enrichment, and were subjected to five successive transfers. After the fifth transfer, cultures were streaked onto fumarate acetate medium agar plates for isolation. Two candidate Δ*imcH* suppressor strains, 5B2 and 5A5, reduced Fe(III) citrate significantly faster than the parent Δ*imcH* strain (Figure 3.1A).

Poised electrodes (+0.24 V *vs.* SHE) were used as another high potential terminal

electron acceptor for enrichment of additional candidate Δ*imcH* suppressor strains. Bioreactors were inoculated with Δ*imcH* strains for selection of suppressor mutations resulting in growth on electrodes poised at high redox potential. After the current densities reached 50 $\mu A.cm^{-2}$, electrodes were harvested for outgrowth on fumarate until $OD_{600} \simeq 0.5$ before inoculating another reactor. The process was repeated for three transfers resulting in isolation of a suppressor strain "C". Selected strain "C" respired electrodes at a significantly faster rate compared to its parent Δ*imcH* strain (Figure 3.1B).

Whole genome re-sequencing using Illumina platform of the candidate strains identified mutations that possibly resulted in gain of function in *G. sulfurreducens* under high redox potential growth conditions. Mapping reads to the lab *G. sulfurreducens* MN1 strain using breseq analysis pipeline [135] revealed all the possible mutations in each of the candidate strains. Predicted mutations with low coverage, low read quality, and low frequency (<60%) were not selected as these could be false positives. Interestingly, three candidates, 5B2, 5A5, and electrode C strain all had unique, non-synonymous single nucleotide polymorphisms in GSU0274 (*cbcL*) (Figure 3.3C). In strains isolated from Fe(III) citrate enrichments, valine residue at 205th position in CbcL was mutated into alanine or glycine, whereas strain "C" from electrode enrichments had a tyrosine residue at 525th position instead of phenylalanine in CbcL.

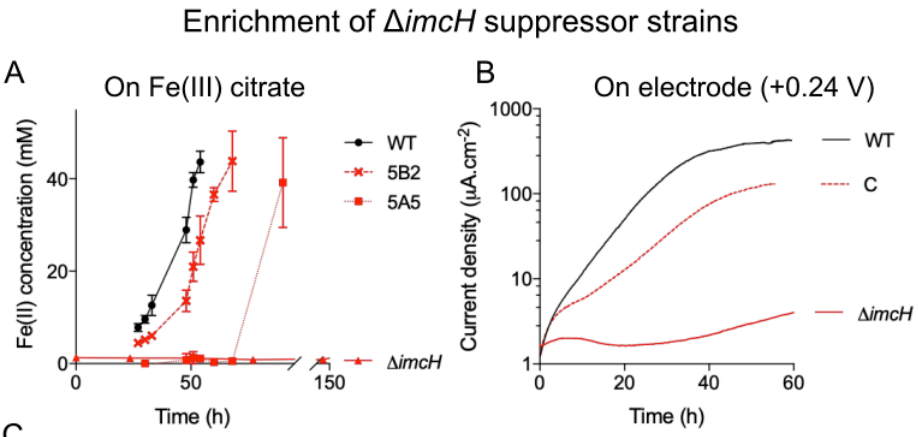

C

Predicted mutations

5A5 strain (parent strain- Δ*imcH*::*kan*^{R})

position	mutation	annotation	gene	description
283,490	T→G	V205G (GTC→GGC)	*GSU0274* →	cytochrome c/cytochrome b
1,017,852	A→G	intergenic (+226/-110)	*GSU0943* → / → *metC-1*	PilZ domain-containing protein/cystathionine gamma-synthase/beta-lyase
2,772,907	+G	coding (1076/1263 nt)	*GSU2508* →	hypothetical protein

5B2 strain (parent strain- Δ*imcH*)

position	mutation	annotation	gene	description
283,490	T→C	V205A (GTC→GCC)	*GSU0274* →	cytochrome c/cytochrome b
810,820	C→T	R133W (CGG→TGG)	*GSU0758* →	hypothetical protein
2,772,907	+G	coding (1076/1263 nt)	*GSU2508* →	hypothetical protein
2,833,482	+C	coding (395/768 nt)	*GSU2565* →	sensor histidine kinase

Electrode "C" strain (parent strain- Δ*imcH*::*kan*^{R})

position	mutation	annotation	gene	description
284,450	T→A	F525Y (TTC→TAC)	*GSU0274* →	cytochrome c/cytochrome b
1,105,291	Δ50 bp	intergenic (+17/+12)	*pbuG* → / ← *GSU1021*	hypoxanthine/guanine transport membrane protein/hypothetical protein
2,772,907	+G	coding (1076/1263 nt)	*GSU2508* →	hypothetical protein
2,774,429	T→G	C38G (TGC→GGC)	*GSU2510* →	SAM-dependent methyltransferase
2,774,454	A→C	H46P (CAC→CCC)	*GSU2510* →	SAM-dependent methyltransferase

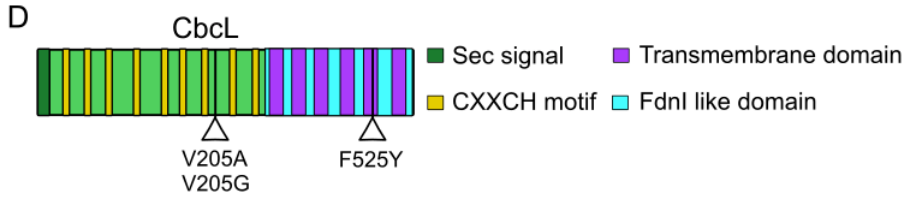

Figure 3.1: **Enrichment analysis of Δ*imcH* yielded suppressor strains with point mutations in *cbcL*.** A. Selected Δ*imcH* suppressor strains 5B2, and 5A5 enriched on Fe(III) citrate medium after five transfers can reduce Fe(III) citrate to WT levels. Fe(III) reduction is measured by taking samples over time for measurement by ferrozine assay. B. High potential electrode enrichment strain "C" selected for further analysis after three successive electrode enrichment rounds, can respire electrodes at a significantly faster rates as compared to the parent Δ*imcH* strain. C. Mapping of short-read sequencing data to the reference *G. sulfurreducens* MN1 sequence using breseq analysis pipeline outputs predicted mutations in the suppressor strains. D. Mapping point mutations to the predicted features of CbcL show one mutation at 205th residue between seventh and eighth CXXCH heme binding domain and other mutation in 525th residue, predicted to be towards the cytoplasmic side of the fifth transmembrane domain of *b*–heme.

ConSurf domain prediction software [62, 138] predicted CbcL V205 to be a non-conserved buried residue between seventh and eighth heme binding domains of *c*–type

cytochrome, and F525 to be a conserved buried residue part of the structural backbone present in the fifth transmembrane domain of *b*–type cytochrome. Changing V to A or G predicts exposure of the 205th residue, whereas changing phenylalanine to tyrosine predicts 525th residue to still be buried in the membrane with prediction of conformational changes. These results suggest that conformational changes in CbcL may have implications in activating CbcL to function at high redox potentials, or these changes may alter the ability of CbcL to interact with other inner membrane or periplasmic electron transfer proteins.

3.4.2 Single amino acid residue change in CbcL confers gain of function in Δ*imcH* to reduce Fe(III) citrate

To test if the point mutations in *cbcL* induced Fe(III) citrate reduction in mutants lacking *imcH*, single nucleotide genomic mutations in *cbcL* were created [89]. Bioreactors containing NB medium with 55 mM Fe(III) citrate and 20 mM acetate were inoculated with *cbcL* point mutant strains lacking *imcH,* and measured for change in reduction potential over time as Fe(III) gets reduced. The Δ*imcH* failed to respire Fe(III) citrate, and did not lower redox potential whereas the WT strain reduced all the available Fe(III) and stabilized at −0.27 V *vs.* SHE as reported earlier (Figure 3.2). Point mutations identified in suppressor strains enriched on Fe(III) citrate (V205A, and V205G) when re-created in Δ*imcH* background reduced Fe(III) citrate to WT levels (−0.27 V *vs.* SHE) with Fe(III) reduction rates comparable to WT (Figure 3.2A). These results support the hypothesis that point mutations in *cbcL* detected in suppressor strains isolated from Fe(III) citrate enrichments restored the ability of Δ*imcH* mutants to reduce Fe(III) citrate. Surprisingly, when

the point mutation identified from electrode enrichments (F525Y) was introduced in Δ*imcH* and inoculated into high potential Fe(III) citrate, a long lag phase of ~80 h occurred before initiation of Fe(III) citrate reduction with eventual reduction of Fe(III) citrate to WT levels (−0.27 V *vs.* SHE) (Figure 3.2A). Point mutations in two separate residues in CbcL showed different phenotypes with the soluble high potential electron acceptor Fe(III) citrate.

One question arising from the CbcL gain of function mutation was if these mutations can also complement lack of CbcBA's electron transfer ability from the inner membrane. CbcBA is another *bc*–type inner membrane cytochrome complex required for reduction of electron acceptors below −0.21 V *vs.* SHE [35]. Re-creating CbcL point mutations in Δ*imcH* Δ*cbcBA* background, and inoculating into Fe(III) citrate containing medium showed that strains with point mutations in CbcL (V205A, V205G, and F525Y) still reduced Fe(III) citrate but failed to lower redox potential below −0.21 V where CbcBA is required, suggesting that these point mutations confer gain of function for high redox potential-dependent electron transfer pathway but not CbcBA-dependent electron transfer pathway (Figure 3.2B).

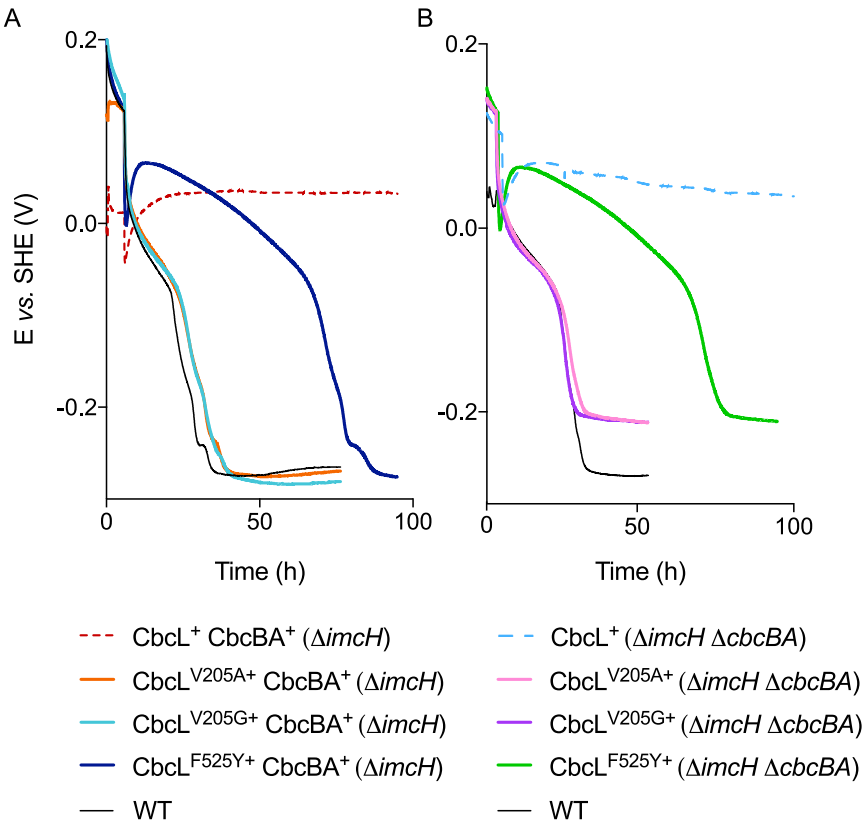

Figure 3.2: **Point mutations in *cbcL* identified from suppressor analysis when re-created in mutants lacking *imcH* allowed Fe(III) citrate reduction.** A. Mutants lacking *imcH* with single nucleotide substitution mutation in *cbcL* ($CbcL^{V205A+}$, $CbcL^{V205G+}$, and $CbcL^{F525Y+}$) can reduce Fe(III) citrate to WT levels whereas Δ*imcH* with wildtype copy of *cbcL* failed to reduce Fe(III) citrate. Point mutation, F525Y in CbcL had a long lag before lowering the redox potential to WT levels. B. Mutants lacking two inner membrane cytochromes *imcH,* and *cbcBA* with point mutations in CbcL still reduced Fe(III) citrate but failed to lower redox potential below −0.21 V *vs.* SHE, the redox potential below which CbcBA is required. This suggests that point mutations in *cbcL* confers the ability for high potential respiration, and that CbcBA is still required for full reduction of Fe(III) citrate. $CbcL^{F525Y+}$ mutant again showed a long lag before initiating reduction and ceased reduction at −0.21 V *vs.* SHE. All experiments were performed in triplicates, and representative data for each strain is shown here.

3.4.3 All CbcL point mutants lacking ImcH can reduce Mn(IV) oxide

From the inner membrane perspective, both Fe(III) citrate and Mn(IV) oxides represent high potential acceptors, and therefore if point mutants in *cbcL* can function at high redox potentials, the phenotypes on Mn(IV) oxide should be similar to the observed phenotypes on Fe(III) citrate.

To test if the different CbcL point mutations in strains lacking *imcH* show similar phenotypes on other high potential electron acceptors, these strains were inoculated in medium containing ~30 mM freshly precipitated Mn(IV) oxide and 10 mM acetate. Synthesis of Mn(IV) oxide results in an amorphous mineral with reported redox potentials >+0.4 V *vs.* SHE [75]. The Δ*imcH* and Δ*imcH* Δ*cbcBA* mutants failed to reduce any Mn(IV) oxide as has been reported earlier (Figure 3.3A, 3.3B). Point mutations in *cbcL* restored the Mn(IV) oxide reduction to WT levels in both Δ*imcH*, and Δ*imcH* Δ*cbcBA* backgrounds (Figure 3.3A, 3.3B). Reduction of Mn(IV) could also be visualized over time as the medium clears when insoluble Mn(IV) gets reduced to soluble Mn(II) (Figure 3.3). Initiation of Mn(IV) reduction occurred without any delay in $CbcL^{F525Y+}$ mutants unlike ~80 h lag in Fe(III) citrate reduction suggesting that these point mutations could be substrate specific in addition to redox potential specificity.

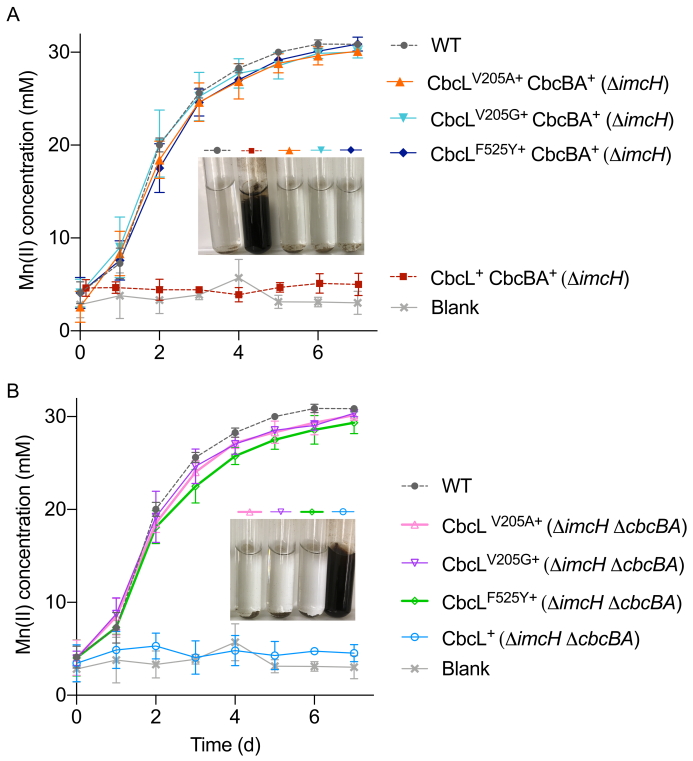

Figure 3.3: **Mn(IV) oxide reduction by Δ*imcH* with point mutations in *cbcL*.** A. Mutants lacking *imcH*, and containing point mutations in *cbcL* (V205A, V205G, and F525Y) fully reduced Mn(IV) oxide at rates similar to WT. Samples were taken twice a day for upto six days. Mn(IV) reduction was calculated by indirectly measuring Fe(II) concentration via ferrozine assay. Inset image shows end point reduction by WT, Δ*imcH*, CbcL^{V205A+} Δ*imcH,* CbcL^{V205G+} Δ*imcH,* and CbcL^{F525Y+} Δ*imcH* cultures shown from left to right respectively. B. Double mutants lacking *imcH* and *cbcBA* with point mutations in *cbcL* could still reduce all available Mn(IV) oxide like WT. Inset image shows end point reduction of Mn(IV) oxide as observed by clearing of the medium. Data represented here is the mean and standard deviation of four replicates (n=4).

3.4.4 CbcL point mutants lacking ImcH do not show lag during Fe(III) oxide reduction, a relatively low potential electron acceptor

Ferric (Fe(III)) oxides represent environmentally relevant electron acceptors for *G. sulfurreducens*. The effective redox potential of Fe(III) oxides varies depending on the particle size, surface area, crystallinity, pH, or Fe(II)/Fe(III) ratio. Hydrous ferric oxides like schwertmannite, ferrihydrite are Fe(III) oxides with high surface area and are predicted to have redox potentials from

+0.1 V to −0.1 V *vs.* SHE. Schwertmannite was synthesized, which transformed into a different mineral form on addition to the medium (pH 6.8). Aging caused by autoclaving can increase the particle size thereby lowering the redox potential of the mineral as compared to the fresh form. Strains lacking *imcH* show a lag when inoculated in medium containing Fe(III) oxides. The length of lag is proportional to the effective redox potential of the Fe(III) oxide mineral, for example– Δ*imcH* had a lag of three days on akaganeite (autoclaved) whereas on freshly synthesized akaganeite mineral, a lag of six days was observed in Δ*imcH* strains [41]. The results suggested that a single mineral form can have different redox potentials, and therefore result in different phenotypes.

To test if mutants containing CbcL variants can still reduce Fe(III) oxides in a redox potential dependent manner, mutants lacking Δ*imcH* and both Δ*imcH* Δ*cbcBA* containing single point mutants in *cbcL* (V205A, V205G, F525Y) were inoculated in medium containing autoclaved and fresh hydrous ferric oxide mineral and 20 mM acetate as electron donor. As expected, Δ*imcH* Δ*cbcBA* had a lag of three days on aged, autoclaved hydrous ferric oxide mineral, and a longer lag of five days on fresh mineral whereas none of the double mutants containing CbcL variants lagged in growth (Figure 3.4A, 3.4C). The strains containing CbcL variants (V205A, V205G, F525Y) initiated Fe(III) oxide reduction like WT suggesting point mutations in CbcL led to gain of function allowing Δ*imcH* strains to reduce Fe(III) oxides at high redox potentials (Figure 3.4A, 3.4C). However, all the double mutant strains (Δ*imcH* Δ*cbcBA*) failed to reduce Fe(III) oxide beyond ~83% reduction as compared to WT corroborating earlier reported results that CbcBA is required for complete reduction of Fe(III) oxides. Single Δ*imcH* strains containing CbcBA, and three variants of CbcL when inoculated in medium containing autoclaved, and fresh hydrous Fe(III) oxide as the electron

acceptor, all the strains had WT like reduction rates, and reduced all available Fe(III) oxide like WT (Figure 3.4B, 3.4D).

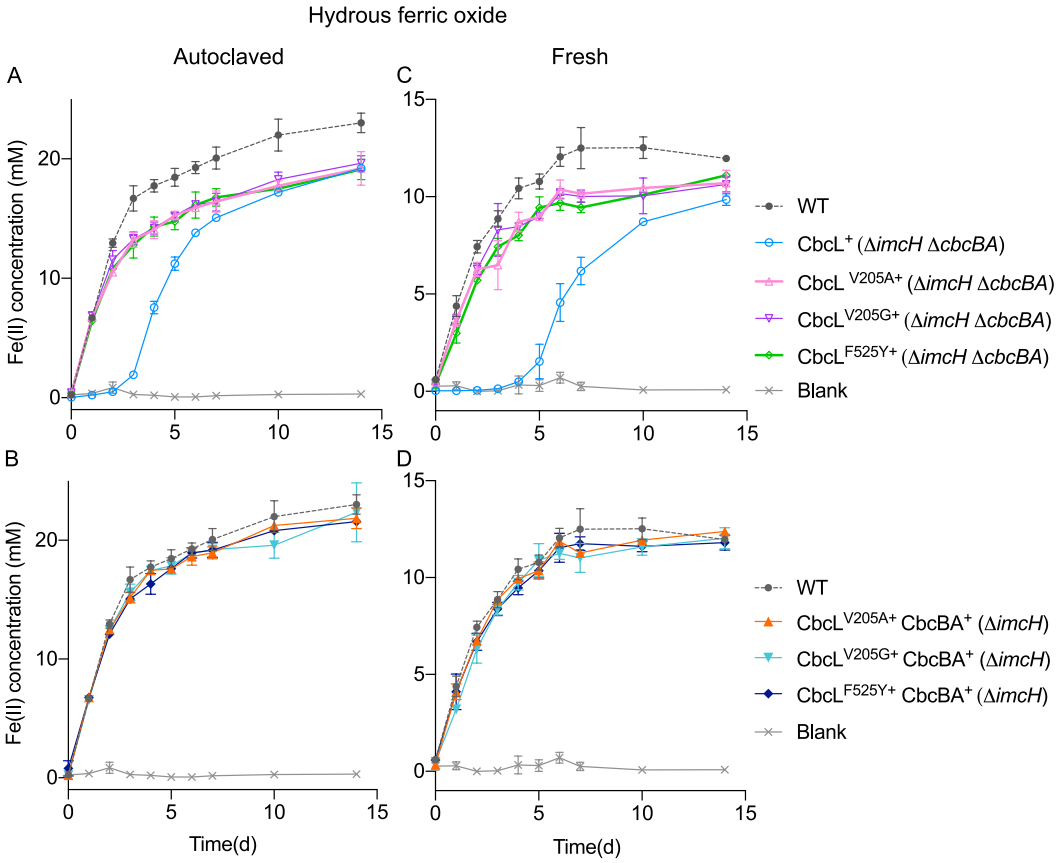

Figure 3.4: **All three point mutants in *cbcL* can reduce different forms of hydrous ferric oxide.** Amorphous Fe(III) oxides were synthesized, and treated two ways–autoclaved, fresh (not autoclaved). Heat treatment reduces the redox potential of Fe(III) oxide whereas fresh Fe(III) oxides maintain relatively high redox potentials. Panel A, and B show Fe(III) oxide reduction by single and double mutants containing variants of CbcL, when synthesized schwertmannite was brought to pH of 6.8 and autoclaved. Panel C, and D show Fe(III) oxide reduction of different mutants when Fe(III) oxide samples were not autoclaved. A and C. Double mutants (Δ*imcH* Δ*cbcBA*) containing wildtype form of CbcL showed a lag of three days (autoclaved), and five days (fresh) before initiating WT rates of autoclaved Fe(III) oxide reduction, and only reduced ~83% of all available Fe(III). Double mutants (Δ*imcH* Δ*cbcBA*) containing all three CbcL variants (V205A, V205G, and F525Y) do not show any lag like WT but cease Fe(III) reduction at ~83%. B. Single Δ*imcH* mutants with single point mutations in *cbcL* reduce autoclaved hydrous ferric oxide like WT, and did not show any lag, characteristic of Δ*imcH*. D. Fresh Fe(III) oxide reduction by single mutant strains in Δ*imcH* containing single point mutations in *cbcL*. All experiments were conducted twice with four replicates each. Data is represented as mean ± standard deviation.

3.4.5 All three suppressor mutants in Δ*imcH* Δ*cbcBA* can respire electrodes poised at high redox potential like WT

Mutants lacking ImcH cannot respire high potential electron acceptors including electrodes poised above 0 V *vs.* SHE [33, 41]. One Δ*imcH* suppressor strain enriched from high potential electrodes had a mutation in 525th residue in the *b*–type domain in CbcL (Figure 3.1). Creating *cbcL* point mutations in strains lacking Δ*imcH* (Δ*imcH,* Δ*imcH* Δ*cbcBA*) conferred an ability in these strains to respire high potential electron acceptors (Figure 3.2, 3.3). However, strains containing $CbcL^{F525Y}$ mutation had a different phenotype compared to strains containing $CbcL^{V205A}$, and $CbcL^{V205G}$ mutations when respiring Fe(III) citrate (Figure 3.2). To compare if there are any phenotypic differences in strains containing point mutations in CbcL, the strains were inoculated in bioreactors containing 40 mM acetate as the carbon source and electron donor, and electrodes poised at +0.1 V *vs.* SHE as the sole electron acceptor. As expected, the Δ*imcH* Δ*cbcBA* strain containing wildtype CbcL failed to respire electrodes, whereas all three strains containing CbcL variants (V205A, V205G, and F525Y) respired electrodes at a similar rate as WT strain and plateaued around the same current density of ~400 $\mu A.cm^{-2}$ around 100 h. Interestingly, mutants identified from suppressor strains enriched on Fe(III) citrate respired electrodes similar to $CbcL^{F525Y+}$ strain (Figure 3.5B) unlike the phenotypic differences observed between strains on Fe(III) citrate (Figure 3.2).

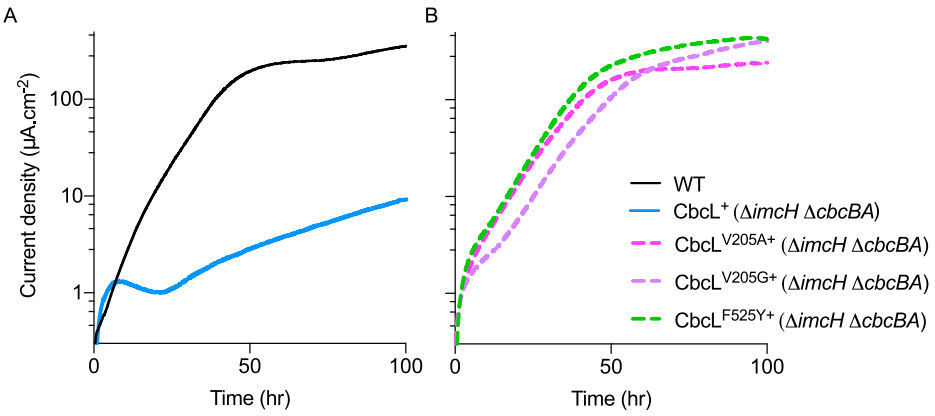

Figure 3.5: **Mutants containing point mutations in *cbcL* in Δ*imcH* Δ*cbcBA* background respire electrodes like WT at +0.1 V *vs.* SHE.** A. Current density measured by WT and CbcL^{+} (Δ*imcH* Δ*cbcBA*) strains over time. CbcL^{+} strain failed to respire electrodes poised at +0.1 V making less than 10 μA.cm^{-2} current after 96 h of inoculation compared to WT producing ~400 μA.cm^{-2}. B. Current production by mutants containing CbcL variants (V205A, V205G, F525Y) in Δ*imcH* Δ*cbcBA* on poised electrodes. Bioreactors were inoculated with mutants after the acetate-fumarate grown cultures reached an OD_{600} of ~0.5. All experiments were performed thrice in triplicates, and representative data is shown here.

3.4.6 CbcL-dependent electron transfer pathway has an oxidative inactivation effect at redox potentials above −0.1 V *vs.* SHE

All the experiments conducted so far measured reduction or respiration of specific electron acceptors under a range of different redox potentials. Electrochemical techniques like cyclic voltammetry can help infer kinetic and thermodynamic properties of redox active systems. Electrochemical analyses of *G. sulfurreducens* biofilms show three major electron transfer pathways with an average midpoint potential of −0.15 V *vs.* SHE when acetate is the electron donor [95, 113, 114, 139]. Cyclic voltammetry analysis of specific inner membrane cytochrome mutants identified midpoint potentials of ImcH-dependent, and CbcBA-dependent electron transfer pathway [34, 35]. The decrease in current observed in *G. sulfurreducens* biofilms grown at −0.145 V, above

-0.1 V measured by impedance spectroscopy [113], and the failure of CbcL$^+$ strain to support respiration at redox potentials above -0.1 V *vs.* SHE (Figure 3.2) leads to the hypothesis that CbcL-dependent pathway functions as a redox switch which requires exposure to low redox potential to allow electron transfer.

To test the redox switch hypothesis, we used double mutant Δ*imcH* Δ*cbcBA* (CbcL$^+$), which allowed us to study the kinetics of CbcL-dependent electron transfer without interference from ImcH or CbcBA. CbcL$^+$ biofilms grown at -0.1 V were subjected to cyclic voltammetry, and current produced is recorded as the redox potential is scanned from -0.55 V to $+0.24$ V at the rate of 1 mV.s^{-1}. Since Δ*imcH* Δ*cbcBA* failed to respire electrodes poised at high redox potentials (Figure 3.5A), to study kinetics of CbcL-dependent electron transfer pathway, Δ*imcH* Δ*cbcBA* were grown on electrodes poised at -0.1 V. The onset potential of Δ*imcH* Δ*cbcBA* (CbcL$^+$) strain is shifted to a more positive value of -0.24 V due to absence of CbcBA-dependent electron transfer activity as compared to -0.28 V in WT when acetate is the electron donor (Figure 3.6A) [35]. As the redox potential is increased slowly, the current production shows a steep increase reaching a maximum value at -0.1 V *vs.* SHE, above which the current starts to drop to about 50% of the maximum even as the redox potential is more thermodynamically favorable (Figure 3.6A). The decrease in current production despite an increase in the driving force showed a "tunnel–diode" effect, which means that at reductive potentials, CbcL-dependent pathway is active, while at oxidative potentials, CbcL-dependent pathway becomes inactive. The first derivative of such voltammograms showed a catalytic peak at low redox potential, and a switch peak at high redox potentials. Plotting the first derivative of Δ*imcH* Δ*cbcBA* revealed two peaks, one catalytic peak at -0.165 V, indicating the

reductive activation potential, and one switch peak at -0.11 V showing the oxidative inactivation potential of CbcL-dependent electron transfer pathway (Figure 3.6B). This system of catalytic activation/inactivation in response to a particular redox potential window is reported in other proteins such as the [FeFe]– or [NiFe]–hydrogenases showing oxidative inactivation at high redox potentials [132].

Point mutations in CbcL identified from suppressor mutation analysis allowed strains lacking ImcH to respire electron acceptors above -0.1 V *vs.* SHE (Figure 3.1) suggesting that these mutations irreversibly lock the CbcL protein in an active confirmation across both high and low redox potentials. If this were the case, cyclic voltammetry analysis of strains containing these mutations in Δ*imcH* Δ*cbcBA* could reveal a sigmoidal curve with no inactivation at high potentials suggesting a wide redox potential window of favorable electron transfer. To test this, $CbcL^{V205A+}$, $CbcL^{V205G+}$, and $CbcL^{F525Y+}$ strains were grown as biofilms on electrodes poised at +0.1 V *vs.* SHE, and subjected to cyclic voltammetry after the current density plateaued at ~300 $\mu A.cm^{-2}$. Biofilms were scanned from -0.55 V to $+0.24$ V at 1 $mV.s^{-1}$, and current produced at each redox potential was measured. As expected, all three strains failed to support electron transfer below -0.24 V as they lack low potential CbcBA-dependent electron transfer pathway (Figure 3.6A) whereas at redox potentials above -0.1 V, current production did not decrease, and instead followed WT like behavior (Figure 3.6A).

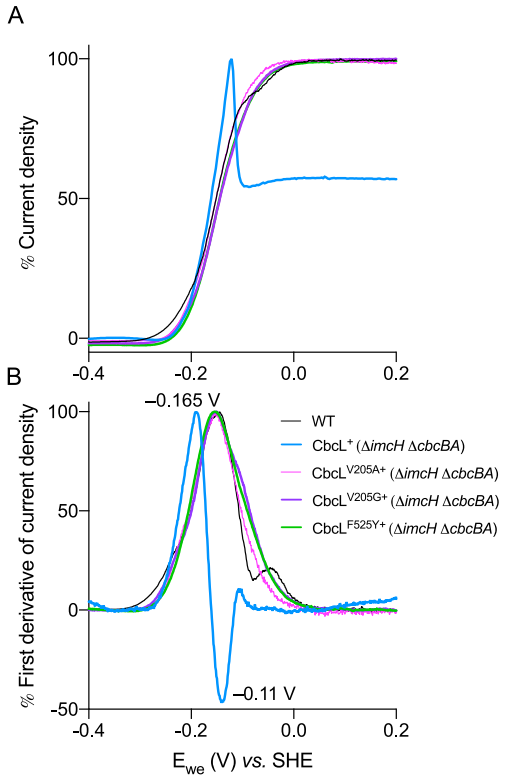

Figure 3.6: **Cyclic voltammetry analysis of CbcL$^+$ biofilms show a midpoint potential of −0.165 V and a lack of high potential dependent electron transfer pathway whereas CbcL$^+$ variants retain the high potential dependent electron transfer feature.** A. *G. sulfurreducens* strains were grown on electrodes poised at +0.1 V *vs.* SHE, and the cyclic voltammetric analysis was performed after 96 h of growth at 1 mV/s. All the mutants show a positive shift in the onset redox potential to −0.24 V *vs.* SHE, same as the onset potential of Δ*cbcBA* [35]. The Δ*imcH* Δ*cbcBA* biofilms showed a decrease in current density above redox potential of −0.1 V whereas all strains containing CbcL variants did not show a decrease in current density, and the CVs followed WT behavior. Reverse scan is shown here. B. First derivative analysis of the reverse scans in A. reveal the redox potential at which maximum rate of electron transfer is observed. CbcL$^+$ biofilms had a midpoint potential of −0.165 V, and the variants had a midpoint potential of −0.15 V like WT biofilms suggesting both high- and low- redox potential dependent electron transfer pathway is active. Data is represented as percentage of current density to show direct comparisons between different traces.

First derivative analysis of the reverse scan of cyclic voltammetry curves also showed no oxidative inactivation peaks, but showed a wide peak with an inflection point at −0.15 V *vs.* SHE (Figure 3.6B). Absence of oxidative inactivation peaks in all strains with mutations in *cbcL* indicate that these mutations activate the CbcL-dependent electron transfer pathway across all redox

potentials above −0.24 V. Comparing the electron transfer kinetics between strains containing CbcL mutations and WT show an overlap on all redox potentials above −0.24 V suggesting that CbcL-dependent pathway is not affected between the redox potential window of −0.24 V and −0.1 V, the required redox window for CbcL-dependent electron transfer, and these mutations acquired electron transfer ability above redox potentials of −0.1 V *vs.* SHE.

3.4.7 CbcL-dependent electron transfer pathway supports lower growth yields

G. sulfurreducens encodes multiple electron transfer pathways allowing conservation of different amounts of energy available from respiration of different electron acceptors [33–35, 41]. *G. sulfurreducens* strains lacking one or more pathways showed different cellular yields per unit of electron acceptor reduced. Strains containing the ImcH-dependent pathway only (Δ*cbcL* Δ*cbcBA*) supported the highest yield of ~200% as compared to WT [35]. One question stemming from this work is associated to the changes in yield caused by the mutations in CbcL. As strains containing point mutations in CbcL, and lacking ImcH support growth at high redox potentials, does the utilization of $CbcL^{V205A+}$–, $CbcL^{V205G+}$–, and $CbcL^{F525Y+}$–dependent pathway affect cellular yields?

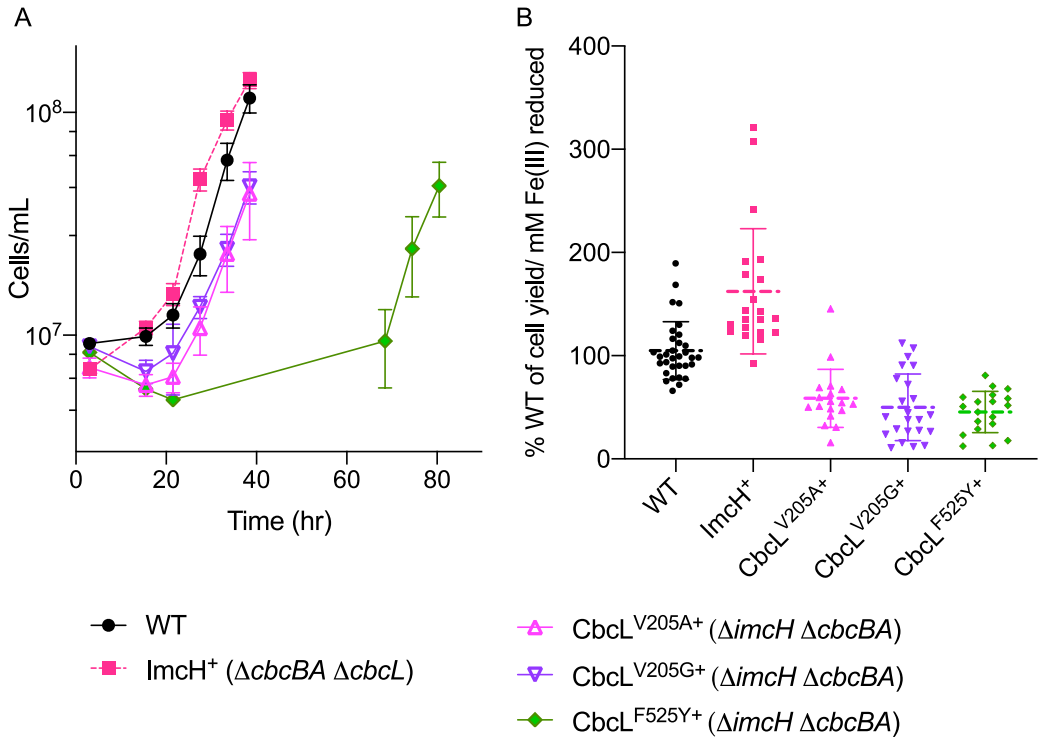

Figure 3.7: **Cell yield (cells/mM Fe(III) reduced) in strains lacking Δ*imcH* Δ*cbcBA* (CbcL^{+}) is significantly lower than yields achieved by WT.** A. Cells measured using flow cytometry from Fe(III) citrate grown cultures. ImcH^{+} strains produced more cells per unit time than WT whereas CbcL^{+} strains produced less number of cells per unit time. Linear regression analysis showed different rates for ImcH^{+} strains and for all three CbcL^{+} variants. B. Mutants lacking *cbcL* and *cbcBA* (ImcH^{+}) had the highest yield corroborating earlier reported results [35,41]. Strains utilizing only CbcL-dependent electron transfer pathway (CbcL^{V205A+}, CbcL^{V205G+}, CbcL^{F525Y+}) had lower cell yields ranging from 59.7% for CbcL^{V205A+}, 50% for CbcL^{V205G+}, and 46% for CbcL^{F525Y+}. Comparing the yields for all three CbcL variants using one-way ANOVA test resulted in a non-significant p value of 0.35. Experiments were performed thrice with eight replicates, and data is represented as mean with standard deviation.

Early experiments measuring yields in Δ*imcH* strains on Fe(III) oxide showed lower cell counts per mM Fe(III) reduced as compared to WT and Δ*cbcL* [134], although these results could be affected by the presence of CbcBA, and attachment of cells to Fe(III) oxide particles. As Δ*imcH* Δ*cbcBA* containing point mutations in CbcL support growth on Fe(III) citrate, direct yield measurement in *cbcL*–only strains was calculated by inoculating CbcL^{V205A+}, CbcL^{V205G+}, and CbcL^{F525Y+} strains in filtered Fe(III) citrate medium and total cells were counted using flow

cytometry. As reported earlier, forcing cells to utilize the ImcH-dependent electron transfer pathway ($ImcH^{+}$) supported the highest cellular yield of 162 ± 60.6% as compared to WT (Figure 3.7B). Interestingly, strains containing only CbcL-dependent electron transfer pathway ($CbcL^{V205A+}$, $CbcL^{V205G+}$, and $CbcL^{F525Y+}$) only supported yields of 58.7± 28.2%, 50.1± 32.2%, and 45.5± 20.1% respectively, as compared to WT (Figure 3.7). These results suggests that mutating single amino acid residues did not increase the yield supporting early evidence that all three inner membrane cytochromes have different H^{+}/e^{-} stoichiometries.

3.5 Discussion

Failure of *G. sulfurreducens* strains lacking *imcH* to respire high potential electron acceptors when *cbcL* is constitutively expressed [34, 35], and CbcL peptides detected in mass spectrometry analysis [37, 38] suggested inactivity of CbcL under high redox potential conditions [33, 41]. In this report we provide an explanation for how *G. sulfurreducens* regulates electron transfer through CbcL using suppressor enrichment analysis. In the absence of a crystal structure of CbcL, suppressor enrichment analysis aided in determination of key amino acid residues involved in regulation of electron transfer through CbcL. Enrichment of suppressor strains to identify important genes and regulatory strategies have been utilized in different bacterial species [140–142]. In this study, suppressor enrichment analysis identified important residues switching the ability of CbcL to function from only low potential to both high and low redox potentials (Figure 3.3, 3.4).

Homology searches and multiple sequence alignments revealed that the V205 residue is not conserved. Glycine and alanine are found in 205th position in CbcL from *Geopsychrobacter electrodiphilus, Geothermobacter hydrogenophilus,* and *Geobacter* strain FeAm09 within *Geobacteraceae* family [143–145]. These strains are found in environments rich in ferrihydrite, an amorphous form of Fe(III) oxide with relatively high redox potential (~0 V *vs.* SHE) [117]. Changing these amino acids can provide structural variability to CbcL affecting the confirmation of the protein, changing how electrons may flow through it. Changing V205 in *c*–type heme domain, and F525 in *b*–type heme domain might change the heme environment by changing the inter-heme distance affecting the rate of electron transfer [146].

CbcL belongs to type–I family of *b*–type diheme quinone oxidoreductase contain six transmembrane domains with five histidines for *b*–type heme coordination. Modeling studies predicted 525th residue to be a conserved residue present in the fifth transmembrane domain located towards the cytoplasmic side of the inner membrane between two conserved histidines required for *b* heme coordination [65, 66]. Mutating F to Y can change the coordination environment allowing the fifth histidine residue to coordinate with one of the heme *b* present towards the cytoplasmic side. These changes can affect the functional properties of *b*–type heme, locking the CbcL protein in active open gated state.

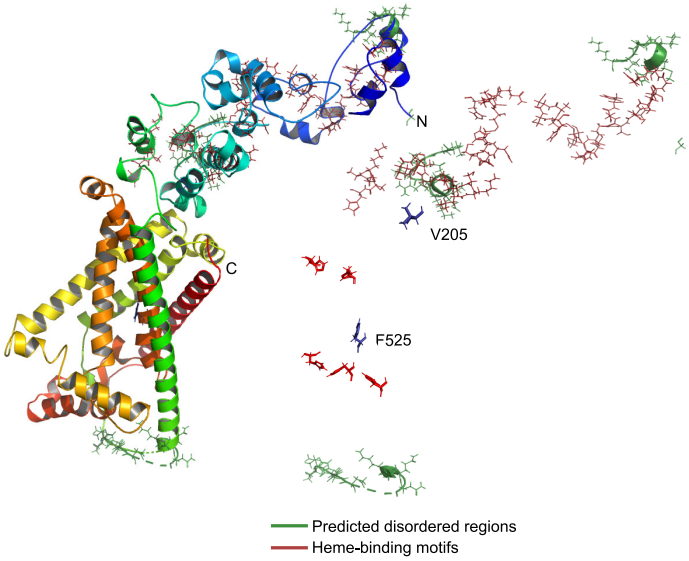

Figure 3.8: **Prediction of CbcL structure using Robetta neural network modeling.** Structure prediction of CbcL using neural network *de novo* approach shows the position V205 to be closest to the periplasmic side of the membrane where electrons flowing from *b*–heme could enter *c*–heme domain. Heme binding motifs are shown in red on the right, and all predicted disordered regions are in green.

Due to the lack of structural information on multiheme cytochromes, CbcL structure was predicted using RoseTTA Fold *de novo* algorithm on Robetta protein prediction server (Baker Lab, University of Washington) [147, 148]. Based on the predicted structure both V205 and F525

appears to be located at key positions probably regulating electron flow from quinone to *b*–type hemes, and from *b*–type heme to *c*–type cytochrome domain. Mutating to V205A or V205G could change the conformation of the periplasmic peptide allowing electron transfer at high redox potentials, and F525Y mutant can change the coordination sphere of heme *b* binding providing access to another H308 instead of H528 coordinating with H354 to bind one *b*–heme (Figure 3.8). The model structure and the results reported in this study depicts the need for biochemical characterization of CbcL.

Electrochemical analysis of $CbcL^{+}$ strain showed a redox switch behavior with reversible inactivation at high redox potentials (Figure 3.6). This redox switch behavior is observed in many enzymes like formate dehydrogenases, and hydrogenases that share domains with CbcL [132,149]. Redox regulation of photosystems is widely studied, and the presence of redox dependent safety valves during electron transfer in photosystem II is reported [150, 151]. Recently published study of redox switches in NADPH–malate dehydrogenase in plants reported regulation by redox switches is essential in fine regulation of the activities under different light conditions for efficient electron transfer [152].

While the ImcH-dependent pathway conserves the most energy, utilization of CbcL-dependent pathway both at high and low redox potentials conserves relatively less energy (Figure 3.7), and CbcBA-dependent pathway doesn't support growth but allows reduction of electron acceptors near the thermodynamic limit of acetate respiration [35]. We also show that CbcL-dependent electron transfer pathway functions as a redox switch allowing electron transfer only below redox potentials of -0.1 V *vs.* SHE (Figure 3.6). Different mutants lacking specific inner

membrane cytochromes could be utilized for building redox sensors in bioelectronic applications. Redox dependent regulation of CbcL, and transcriptional regulation of CbcBA suggest multiple regulatory regimes governing the differential utilization of electron transfer pathways across the inner membrane of *G. sulfurreducens*.

Chapter 4

Visualizing redox potential dependent stratification of *Geobacter sulfurreducens* biofilms.

Komal Joshi, Chi Ho Chan, Daniel R. Bond

(manuscript in preparation for submission)

4.1 Summary

Extracellular electron transfer allows microorganisms to use insoluble substrates as electron acceptors. *Geobacter sulfurreducens* links oxidation of acetate in the cytoplasm to the reduction of extracellular electron acceptors such as metal oxides, or poised conductive surfaces such as electrodes. *G sulfurreducens* forms over 20 μm thick conductive biofilms linked by a series of *c*–type cytochromes, when poised electrode serves as the electron acceptor. Although metabolic heterogeneity and environmental factors regulating biofilm structure has been studied extensively in pathogenic bacteria, it remains largely unknown what controls the structure and metabolic activity of cells in electroactive biofilms of *G. sulfurreducens*. The presence of recently described separate electron transfer pathways out of the inner membrane in *G. sulfurreducens* under high *vs.* low redox potential conditions suggested a mechanism for survival and advantage over other organisms in different regions of the electrode biofilm. Confocal Raman spectroscopy analysis, and electrochemical analysis of *G. sulfurreducens* biofilms showed that cells experience a gradient of redox potentials from poised electrode potential at the surface to a lower redox potential at the top of the biofilm. *G. sulfurreducens* cells within a biofilm also show a gradient of anabolic activity with cells closest to the electrode reported to be the most active. By co-inoculating electrodes with mutants that can only respire within certain reduction potential windows and visualizing the electrode biofilm expressing florescent proteins optimized for *G. sulfurreducens*, we report that cells favoring high redox potential dominated near the electrode surface, and cells favoring low redox potential below −0.13 V *vs.* SHE were primarily found in a band >15 μm from the high potential

electrode. When mixtures of these high and low redox potential-requiring cells were inoculated into reactors for growth on electrodes poised at +0.24 V *vs.* SHE, biofilms always stratified to reveal the low-potential strains in a layer farthest from the electrode. Control experiments mixing vGFP- and mScarlet-expressing wild type strain did not produce the same stratification. These new data, using fluorescently-labeled inner membrane cytochrome mutants, combined with recent nanoSIMS evidence for metabolic stratification, suggests that the fundamental limitation to current production in *Geobacter*-dominated microbial electrochemical systems is the decrease in redox potential over distances greater than 20 μm.

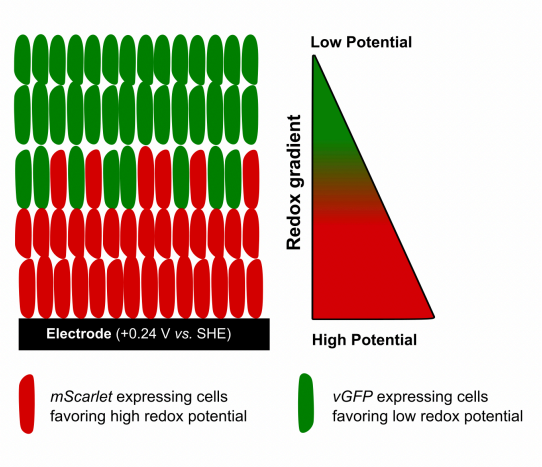

Figure 4.1: Graphical summary: A gradient of redox potential causes spatial stratification of electroactive biofilms.

4.2 Introduction

The majority of bacteria in the environment are found to be surface-attached, present in structured microbial communities [153, 154]. Biofilms represent an enclosed system of same or different species of microbial cells embedded in an extracellular matrix attached to a surface providing persistence to microorganisms in constantly changing environmental conditions [153, 155]. Bacteria in biofilms experience different growth conditions as compared to planktonic growth conditions resulting in different metabolic activities, and gene expression profiles within the micro-compartments of a biofilm. Microbial biofilm properties are defined by the structure of biofilms, availability of nutrients, and physiological activity of the community [154, 155]. Biofilms play detrimental roles in infections [156], biofouling [157, 158] and beneficial roles like their use as living catalysts [159], biogeochemical cycling of elements in water, soil as well as subsurface environments [160, 161].

Same or multispecies biofilms are spatially heterogeneous containing subpopulations with different metabolic activities stratified into different regions within a biofilm [162, 163]. Physiological heterogeneity can be easily explained using the example of a biofilm utilizing oxygen as its terminal electron acceptor: diffusion and subsequent utilization of oxygen causes the inner core cells to switch to anaerobic metabolism [164, 165]. Species stratification is also one of the common features of a biofilm where different species utilize different electron acceptors in an environment. For example, biofilms enriched on anodes in microbial fuel cells show outer layers of the biofilms is enriched in species breaking down complex carbon compounds and consuming oxygen whereas

the innermost layers are occupied by small chain fatty acids utilizing anaerobic bacteria capable of extracellular electron transfer like *Geobacter* and *Shewanella* species [166–168].

Geobacter species acquire energy by coupling the intracellular oxidation of organic compounds such as acetate to the reduction of soluble or insoluble electron acceptors such as fumarate, Fe(III) citrate, Fe(III) oxide, Mn(IV) oxide, poised electrodes or syntrophic partners [13, 39, 40, 42, 43, 80, 82, 169]. *Geobacter sulfurreducens* has the ability to form multi-cell layer conductive biofilms when respiring insoluble electron acceptors [40, 41, 113, 114]. The *G. sulfurreducens* genome encodes over hundred *c*–type cytochromes forming a chain of redox active electron transfer proteins linking intracellular oxidation to extracellular reduction [36]. Although the complete electron transfer chain still remains unknown, three main energy conserving inner membrane cytochrome (ImcH, CbcL, and CbcBA) dependent electron transfer pathways have been identified [33–35,41]. ImcH (GSU3259) is a seven heme containing *c*–type cytochrome required for respiration of high redox potential (> -0.1 V *vs.* SHE) electron acceptors [33], CbcL (GSU0274) is a *bc*–type nine heme containing *c*–type cytochrome, and diheme containing *b*–type cytochrome required for respiration of low potential electron acceptors (< -0.1 and > -0.21 V *vs.* SHE) [34] whereas CbcBA (GSU0593–0594), another *bc*–type cytochrome complex containing seven *c*–type hemes and two *b*–type hemes is required for the reduction of electron acceptors below the redox potential of -0.21 V *vs.* SHE [35].

Despite applications of *G. sulfurreducens* electroactive biofilms in sensing heavy metal pollutants in the environment or in self-assembling bioelectronic circuits [23, 170], factors determining the structure and morphology of electroactive biofilms remains unknown.

Fluorescent microscopy studies [171–173] provided evidence for fluorescent probe detection in *G. sulfurreducens* and visualization of *G. sulfurreducens* biofilms. Modeling studies [113, 124, 139, 174], and spectral and electrochemical analysis [122, 123, 175–177] of *G. sulfurreducens* biofilms reported accumulation of reduced cytochromes suggesting formation of a redox gradient away from the electrode surface. Stable isotope probing coupled to nanoscale secondary ion mass spectrometry (nanoSIMS) analysis of *G. sulfurreducens* biofilms showed that highest metabolic activity in cells growing closest to the electrode with a linear decline in metabolic activity away from the electrode surface [120]. When biofilms were grown at high redox potential (+0.24 V *vs.* SHE), the rate of biomass formation as a function of distance showed two maxima suggesting the presence of two anabolic processes whereas low redox potential (−0.1 V *vs.* SHE) grown *G. sulfurreducens* biofilms showed a steeper decline in metabolic activity away from the surface of the electrode [120]. We hypothesize that utilization of different inner membrane cytochrome (ImcH or CbcL) dependent electron transfer pathways dictate the different anabolic processes observed in *G. sulfurreducens* biofilms.

In this study, we describe the factors controlling the morphology and structure of *G. sulfurreducens* biofilms. Using improved fluorescent proteins (vGFP and mScarlet), we show that *G. sulfurreducens* cells grow vertically in a biofilm suggesting that cells that first attach to the electrode surface divide with daughter cells, forming clonal pillars away from the surface of the electrode. These results support the recent report that when *Shewanella oneidensis* were inoculated in a ratio of 9:1 with equal access to stable non-degrading electron acceptor such as the surface of an electrode, the cells to first attach to the electrodes maintain their location (population) even after

365 generations, as detected by confocal fluorescence microscopy [178].

We also provide evidence for redox dependent metabolic stratification in *G. sulfurreducens* biofilms when grown on a high potential electrode surface (+0.24 V *vs.* SHE) using engineered strains expressing vGFP or mScarlet containing only one relevant redox dependent inner membrane cytochrome ($ImcH^+$ or $CbcL^+$). Imaging of biofilms grown at +0.24 V *vs.* SHE inoculated with $ImcH^+$ and $CbcL^+$ cells, show distinct layers of $ImcH^+$ and $CbcL^+$ cells suggesting the cells closest to the electrode surface utilize ImcH-dependent electron transfer pathway, and cells growing at a distance greater than 10 μm utilize CbcL-dependent electron transfer pathway. These results, combined with the recent nanoscale secondary ion mass spectrometry (nanoSIMS) analysis of metabolic stratification in *G. sulfurreducens* biofilms [120] provide an explanation for the limiting thickness of the current contributing biofilm.

4.3 Materials and Methods

4.3.1 Growth and medium conditions.

G. sulfurreducens strains, pK18mobsacB gene deletion plasmids and Tn7-based integration vectors are listed in Table 4.1. All strains were grown from isolated colonies from −80 °C DMSO stocks. Acetate (20 mM) and fumarate (40 mM) in a bicarbonate-buffered anoxic basal medium were used for routine growth and strain construction in liquid under N_2:CO_2 (80:20) or on semisolid surface agar (1.5%) under N_2:CO_2:H_2 (75:20:5) atmospheres [33, 89]. When poised electrodes were used as the electron acceptor, NaCl (50 mM) was added to maintain a similar ionic strength. The pH of the medium was adjusted to 6.8 before adding 2 g/L sodium bicarbonate, then sparged with N_2:CO_2 (80:20) passed over a heated, reduced copper column to remove trace O_2. Biofilm growth was initiated with a 25% inoculum of fumarate grown *G. sulfurreducens* cultures as they nearly depleted fumarate in the medium (~ 0.5 OD_{600}) in 15 mL reactor volume.

Strain or Plasmid	**Description or relevant genotype**	**Source or reference**
Geobacter sulfurreducens strain		
G. sulfurreducens PCA	Wildtype	Lab culture collection
DB1717	ΔGSU0593-94 (Δ*cbcBA*)	[35]
DB868	ΔGSU0274 (Δ*cbcL*)	[34]
DB1719	ΔGSU0593-94 ΔGSU0274 (Δ*cbcBA* Δ*cbcL*)	[35]
DB1718	ΔGSU0593-94 ΔGSU3259 (Δ*cbcBA* Δ*imcH*)	[35]
DB1964	Tn7::P_{ppcA} - *vsfGFP-0v2* (vGFP)	This study
DB1965	Tn7::P_{ppcA} – *mScarlet* (mScarlet)	This study

DB1969	ΔGSU0593-0594 ΔGSU0274 (Δ*cbcBA* Δ*imcH*) Tn7::P_{ppcA} -*vsfGFP-0v2* (vGFP)	This study
DB1975	ΔGSU0593-0594 ΔGSU0274 (Δ*cbcBA* Δ*cbcL*) Tn7::P_{ppcA} -mScarlet (mScarlet)	This study
DB2001	ΔGSU0274 (Δ*cbcL*) Tn7::P_{ppcA} -*vsfGFP-0v2* (vGFP)	This study
DB2003	ΔGSU0593-0594 (Δ*cbcBA*) Tn7::P_{ppcA} -*vsfGFP-0v2* (vGFP)	This study
***E. coli* strains**		
S17-1	*recA pro hsdR RP4-2-Tc::Mu-Km::Tn*7	[179]
MFDpir	RP4-2-Tc::[Δ*Mu1::aac(3)IV*-Δ*aphA*-Δ*nic35*-Δ*Mu2::zeo*] Δ*dapA::(erm-pir)* Δ*recA*	[92]
MFDpir/pTNS3	MFDpir with plasmid expressing *tnsABCD*	[90]
Plasmids		
pk18mobsacB	SacB encoding scarless deletion vector	[89]
pDGSU0274	Flanking regions of GSU0274 (*cbcL*) in pK18mobsacB	[34]
pDGSU3259	Flanking regions of GSU3259 (*imcH*) in pK18mobsacB	[89]
pDGSU0593-0594	Flanking regions of GSU0593-0594 (*cbcBA*) in pK18mobsacB	[35]
pTn7C146	Tn7 integrative vector, derivative of pTJ1	[34]
pTn7-Geo7	The GSU0612 (*ppcA*) promoter-RBS with an MCS sequence synthesized and cloned into a derivative of pTn7C146	This study
pTn7-Geo7-vsfGFP-0 v2	*G. sulfurreducens* codon optimized *vsfGFP-0* variant (vGFP) sequence synthesized and cloned into a derivative of pTn7-Geo7 under the control of *ppcA* promoter	This study
pTn7-Geo7-mScarlet	*G. sulfurreducens* codon optimized *mScarlet* (mRFP) sequence synthesized and cloned into a derivative of pTn7-Geo7 under the control of *ppcA* promoter	This study

Table 4.1: Strains and plasmids used in this study

4.3.2 Strain construction.

Primer and DNA fragment sequences used for plasmid constructs are in Table 4.2. SacB-sucrose counter-selection gene deletion vectors were used to generate scarless gene deletions in *G. sulfurreducens* [89]. Around 750 bp flanking sequences of the targeted genes were cloned into the pK18mobsacB plasmid. S17–1 conjugative donor cultures carrying the *sacB* plasmids were pelleted with recipient *G. sulfurreducens* cultures, mixed on top of a 0.22 μm pore-sized filter set on acetate-fumarate agar plates inside an anaerobic chamber at 30 °C, incubated for 4 hours before streaking the mixture onto acetate-fumarate plates with 200 μg/ml kanamycin. Gene deletion mutant was selected on acetate-fumarate plates containing 10% sucrose and confirmed using PCR with primers flanking the deletion site [89]. DNA sequences for a modified green (vsfGFP-0, vGFP) and red (mScarlet) fluorescent proteins were codon optimized based on the *G. sulfurreducens* codon table using the "guided random" method calculated by OPTIMIZER [180, 181]. vGFP and mRFP under the control of the *G. sulfurreducens ppcA* promoter were integrated into the chromosome downstream of the *glmS* gene using Tn7 integrative plasmids [91, 93]. MFDpir conjugative donor cultures carrying vGFP or mRFP, together with a separate MFDpir culture carrying the pTNS3 helper plasmid were pelleted with recipient *G. sulfurreducens* cultures. Integrants were selected on agar plates with 200 μg/ml kanamycin.

DNA fragment synthesized or primer	Sequence (5'-3')	Restriction site
vsfGFP-0	CATATGTCGAAGGGCGAGGAGCTCTTCA CCGGGGTTGTGCCCATCCTCGTCGAACT GGACGGCGATGTCAACGGTCACAAGTTC TCGGTTCGGGGCGAGGGCGAGGGGGACG CCACCAACGGCAAGCTGACCCTCAAGTT CATCTGCACCACCGGGAAGCTCCCCGTG CCTTGGCCTACCCTGGTGACGACACTGA CCTACGGAGTGCAATGCTTCTCACGCTA CCCGGACCACATGAAGCGGCACGATTTC TTCAAGTCCGCCATGCCCGAAGGCTACG TGCAGGAGCGCACCATCTCCTTCAAGGA CGATGGGACTTATAAGACCCGGGCGGAA GTGAAATTCGAAGGAGACACCCTGGTTA ACCGCATAGAGCTTAAGGGTATCGATTT TAAGGAAGACGGCAATATCCTCGGGCAT AAACTGGAGTACAACTTTAACTCACATA ACGTCTATATCACCGCCGACAAGCAGAA GAATGGTATTAAGGCCAACTTTAAGATC CGGCATAACGTGGAGGACGGATCGGTCC AGCTGGCCGATCACTACCAGCAGAACAC CCCCATCGGCGACGGCCCCGTCCTGCTT CCCGACAACCACTATTTGAGCACGCAGT CCGTCCTTAGCAAGGACCCGAACGAGAA ACGGGATCACATGGTGCTCCTGGAATTC GTTACGGCGGCCGGGATCGCCCAGGTAC AACTGGTCGAGAGCGGAGGCGCCTTGGT CCAGCCGGGCGGCTCCCTGCGGCTGTCC TGTGCGGCTTCCGGGTTCCCGGTGAACA GGTACAGCATGCGTTGGTACAGGCAAGC GCCCGGCAAGGAACGTGAATGGGTTGCG GGCATGTCCTCCGCGGGCGACCGGTCCT CCTATGAGGATTCGGTAAAAGGACGTTT CACCATTTCACGGGATGACGCGCGCAAC ACCGTCTACCTGCAGATGAATTCCCTGA AGCCGGAGGACACCGCCGTGTACTATTG TAACGTCAACGTTGGCTTTGAGTACTGG GGGCAGGGCACCCAGGTGACCGTGTCGT GAGTGCAC	NdeI, ApaLI

vsfGFP-0v2	CATATGAGGTCAGGCGGAATGGCTATG TCGAAGGGCGAGGAGCTCTTCACCGG GGTTGTGCCCATCCTCGTCGAACTGGA CGGCGATGTCAACGGTCACAAGTTCTC GGTTCGGGGCGAGGGCGAGGGGGACG CCACCAACGGCAAGCTGACCCTCAAGT TCATCTGCACCACCGGGAAGCTCCCCG TGCCTTGGCCTACCCTGGTGACGACA CTGACCTACGGAGTGCAATGCTTCTCA CGCTACCCGGACCACATGAAGCGGCA CGATTTCTTCAAGTCCGCCATGCCCGA AGGCTACGTGCAGGAGCGCACCATCT CCTTCAAGGACGATGGGACTTATAAGA CCCGGGCGGAAGTGAAATTCGAAGGA GACACCCTGGTTAACCGCATAGAGCTT AAGGGTATCGATTTTAAGGAAGACGGC AATATCCTCGGGCATAAACTGGAGTAC AACTTTAACTCACATAACGTCTATATCA CCGCCGACAAGCAGAAGAATGGTATT AAGGCCAACTTTAAGATCCGGCATAA CGTGGAGGACGGATCGGTCCAGCTGG CCGATCACTACCAGCAGAACACCCCC ATCGGCGACGGCCCCGTCCTGCTTCC CGACAACCACTATTTGAGCACGCAGT CCGTCCTTAGCAAGGACCCGAACGA GAAACGGGATCACATGGTGCTCCTG GAATTCGTTACGGCGGCCGGGATCG CCCAGGTACAACTGGTCGAGAGCGG AGGCGCCTTGGTCCAGCCGGGCGG CTCCCTGCGGCTGTCCTGTGCGGCT TCCGGGTTCCCGGTGAACAGGTAC AGCATGCGTTGGTACAGGCAAGCG CCCGGCAAGGAACGTGAATGGGTTG CGGGCATGTCCTCCGCGGGCGAC CGGTCCTCCTATGAGGATTCGGTAA AAGGACGTTTCACCATTTCACGGGA TGACGCGCGCAACACCGTCTACCT GCAGATGAATTCCCTGAAGCCGGAG GACACCGCCGTGTACTATTGTAACG TCAACGTTGGCTTTGAGTACTG GGGGCAGGGCACCCAGGTGACCG TGTCGTGAGTGCAC	NdeI, ApaLI

mScarlet	CATATGAGCAAGGGGGAGGCGGT CATTAAGGAGTTCATGCGGTTCAAA G TCCACATGGAGGGCAGCATGAACG GCCACGAATTCGAAATTGAAGGGG AGGGTGAAGGCAGGCCTTACGAA GGCACCCAGACCGCCAAGCTCAA AGTCACTAAGGGCGGGCCCTTGCC CTTCTCCTGGGACATCCTCTCGCC GCAGTTCATGTACGGATCCCGCGC CTTCACAAAGCACCCAGCCGACA TCCCCGACTATTATAAGCAGTCCT TCCCCGAAGGTTTCAAGTGGGAGA GGGTCATGAACTTCGAGGACGGCGG CGCCGTGACCGTGACGCAGGACAC CTCGCTGGAAGACGGTACCCTGATC TACAAGGTCAAGCTCCGCGGCACCA ACTTCCCCCCCCGATGGCCCCGTGATG CAGAAGAAGACAATGGGCTGGGAA GCATCGACCGAACGCCTGTACCCTG AAGATGGCGTGCTCAAGGGCGATAT AAAGATGGCCCTGCGGCTGAAGGA CGGCGGTCGGTACCTCGCTGACTTT AAGACCACCTATAAGGCCAAGAAG CCAGTCCAGATGCCCGGCGCCTACA ACGTGGACCGGAAGCTGGACATCA CGAGTCATAACGAGGACTACACCGT CGTGGAACAGTATGAACGGTCGGAA GGCCGGCACTCGACGGGAGGCATG GATGAGCTGTATAAGTGAGTGCAC	NdeI, ApaLI
Primer 614	TAGGCCATGATGCTCATTCTG	
Primer 714	GTTCAACAGACAGCCTTCGTT	

Table 4.2: Primers used in this study.

4.3.3 Improving fluorescent protein detection in *G. sulfurreducens.*

Visualizing *G. sulfurreducens* biofilms using fluorescent proteins is difficult due to the small size of the *Geobacter* cell, with a volume of approximately a tenth of *Escherichia coli*, the strict oxygen requirement of the fluorophore, and expression systems not optimized for *Geobacter*. To overcome these challenges, first, the brightest green fluorescent (*vsfGFP-0*) [182] and red fluorescent protein (*mScarlet*) coding genes [183] were selected and recoded to match the normal distribution of *G. sulfurreducens* genes to reduce any translation barriers, then both genes were expressed under the control of the promoter of one of the highest expressing genes, *ppcA* (GSU0612) under fumarate or electrode growth conditions [30]. A fortuitous in-frame mutation that added 21 bp (coding for MRSGGMA) to the 5' end of the gene encoding vsfGFP-0 was isolated during gene assembly that produced a vsfGFP-0 (vsfGFP-0v2) variant four times brighter than vsfGFP-0 when expressed in *G. sulfurreducens.* When these redesigned fluorophore sequences were integrated downstream of the *glmS* gene in the chromosome using Tn7 and expressed from the *ppcA* promoter (Figure 4.2), brief exposures to oxygen present in atmosphere without fixation was adequate to mature both fluorophores for detection using a standard fluorescence microplate reader, epifluorescence microscope, and confocal microscope with excitation and exposure levels that did not cause significant photobleaching.

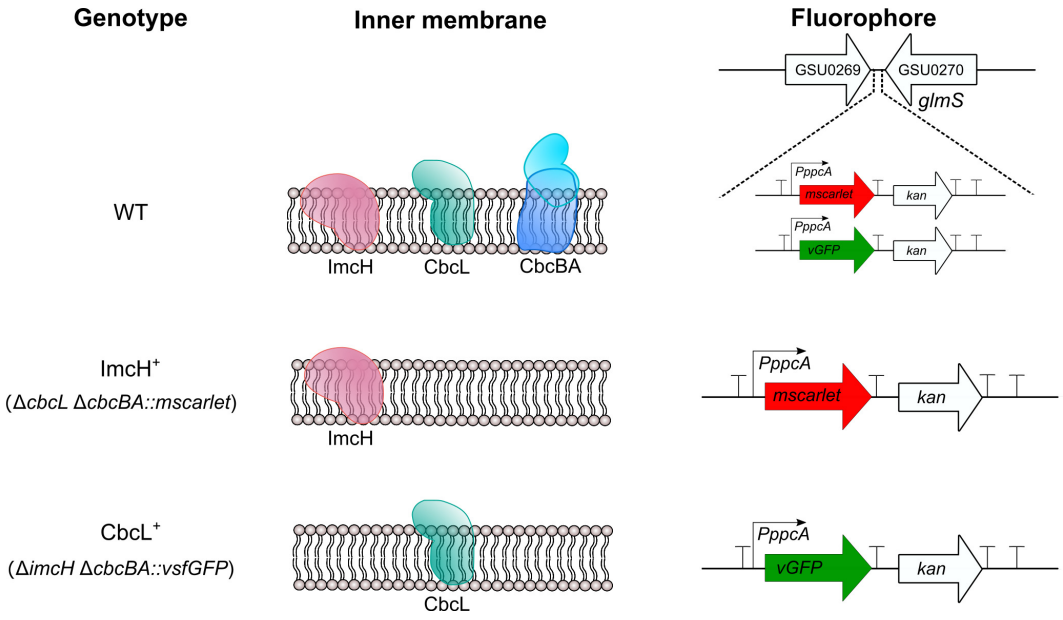

Figure 4.2: **Schematics of integrating genes encoding fluorescent proteins on to *G. sulfurreducens* chromosome.** pTn7 plasmid expressing either vGFP or mScarlet encoding genes under the control of *ppcA* promoter was integrated downstream of the *glmS* (GSU0270) on to the *G. sulfurreducens* chromosome. Both plasmids with vGFP and mScarlet were integrated into WT *G. sulfurreducens* creating WT::Tn7-P_{ppcA}*vGFP* or WT::Tn7-P_{ppcA}*mScarlet*. pTn7-P_{ppcA}-*mScarlet* was cloned into *G. sulfurreducens* strain lacking inner membrane cytochromes CbcL and CbcBA, required for low potential respiration ($ImcH^+$), and pTn7-P_{ppcA}-*vGFP* was cloned into a *G. sulfurreducens* strain containing only CbcL (Δ*imcH* Δ*cbcBA*), an inner membrane cytochrome essential for respiration of electron acceptors below −0.1 V *vs.* SHE. Different *G. sulfurreducens* strains containing vGFP or mScarlet allowed a way to visualize metabolic stratification of electroactive biofilms.

4.3.4 Electrochemical measurements of *G. sulfurreducens* biofilm.

To grow *G. sulfurreducens* biofilms on electrodes, we assembled three-electrode single chambered reactors as previously described [94, 95]. Briefly, graphite electrodes with a 3 cm^2 surface area were polished using 1,500–grit wet/dry sandpaper and attached to platinum wire to serve as the working electrode. A bare platinum wire served as the counter electrode. A saturated calomel reference electrode maintained the working potential of the graphite electrode to +0.24 V or −0.13 V *vs.* standard hydrogen electrode (SHE) using a VMP3 multichannel potentiostat (Biologic).

Reactor headspace was degassed using 80:20 N_2:CO_2 prior to inoculation and maintained for the duration of the experiment. Reactor temperature was maintained at 30 °C using a heated circulating water bath. Biofilm growth using poised electrodes as the sole electron acceptor was measured as current increase recorded every two minutes using EC–Labs (Biologic). For cyclic voltammetry measurements, the working electrode potential was cycled from -0.5 V to $+0.24$ V *vs.* SHE and back to -0.5 V *vs.* SHE twice at the rate of 1 mV/s, and the current produced by biofilms was measured as a result of changing working electrode potential. Second scan was used for data analysis.

4.3.5 Confocal imaging of *G. sulfurreducens* electrode biofilm.

G. sulfurreducens biofilms on 3 cm^2 graphite electrodes were gently rinsed once to remove any loosely attached cells with basal medium lacking any electron donor or acceptor then placed onto custom 3D-printed holders (Figure 4.3) that raised the surface of the biofilm ~0.2 mm above a 0.17 mm microscope cover glass. The chamber was sealed with vacuum grease and filled with fresh oxic basal medium. The biofilm was imaged using a Nikon A1R confocal microscope equipped with a 20× water immersion objective with a working distance of 0.8 mm. Lasers (561 and 488 nm) in sequential mode were used to excite biofilms expressing mScarlet and vGFP. A laser power of 1.1% with 30% gain was used for the 488 nm laser for vGFP, and 20.8% laser power with 60% gain was used for the 561 nm laser for mScarlet. Numerical aperture (NA) setting of 0.95, pinhole of 19.16 μm, and z-step of 0.24 μm, and resonant mode detector was used for capturing all the images. Noise in confocal images was reduced using Denoise.ai (Nikon) and analyzed using Fiji

[184]. The 3D-printed chambers and confocal imaging were performed at the University Imaging Centers (UIC) at the University of Minnesota with the assistance of UIC staff.

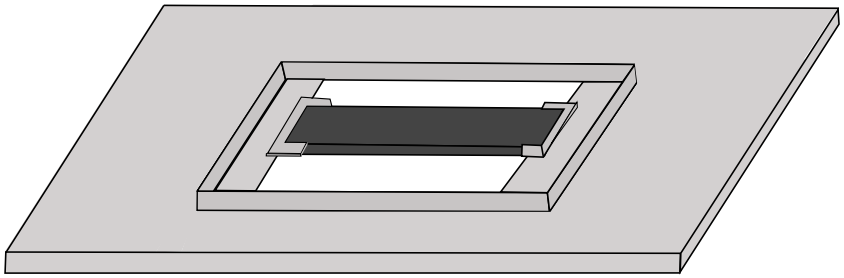

Figure 4.3: **Custom designed 3D-printed holder for placing electrodes for imaging.** To prevent damaging the biofilms by directly placing them on the coverslip, a customized hollow electrode holder was designed to raise the electrode 0.2 mm from the surface of the cover glass. The electrode holder is held in place on a 0.17 mm cover glass using a thin layer of grease. Adding fresh aqueous oxic basal medium under the electrode ensured consistent imaging with the same refractive index when using a 20x water immersion objective.

4.4 Results

4.4.1 Visualizing *G. sulfurreducens* strains expressing vGFP or mScarlet as biofilms on poised electrodes

G. sulfurreducens is a model organism to study extracellular electron transfer, as it can grow by forming multilayered biofilms when a poised electrode serves as the sole electron acceptor [40]. Most of the earlier studies visualizing *G. sulfurreducens* biofilms either involved staining biofilms [171–173] with a fluorescent dye or imaging them using scanning electron microscopy [40, 173, 185]. All of these techniques require disruptive processing of biofilms by either fixing them before visualization or multiple steps of staining and washing the biofilms with fluorescent dyes and then placing them directly on a microscope slide for visualization, which could yield highly variable results. The improved fluorescent protein production in *G. sulfurreducens*, combined with a customized 3D-printed electrode holder, and an artificial intelligence software for noise reduction, denoise.ai (Nikon) allowed direct visualization of *G. sulfurreducens* biofilms and its micro-structures by keeping the biofilms intact.

The *vGFP* and *mScarlet* genes were expressed constitutively but not matured as oxygen is required for cyclization and maturation of the fluorophore [186, 187]. Incorporation of an oxygen atom during cyclization of the fluorophore releases hydrogen peroxide causing oxidative stress to the cells. Since *G. sulfurreducens* cultures were grown under strict anaerobic conditions, maturation reaction could not take place. No growth defect was observed between *G. sulfurreducens* strains labeled with vGFP or mScarlet and non-labeled strain suggesting strains expressing *vGFP* or *mScarlet* did not experience oxidative stress. *G. sulfurreducens* expressing either *vGFP* or *mScarlet*

were inoculated into bioreactors with electrodes poised at +0.24 V *vs.* SHE, and current production was recorded over time as a measure for growth [95, 114]. Similar current densities were observed for WT expressing either *vGFP* or *mScarlet* as compared to non-fluorescent WT strain suggesting no growth defect from constitutive expression of both the fluorophores. When the current density reached ~350 $\mu A.cm^{-2}$ (60 h after inoculation), electrodes were harvested for imaging, and exposure to oxygen at the end after electrodes were harvested was sufficient for maturation of the fluorophores making visualization possible.

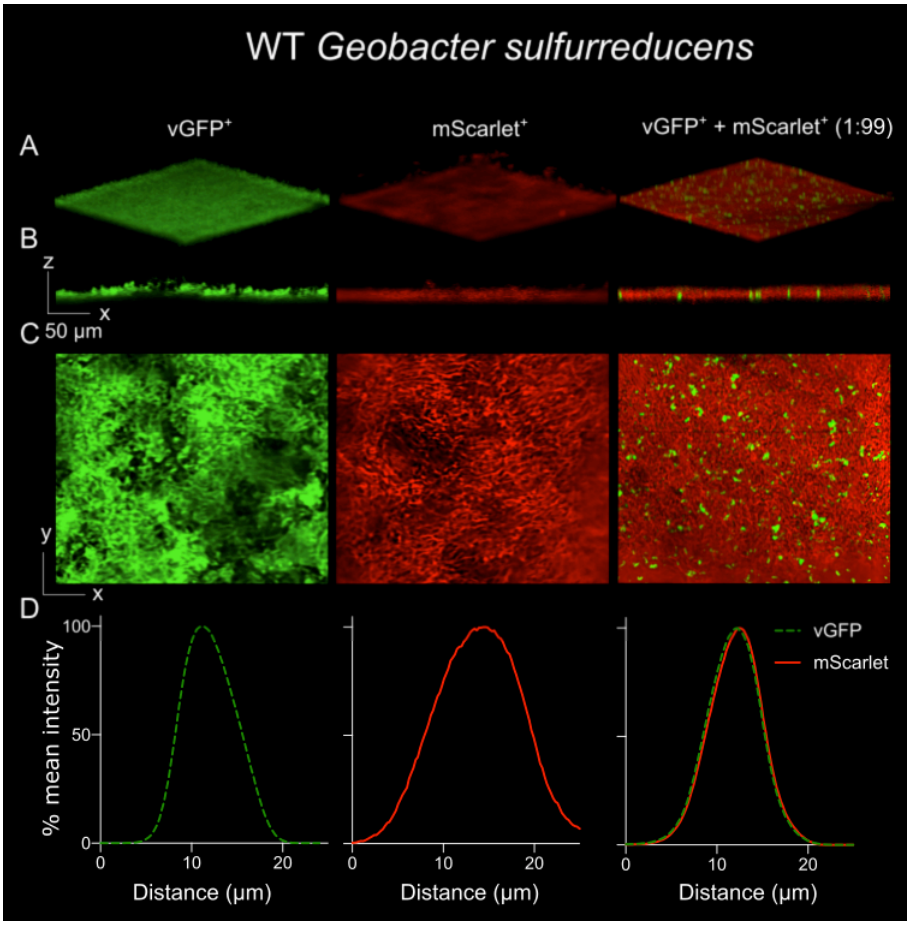

Figure 4.4: ***G. sulfurreducens* biofilms when grown on electrodes can be visualized with improved versions of vGFP and mScarlet.** A. Confocal fluorescence microscopy images for WT *G. sulfurreducens* labeled with vGFP (left), labeled with mScarlet (middle), and biofilms when WT:vGFP and WT:mScarlet were co-inoculated in a ratio of 1:99. B. Biofilms images are represented as volume view, side view (x-z plane), C. top view (x-y plane). D. Mean intensity z-axis profiles for each biofilm as a function of distance show a bell shaped curve. When the WT:vGFP and WT:mScarlet were co-inoculated, *G. sulfurreducens* biofilms structured as pillars can be visualized, and the intensity profiles for vGFP and mScarlet shows overlap of the profiles suggesting WT:vGFP cells and WT:mScarlet cells grow upwards from the surface of the electrode.

Both WT:vGFP and WT:mScarlet biofilms show uniform coverage of the electrode surface (Figure 4.4A). The top panel in Figure 4.4A shows a full z-stack of the imaged 512 µm × 512 µm area of the electrode. The thickness of the biofilm was measured to be ~15–20 µm. Middle panel (Figure 4.4B) shows side view of the biofilm representing the thickness of the biofilms.

Top view (Figure 4.4C) represented by the x-y plane shows an image of a single z-step for both WT:vGFP and WT:mScarlet. Using the electrode holder and denoising software allowed resolution of microstructures within the biofilms. Mean intensity z-axis profiles of each fluorophore represents spatial distribution of the labeled cells as measured by average emission intensity of vGFP or mScarlet at each z-step volume from electrode surface to the top of the biofilms (Figure 4.4D).

4.4.2 Co-inoculation of green and red fluorescent *G. sulfurreducens* reveals pillar-structured biofilms

After visualization of WT:vGFP and WT:mScarlet biofilms independently, we could now visualize how *G. sulfurreducens* cells colonize electrodes and how the biofilms are structured when a poised electrode is the sole electron acceptor. When bioreactors were inoculated with a mixture of otherwise isogenic WT *G. sulfurreducens* strains expressing either vGFP or mScarlet at a 1:99 ratio, confocal microscopy of the electrode biofilm at 60 hours post inoculation revealed that cells grew upwards away from the electrode surface forming pillars of clonal cells (Figure 4.4A). Co-inoculation of 1% WT:vGFP and 99% WT:mScarlet helped to demonstrate the dynamics of early attachment phase of electroactive biofilm formation of *G. sulfurreducens* cells.

Pillar like structures formed when a mixture of both green and red fluorescent protein expressing WT cells suggested once cells attach to the electrode surface, the daughtering cells are pushed outward without any apparent mixing of cells expressing *mScarlet* in the green cell pillars (Figure 4.4A). These results showing pillar-structured biofilm formation corroborates earlier reports that *G. sulfurreducens* forms mushroom-like vertical structures as the biofilms mature [171, 173,

188] grow upwards instead of growing horizontally on the surface of the electrode. It is recently reported that when two differentially growing *Shewanella oneidensis* strains were co-inoculated into bioreactors, the ratio of surface attached cells remained stable with perturbations and strain growth rate differences [178]. The formation of sparse green pillar structures without any mixing with WT:mScarlet cells aligns with reported results of no interactions within competing cells once the electrode surface is claimed. Plotting mean intensity values for both red and green fluorophore over distance from the electrode surface shows complete overlap of the intensity profiles (Figure 4.4B) suggesting independent parallel growth of both WT:vGFP and WT:mScarlet strains perpendicular to the surface of the electrode.

4.4.3 Inner membrane cytochrome *G. sulfurreducens* mutants form distinct redox dependent stratified layered biofilms at high potential (+0.24 V *vs.* SHE).

The *G. sulfurreducens* cells cease to contribute to current production as the biofilm thickness approaches 20 μm, suggesting a distance penalty as cells grow farther away from the electrode surface. Earlier studies have reported that *G. sulfurreducens* cells experience a redox gradient when growing in a biofilm [123, 176, 189]. Conductive biofilm studies using Raman spectroscopy, scan rate analysis, and modeling studies also suggests *G. sulfurreducens* cells experience metabolic and redox heterogeneity within the biofilm [121, 124, 174, 190]. *G. sulfurreducens* genome encodes over seventy multiheme cytochromes [36], out of which three multiheme cytochromes have been characterized to be essential for growth at different redox potentials. ImcH, a seven heme *c*–type cytochrome is required for growth with high potential

electron acceptors above −0.1 V *vs.* SHE [33], CbcL, a *bc*–type cytochrome complex with nine *c*–type hemes, and a diheme *b*–type cytochrome essential for respiration of low potential electron acceptors below −0.1 V *vs.* SHE [34], and CbcBA, seven heme containing *bc*–type cytochrome complex required for reduction of electron acceptors below −0.21 V *vs.* SHE [35].

We hypothesized that the redox potential decreases as cells layers upwards away from the surface of electrode poised at +0.24 V *vs.* SHE, and that cells utilize different inner membrane cytochrome-dependent electron transfer pathways at the surface of the electrode *vs*. at the top layer of the biofilm. *G. sulfurreducens* mutant lacking CbcL and CbcBA (Δ*cbcBA* Δ*cbcL*) able to only respire high potential electron acceptors was engineered to express *mScarlet* ($ImcH^+$:mScarlet), and mutant lacking ImcH and CbcBA (Δ*cbcBA* Δ*imcH*) able to only respire low potential electron acceptors was engineered to express *vGFP* ($CbcL^+$:vGFP) constitutively allowing tracking spatial location of these strains within a biofilm.

$ImcH^+$:mScarlet respires high potential electrodes, forming biofilms of comparable thickness to WT *G. sulfurreducens* biofilms in images around 60 h after growth on electrodes poised at +0.24 V *vs.* SHE. In contrast, when $CbcL^+$:vGFP was inoculated with electrodes poised at +0.24 V *vs.* SHE, it failed to respire electrodes, and did not form any biofilm when imaged around 80 h after inoculation (Figure 4.5A,E). When both $ImcH^+$:mScarlet and $CbcL^+$:vGFP strains were mixed in a ratio of 1:2 and inoculated into bioreactors with electrodes poised at high redox potential. When the electrode was imaged 60 h after inoculation, both strains stratified into two separate layers in a biofilm with $ImcH^+$ cells only growing in a layer closest to the electrode whereas $CbcL^+$ cells formed a layer above the $ImcH^+$ layer (Figure 4.5B). The distinct stratification into layers parallel

to the surface of the electrode suggested cells experience low reduction potentials >10 μm away from the electrode surface. Viewing each image slice as a montage shows the absence of green fluorescing $CbcL^+$ cells in the early layers of the biofilm, followed by layers where both strains co-exist, and then an absence of red fluorescing $ImcH^+$ cells in the top layers of the biofilm furthest away from the electrode (Figure 4.5C). Mean intensity profiles of each fluorescent protein also both strains dominated in different spatial locations in the biofilm (Figure 4.5D).

To test if the $CbcL^+$ cells growing above $ImcH^+$ cell layers can still transfer electrons to the electrode, electron transfer kinetics was measured using cyclic voltammetry by scanning the working electrode potential from -0.5 V to $+0.24$ V *vs.* SHE at 1 mV/s and recording the current output at each redox potential [48, 95, 114]. WT *G. sulfurreducens* biofilms have an onset potential of -0.28 V *vs.* SHE when acetate is the electron donor [114], whereas the mutant lacking both low potential favoring inner membrane cytochromes, $ImcH^+$ (Δ*cbcBA* Δ*cbcL*) have onset potential positively shifted to -0.15 V [35]. The mixture of $ImcH^+$(Δ*cbcBA* Δ*cbcL*) and $CbcL^+$(Δ*cbcBA* Δ*imcH*) cells shows an intermediate phenotype, with onset potential shifting negatively to -0.21 V, suggesting $CbcL^+$ cells growing in a layer away from the electrode are still able to transfer electrons through the $ImcH^+$ cells layers (Figure 4.5F).

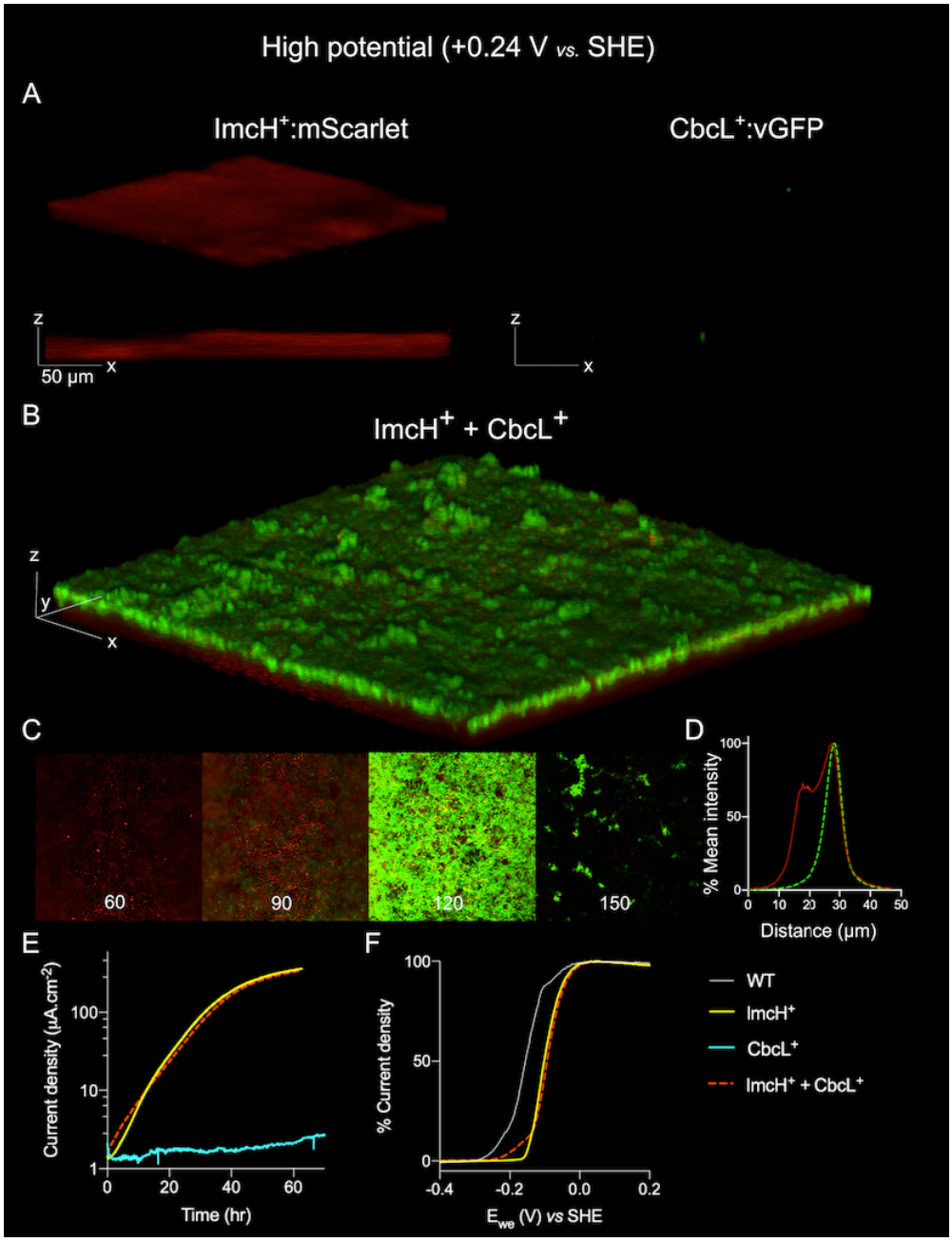

Figure 4.5: ***G. sulfurreducens* mutants containing either ImcH or CbcL when co-inoculated form redox dependent distinctive layered biofilms at high redox potential (+0.24 V *vs.* SHE).** A. Confocal microscopy images of ImcH$^+$:mScarlet and CbcL$^+$:vGFP biofilms when inoculated into bioreactors independently and electrodes were poised at +0.24 V. ImcH$^+$:mScarlet cells attached to the electrodes and developed biofilms comparable to WT whereas CbcL$^+$:vGFP cells failed to form a biofilm and grow at high redox potential shown as 3D volume view of z-stack as well as the side view (x-z plane). B. When ImcH$^+$:mScarlet and CbcL$^+$:vGFP cells were co-inoculated, confocal microscopy images of the biofilms formed show layered structure with ImcH$^+$ cells growing in a separate layer closest to the electrode whereas CbcL$^+$ cells attach and grow multilayered biofilms on top of ImcH$^+$ biofilms. C. Top view (x-y plane) of different slices throughout the z-stack showing a progression of the formation of biofilm structure. D. Mean intensity profile of vGFP

and mScarlet fluorophores measured across the z-axis. E. Growth of ImcH$^+$, CbcL$^+$, and ImcH$^+$ + CbcL$^+$ biofilms measured over time when the electrodes were poised at +0.24 V *vs.* SHE. CbcL$^+$ cells were unable to grow at high potential whereas ImcH$^+$ as well as ImcH$^+$ + CbcL$^+$ mixed culture biofilms produced comparable current densities at ~60 h when the biofilms were imaged. F. Cyclic voltammetry of ImcH$^+$ + CbcL$^+$ biofilms show an intermediate phenotype between ImcH$^+$ biofilms and WT biofilms grown at high redox potential. Experiments were performed in triplicates and representative data is shown here.

4.4.4 Time series of biofilm formation shows CbcL$^+$ cells initiate attachment and colonization after 40 h of co-inoculation with ImcH$^+$ cells at high potential.

ImcH$^+$ and CbcL$^+$ cells stratify into two distinct zones in a high potential growing biofilm when imaged at 60 h (Figure 4.5B). We hypothesized that CbcL$^+$ cells only attach and colonize when the redox potential favorable for growth of CbcL$^+$ cells is established (<-0.1 V *vs.* SHE). To test our hypothesis of redox potential dependent colonization by *G. sulfurreducens* mutants, six reactors were inoculated with ImcH$^+$ and CbcL$^+$ strains at a ratio of 1:2, and two electrodes each were harvested at 42 h, 66 h, and 90 h for imaging. These three times were chosen to represent different growth stages of *G. sulfurreducens* biofilms– exponential (between 100–300 $\mu A.cm^{-2}$), late exponential (~330 $\mu A.cm^{-2}$), and stationary phase when current production plateaus (~400 $\mu A.cm^{-2}$) [114] (Figure 4.6A). *G. sulfurreducens* forms monolayer on the surface of electrode when the current densities are below 75 $\mu A.cm^{-2}$ [114].

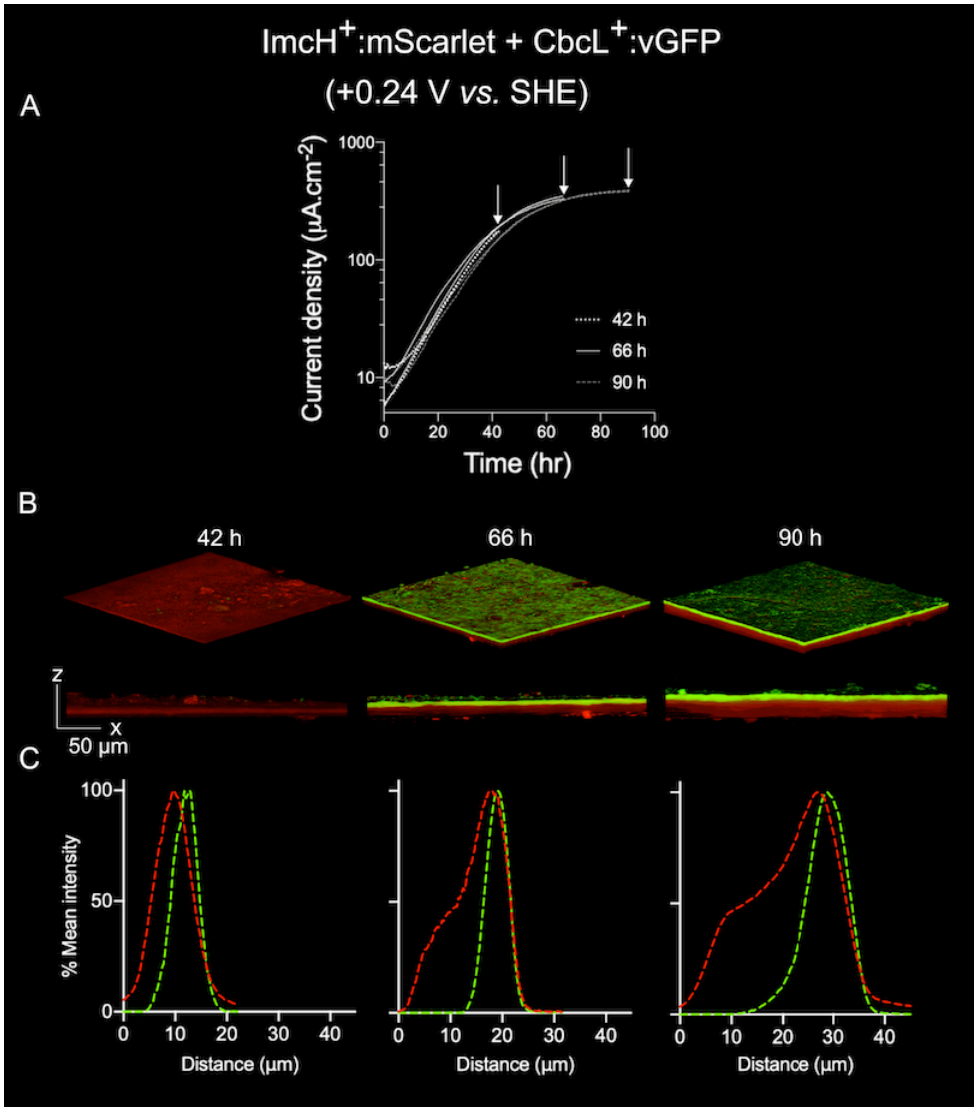

Figure 4.6: **Time series confocal imaging of ImcH$^+$:mScarlet + CbcL$^+$:vGFP biofilm development at high redox potential reveals CbcL$^+$ cells start attachment and growth on to the ImcH$^+$ biofilm only when the redox potential drops.** A. Growth measured as current density (µA.cm^{-2}) over time of *G. sulfurreducens* biofilms when ImcH$^+$:mScarlet and CbcL$^+$:vGFP strains are co-inoculated in the ratio of 1:2. Arrows represent the times when electrodes were harvested from independent bioreactors for imaging. B. Volume view and side view of the full biofilm at 42 h (exponential phase), 66 h (late exponential–early stationary phase), and 90 h (stationary phase). Side view (x-z plane) shows increase in biofilm thickness over time as well as the stratification of ImcH$^+$ and CbcL$^+$ cells in a developed biofilm. C. Mean intensity profile over distance from the electrode surface measured as intensity of each fluorophore along the z-axis (z step = 0.24 µm). Experiments were performed in duplicates (n=2) and representative images from each time point is shown.

If CbcL$^+$ initiate attachment in early stages of biofilm growth, imaging biofilms

~40 h would show a layer of CbcL$^+$:vGFP cells or CbcL$^+$:vGFP cells randomly mixed with ImcH$^+$:mScarlet cells. When electrodes were harvested at 42 h and imaged, the biofilms were thin, composed of red fluorescing ImcH$^+$:mScarlet cells (Figure 4.6B) suggesting CbcL$^+$ cells do not initiate attachment and colonization at this early phase of biofilm growth. The failure of CbcL+ cells to initiate growth during exponential phase also suggests that during exponential growth phase, all cells experience high redox potential. When the biofilms were imaged at ~60 h, when current density reached between 330–350 μA.cm^{-2}, biofilms were seen to be composed of stratified layers, with ImcH$^+$ cells in the layer near the electrode, and CbcL$^+$ cells forming a layer above ImcH$^+$ biofilm layer (Figure 4.6B) indicating the redox potential of the top of the biofilm decreases below -0.1 V *vs.* SHE. The biofilms were also observed to be of increased thickness as compared to biofilms imaged at 42 h (Figure 4.6B, C).

Biofilms imaged at 90 h when the current plateaued (Figure 4.6B) showed increased thickness of individual ImcH$^+$ and CbcL$^+$ layers, suggesting cells in each layer continue to grow even when the total current production is not increasing. These results corroborate earlier reports showing the increase in protein concentration on the electrode, but a plateau of current, and nanoSIMS imaging of long term biofilms suggesting the biofilm thickness continues to increase but the metabolic activity is similar to that of the exponential phase biofilms [114, 120] (Figure 4.6C). Late stage biofilms were delicate to handle as some parts of the biofilm sloughed off on to the cover slip during imaging adding variability and causing difficulty in measuring the thickness of the biofilms (Figure 4.6B,C).

4.4.5 Low potential grown *G. sulfurreducens* biofilms do not produce a layered structure as observed at high potentials.

To test if the low redox potential growth conditions also produced stratified biofilms, *G. sulfurreducens* strains were inoculated into bioreactors for growth at low redox potential (−0.13 V *vs.* SHE). Below redox potentials of −0.13 V *vs.* SHE, ImcH^{+} (Δ*cbcBA* Δ*cbcL*) fails to grow [35]. At low redox potentials, *G. sulfurreducens* alters its electron transfer pathway from ImcH-dependent electron transfer to CbcL- and CbcBA-dependent electron transfer [33–35,41]. WT *G. sulfurreducens,* when inoculated into the bioreactors for growth on electrodes poised at −0.13 V *vs.* SHE produced current densities comparable to CbcL^{+}:vGFP (Δ*cbcBA* Δ*imcH*), and when both ImcH^{+}:mScarlet and CbcL^{+}:vGFP strains were co-inoculated (Figure 4.7C).

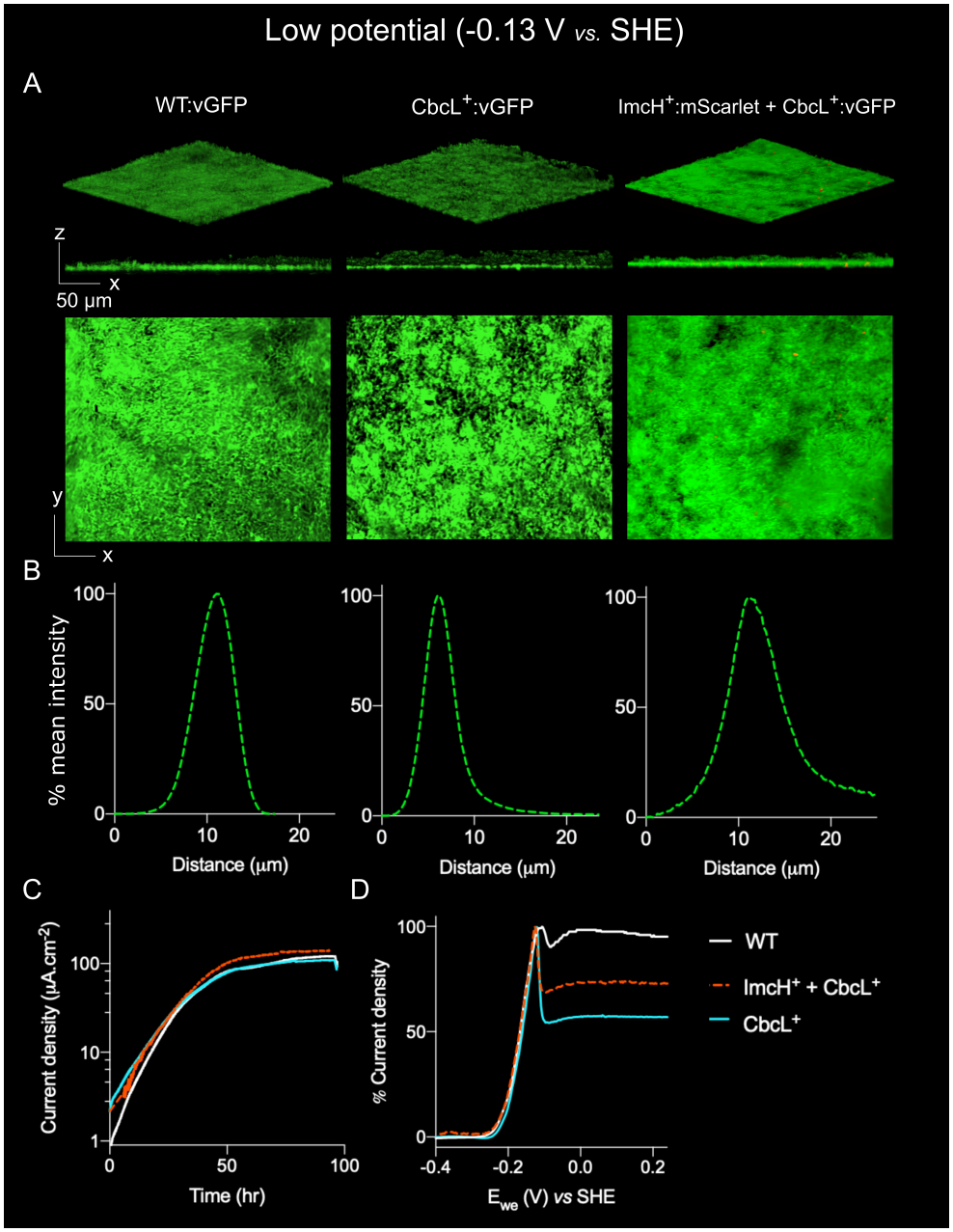

Figure 4.7: **CbcL is essential for growth of *G. sulfurreducens* biofilms at −0.13 V *vs.* SHE.** A. Confocal fluorescence microscopy images of *G. sulfurreducens* biofilms grown at low redox potential (−0.13 V *vs.* SHE). Top panel shows the volume view of WT:vGFP, CbcL$^+$:vGFP, and ImcH$^+$:mScarlet + CbcL$^+$:vGFP biofilms, middle panel shows the side view of all three biofilms, and bottom panel shows x-y plane (top view) of the biofilms. B. Mean fluorescent intensity profile of the biofilms imaged and shown in panel A. C. Current densities produced by each biofilm. D. Reverse scan of cyclic voltammetry curve of WT, CbcL$^+$, and ImcH$^+$ + CbcL$^+$biofilms showing a sharp decrease in current at high potential regions suggesting lack of a high redox potential pathway in CbcL$^+$ and ImcH$^+$ + CbcL$^+$ biofilms. Representative data from experiments conducted in triplicates are shown here.

Due to the slow growth rate of *G. sulfurreducens* at lower redox potentials, the biofilms grown at −0.13 V *vs.* SHE were imaged at ~100 h, when current densities reached around 120 μA.cm^{-2} (Figure 4.7C). WT *G. sulfurreducens* biofilms grown at low redox potential formed thin biofilms (~10 μm) similar to CbcL^{+} biofilms (Figure 4.7A,B). When ImcH^{+} and CbcL^{+} cells were co-inoculated in the ratio of 1:2, if both the strains grew, both red and green fluorescing cells would be present in the biofilm, but only CbcL^{+}:vGFP cells colonized and formed a biofilm. The inability of ImcH^{+} cells to grow and form a biofilm at −0.13 V *vs.* SHE suggests that at low redox potential, the ImcH-dependent electron transfer pathway is not active, consistent with earlier reported data. At low redox potentials, the imaged biofilms were thin, and showed more variability in electrode surface coverage with no cell attachment in some regions as is visible in the volume view and side view of the biofilms, suggesting that *G. sulfurreducens* is more sensitive to low redox potentials as the energy available is close to the thermodynamic limit of acetate respiration (Figure 4.7A). This variability in coverage and thickness also affected the mean intensity profile of the biofilms (Figure 4.7B).

Cyclic voltammetry analysis to measure catalytic current or electron transfer rate at a range of redox potentials for WT *G. sulfurreducens* biofilms (Figure 4.7D) overlaps with the catalytic curve when the biofilms were grown at high redox potential (Figure 4.5F) [95, 114]. When CbcL^{+} (Δ*cbcBA* Δ*imcH*) biofilms were subjected to cyclic voltammetry analysis, there was a drop in current production by about 50% at redox potentials above −0.1 V *vs.* SHE, indicating the lack of ImcH-dependent electron transfer pathway. The same phenotype was observed when both ImcH^{+} and CbcL^{+} cells were co-inoculated for biofilm formation at −0.13 V *vs.* SHE (Figure

4.7D). Overall, at lower redox potentials ImcH$^+$ + CbcL$^+$ did not produce layered stratified biofilms, indicating the redox potential decreases from -0.13 V to even lower redox potentials as cells form layers away from the electrode surface.

4.4.6 Spatial organisation of *G. sulfurreducens* strains within a biofilm is defined by the utilization of specific inner membrane cytochrome-dependent electron transfer pathway.

To confirm that *G. sulfurreducens* biofilms stratify based on redox potential, a WT strain expressing mScarlet and CbcL$^+$ strain expressing vGFP were co-inoculated into bioreactors with electrodes poised at high and low redox potentials. At high redox potential, WT can utilize the ImcH-dependent electron transfer pathway at high redox potentials, and should form biofilms thicker than ImcH$^+$ biofilms, and CbcL$^+$ cells would initiate attachment and colonization on top of WT biofilms when the redox potential is below -0.1 V *vs.* SHE. Biofilms imaged after 60 h of inoculation when the current densities reached ~350 μA.cm^{-2}, show stratified layers with WT at the layer closest to the electrode, and CbcL$^+$ invading layer ~10 μm away from the electrode surface (Figure 4.8A). Visualizing individual z-slices also shows absence of CbcL$^+$ cells (expressing vGFP) in the layers closest to the electrode. Side views of the biofilm also show clear stratification with some pillars of WT:mScarlet cells in the CbcL$^+$ layer, as WT can also respire at low redox potentials by altering from ImcH- to CbcL-dependent electron transfer pathway. Measuring fluorescence intensities for each fluorophore and plotting them as a function of distance also show separation of WT and CbcL$^+$ cells with WT dominating layers near the electrode surface poised at $+0.24$ V

and CbcL$^+$ cells only in layers >10 µm from the electrode (Figure 4.8C).

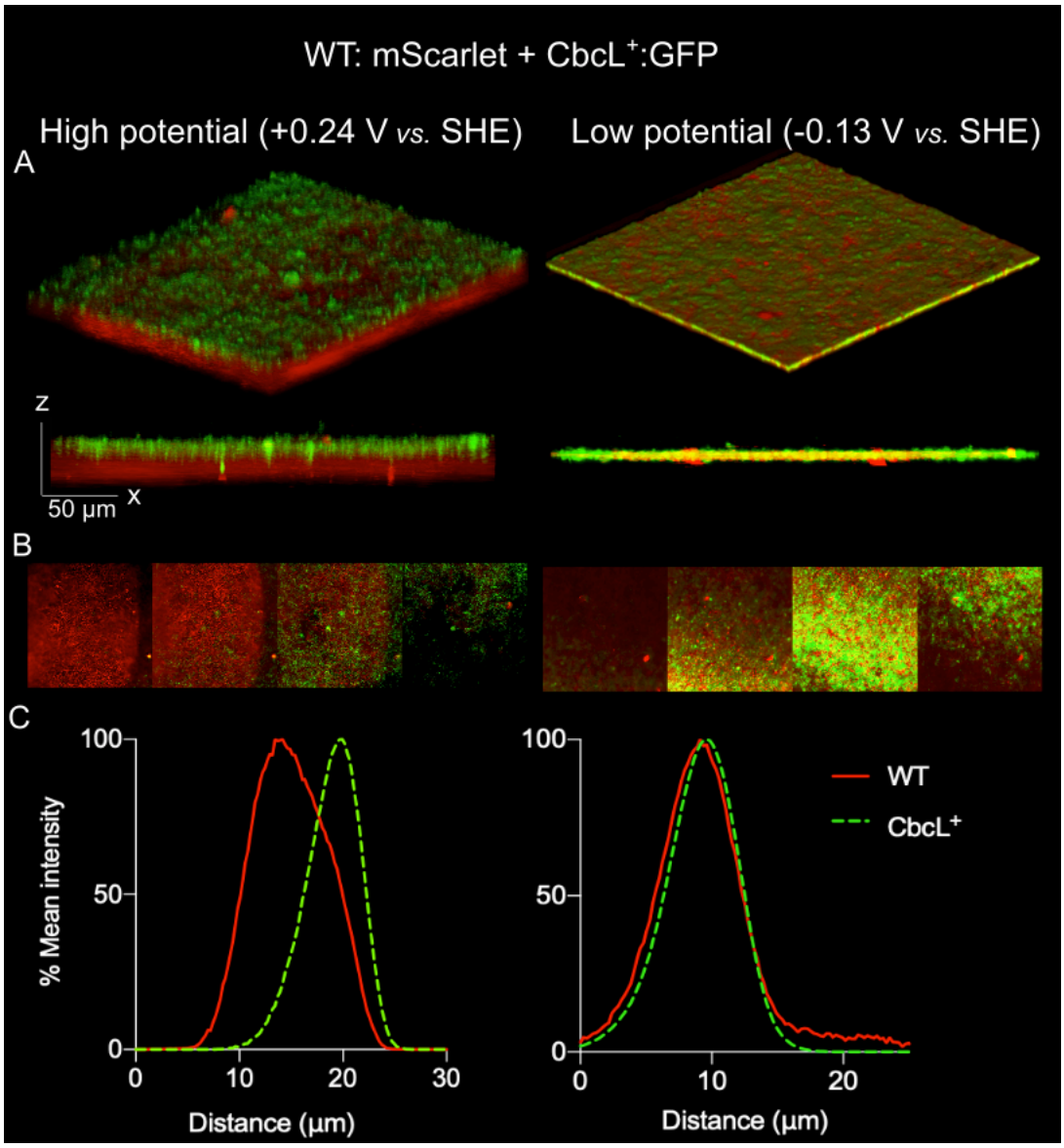

Figure 4.8: **WT and CbcL$^+$ strains when co-inoculated formed stratification patterns depending on the utilization of inner membrane cytochromes required at high *vs.* low redox potentials.** A. Volume view and side view of biofilms grown at high redox potential (+0.24 V *vs.* SHE) and low redox potential (−0.13 V *vs.* SHE). The reactors were inoculated with WT:mScarlet and CbcL$^+$:vGFP strains mixed in a ratio of 1:2. B. Top view (x-y plane) of different z-slices from one closest to the electrode to the top layers showing progression of biofilm structure formation. At high redox potentials, redox dependent stratified layers were observed whereas pillar-like structures at low redox potential grown biofilms were seen. C. Mean profile intensities for vGFP and mScarlet represented as a function of distance from the electrode surface. At high redox potentials, the separation of peaks for both red and green fluorescence intensities show two separate regions where WT and low potential favoring cells are dominant. At low redox potentials, the peaks overlap

consistent with a pillared structured biofilm as viewed in Figure 4.4. The experiments were conducted in triplicates and representative data for each condition is reported here.

When WT:mScarlet and CbcL$^+$:vGFP strains were co-inoculated when electrode was poised at -0.13 V, both WT and CbcL$^+$ grew intermixed at low redox potential, forming a vertical structured biofilm (Figure 4.8A). Both WT:mScarlet and CbcL$^+$:vGFP can equally access electrode surface, and as observed earlier, cells that first attach to the electrode surface stay attached and daughter cells grow outwards perpendicular to the electrode surface (Figure 4.4) [178]. Volume and side views of the biofilm shows both WT:mScarlet and CbcL$^+$:vGFP cells are mixed throughout the biofilm (Figure 4.8A). Mean intensity profile also shows overlap of both the fluorophores consistent with pillar-structured biofilms (Figure 4.8C). These results provide evidence for stratification of *G. sulfurreducens* biofilms depending on the utilization of specific inner membrane cytochromes based on redox potential.

4.5 Discussion

Physiological heterogeneity in biofilms is widely researched [155, 191, 192], and is dependent on a range of factors such as genetic factors, physicochemical environmental factors, or mechanical factors. Chemical gradients like oxygen, pH, sulfate, hydrogen within biofilms are widely reported. Oxygen gradients in aggregates and biofilms have been the most studied chemical gradients in biofilms, visualized by utilizing a fluorescent protein expressed under the control of oxygen concentration sensitive promoter [193], or by direct measurement using microelectrodes [194]. *G. sulfurreducens* cells growing in a biofilm experience a gradient of redox potentials [123], and anabolic activity [120]. It was not clear why *G. sulfurreducens* biofilms self-restrict growth after reaching a certain height (~20 μm) [173], or the factors causing the decline in anabolic activity with respect to distance. In this report, we show that redox potential controls the thickness of biofilms, and that specific inner membrane cytochromes required for respiration at different redox potential windows are utilized in different spatial locations within biofilms.

Preliminary experiments of *G. sulfurreducens* cells expressing green or red fluorescent protein required 100% laser power with high gain settings (>50%) for visualization. Using high laser power caused photobleaching resulting in decrease in fluorescence intensities even before the completion of image acquisition. In addition, *G. sulfurreducens* encodes around seventy *c*–type cytochromes [36]. The emission spectra for cytochromes lies between the wavelengths of 500–650 nm [195, 196], causing autofluorescence of cytochromes to amplify the emission signals for both green and red fluorescent proteins, making it difficult to differentially identify spatial location of

strains expressing green or red fluorescent protein. Protein engineering approaches to improve photostability, maturation time, and brightness involve adding point mutations as well as adding small peptides to N– and C–terminal of the fluorescent proteins [182, 197–199]. For example– replacing a six amino acid peptide (MDSTES) to the N–terminal of superfolder GFP (msfGFP) yielded in a less cytotoxic, photostable brighter variant compared to the earlier versions [199]. Mutations in N–terminal peptides are expected to reduce non-specific interactions, increasing stability of the fluorescent protein. A random addition of seven amino acids MRSGGMA at N–terminal of vsfGFP-0 yielded in a variant that was four times brighter and more photostable in *G. sulfurreducens*. The laser power used to detect *G. sulfurreducens* expressing vsfGFP-02 (vGFP) was only 1.1% compared to 100% in the early experiments, also lowering the absorption and emission by cytochromes at GFP wavelengths.

Spectroscopic studies measuring redox status of actively growing *G. sulfurreducens* biofilms reported *c*–type cytochromes beyond a few cell layers remained in the reduced state even when the electrode potential was oxidizing (+0.24 V *vs.* SHE) [176, 200]. Other studies reported a redox gradient suggesting reduced state of redox active components increases with increased distance [122], and that at 15 μm distance away from the oxidizing electrode (+0.5 V *vs.* SHE) surface, *G. sulfurreducens* cells experience a redox potential of −0.26 V *vs.* SHE [123] showing 56% of the biofilm is reduced 15 μm away from high potential electrode. NanoSIMS analysis of *G. sulfurreducens* biofilms to measure anabolic activity revealed a small amount of anabolic activity between 10–15 μm from the electrode surface [120]. The differential redox dependent stratification of *G. sulfurreducens* biofilms at high redox potential (Figure 4.5) with $ImcH^{+}$ cells growing only

closest to the electrode and $CbcL^+$ cells growing at distances >10 μm from the electrode surface provides an explanation for the reduced redox state and secondary anabolic activity in high potential grown *G. sulfurreducens* biofilms.

Interestingly, even though $ImcH^+$ + $CbcL^+$ biofilms grown at high redox potentials help explain the anabolic activity patterns of *G. sulfurreducens* biofilms [120], cyclic voltammetry of $ImcH^+$ + $CbcL^+$ biofilms showed only partial complementation (Figure 4.5F). Marsili *et al.* reported that exposing biofilms to low or high redox potential briefly did not change the electron transfer mechanism [114]. Low redox potential grown biofilms did not show increase in metabolic activity when the electrode potential was increased to +0.24 V briefly [120], suggesting that there may be different conductive pathways active under different redox potentials. When *G. sulfurreducens* biofilms were grown at +0.1 V *vs.* SHE and then periodically discharged by disconnecting the circuit, there was an overall increase in current density as well as charge carrier concentrations as compared to biofilms grown at constant redox potential [188]. Our intermediate electron transfer kinetics phenotype measured using cyclic voltammetry suggests that *G. sulfurreducens* not only utilizes specific inner membrane cytochrome dependent electron transfer pathways at different spatial locations within a biofilm but also may show a redox based specificity in the conductive network. This specificity could be a result of specific partnerships between inner membrane, periplasmic, outer membrane or extracellular cytochromes.

With improved tools to visualize *G. sulfurreducens* strains using fluorescent protein expression combined with the characterization of many multiheme *c*–type cytochromes, engineering biological sensors using whole cells for measurement of redox potentials in different environment is

now possible. Inner membrane cytochrome specific electron transfer pathways dominating different spatial regions of *G. sulfurreducens* biofilms opens up the possibility to investigate the specificity of other redox active components involved in electron transfer through *Geobacter* biofilms. Fusions of different *G. sulfurreducens* promoters and the improved fluorescent proteins could also be used to detect expression of specific genes involved in electron transfer and biofilm formation.

Chapter 5

Conclusions and Future directions

Komal Joshi

The work presented in the thesis provides answers to some of the long standing questions about electron transfer across the inner membrane in *G. sulfurreducens.* Evidence on how *G. sulfurreducens* alters its respiratory strategy based on the redox potential of the electron acceptors is also presented. With three known inner membrane cytochromes, five periplasmic cytochromes, at least five outer membrane conduits, and at least three extracellular cytochromes playing a role in electron transfer, discovery of other cytochrome complexes might complicate the already complex electron transfer pathways of *G. sulfurreducens.*

Chapter 2 in this thesis characterized another inner membrane cytochrome complex in *G. sulfurreducens*, and for the first time linked the regulation of genes encoding cytochrome complexes involved in electron transfer to a transcription factor. Some questions that still remain unanswered:

1. What other genes are regulated by BccR (GSU0598), and what is the role of GSU0599, a histidine kinase in regulation of *cbcBA* operon? Comparison of transcriptional data of WT *G. sulfurreducens* and Δ*bccR* under Fe(III) citrate growth conditions, revealed some candidate genes whose expression significantly changed in Δ*bccR.* Most of the genes with significantly high or low expression are annotated as hypothetical proteins. The other two candidates *hgtR* (GSU3364) coding for RpoN-dependent transcription repressor shown to be involved when hydrogen is the electron donor, and *cysD* (GSU1717) encoding ATP-sulfurylase small subunit predicted to be involved in sulfate reduction. Further studies utilizing genetic approach could be informative. Other methods could be building library of mutants expressing an antibiotic resistant gene or a nano-luciferase gene under the control of the *cbcBA* operon's promoter, and screening for mutants

with desired phenotypes. The gene upstream of GSU0598 encodes a histidine kinase (GSU0599). Creation of ΔGSU0599 mutant could help determine the role of this histidine kinase in induction of the *cbcBA* operon, and other yet unknown genes. Genetic approaches combined with biochemical analysis would be helpful in determining how BccR senses the redox potential, and what is the cascade of factors involved in the process.

2. Does OmcQ (GSU0592), a twelve heme containing *c*–type cytochrome interact with CbcBA in electron transfer? Transcriptional analysis under fumarate, poised electrodes (+0.24 V *vs.* SHE), and Fe(III) citrate revealed that *omcQ* is constitutively expressed, and it is not a part of the *cbcBA* operon. OmcQ is annotated as part of the Cbc5 quinone oxidoreductase cluster, but its role in electron transfer is still not clear. Δ*omcQ* has been created but requires experimentation to determine if there is a defect in electron transfer under any of the commonly used electron acceptors. Homology searches show *omcQ* next to the *cbcBA* genes in many Desulfuromonadales, suggesting an evolutionary relationship between CbcBA and OmcQ.

Chapter 3 in this thesis provides an explanation for the inactivity of CbcL-dependent electron transfer pathway even when the redox potential is favorable for electron transfer to the extracellular acceptors. Suppressor enrichment analysis identified two key residues (V205, and F525) in CbcL, that might be involved in gating of electrons at high redox potentials. Mutating these residues– V205A, V205G, F525Y allowed CbcL–dependent electron transfer pathway to function at high redox potentials. However, these CbcL variant containing strains did not have increased yield as would be expected from a cytochrome functioning in complementation to Δ*imcH*, suggesting that the H^+/e^- stoichiometry does not change. Structural information for CbcL, and its variants using

X–ray crystallography, or cryoEM techniques would provide concrete evidence for conformational changes in CbcL as a function of redox potential. Mutating specific histidine residues predicted to be involved in heme coordination would be helpful in determining the mid-point potentials of individual hemes, and the subsequent electron flow through the protein as has been recently reported in nitrite reductase, NrfA from *Geobacter lovleyi* [201].

Chapter 4 in this thesis utilized codon optimized engineered fluorescent proteins (mScarlet, and vGFP) to image the structure of *G. sulfurreducens* biofilms. Mixing mutants lacking specific inner membrane cytochromes constitutively expressing different fluorescent proteins confirmed the presence of a redox gradient within *G. sulfurreducens* biofilms. Metabolic stratification, and spatial heterogeneity of *G. sulfurreducens* show that cells experiencing redox potentials > −0.1 V *vs.* SHE utilizes ImcH-dependent pathway at the level of the inner membrane, and cells experiencing low redox potentials < −0.1 V utilizes CbcL-dependent pathway. Under high potential growth conditions, the secondary peak observed at ~10 μm in nanoSIMS analysis of WT *G. sulfurreducens* can now be attributed to the anabolic activity of CbcL-dependent pathway. Initial experiments expressing GFP under the control of *cbcBA* operon's promoter revealed a thinner fluorescent layer as compared to the ones reported in chapter 4 (Figure 5.1).

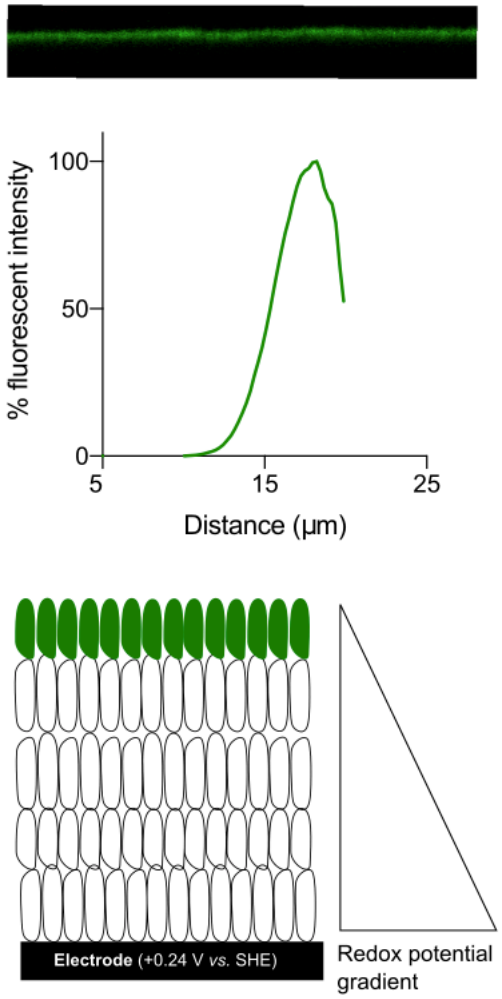

Figure 5.1: **CbcBA is expressed only in the top layer of the *G. sulfurreducens* biofilms.** WT *G. sulfurreducens* strain expressing GFP under the control of *cbcBA* operon promoter (GSU0597) were inoculated into bioreactors for growth on electrodes poised at +0.24 V. The biofilms were imaged using fluorescence microscopy showed green fluorescence present only in the top few layers of the biofilms. Top panel shows side view of the biofilms, bottom panel represents % fluorescence intensity of GFP as a function of distance, and bottom panel shows a cartoon model of the biofilm with lowest potential experiencing cells farthest from the electrode surface.

While cells expressing GFP were found to be located at the top layers of the biofilm, the electrode surface could not be accurately determined due to the lack of constitutive expression of a fluorescent protein. Developing strategies for expressing both fluorescent proteins in one *Geobacter* cell– one under the control of constitutive promoter, and the other one under regulated promoter, only

expressed under specific growth conditions would be useful in imaging the full biofilm stack from the electrode surface to the top of the biofilm. The engineered strains could also be grown in Fe(III) citrate medium which represents a range of redox potentials (high potential under fully oxidized state, and decreases as Fe(III) citrate gets reduced), and the population ratio of different strains at different stages of growth could be measured via flow cytometry. The results obtained could be utilized to precisely quantify the population ratios without the variability introduced during biofilm imaging.

The structures of multiheme cytochrome complexes including MtrCAB complex from *Shewanella* spp. [26], and OmcS "cytochrome nanowires" from *G. sulfurreducens* [23] using cryogenic electron microscopy (cryoEM) have recently been reported. These structures provide a strategy for elucidation of cryoEM structures of other multiheme cytochromes like OmcZ, CbcL, ImcH, CbcBA, OmcB, ExtA etc. Biochemical information gained from the structures will help in determining the electron transfer through these cytochromes at molecular level. The structural information would provide candidates for engineering protein variants for synthetic electron transfer chains.

Bibliography

[1] Thauer, RK, Jungermann, K, Decker, K (**1977**), Energy conservation in chemotrophic anaerobic bacteria. *Bacteriological Reviews*, 41(1):100–180, doi:10.1128/mmbr.41.3.809-809.1977.

[2] Schoepp-Cothenet, B, van Lis, R, Atteia, A, *et al.* (**2013**), On the universal core of bioenergetics. *Biochimica et Biophysica Acta (BBA)-Bioenergetics*, 1827(2):79–93, doi:10.1016/j.bbabio.2012.09.005.

[3] Mitchell, P (**1961**), Coupling of phosphorylation to electron and hydrogen transfer by a chemi-osmotic type of mechanism. *Nature*, 191(4784):144–148, doi:10.1038/191144a0.

[4] Mitchell, P (**1966**), Chemiosmotic coupling in oxidative and photosynthetic phosphorylation. *Biological Reviews of the Cambridge Philosophical Society*, 41(3):445–502, doi:10.1111/j.1469-185x.1966.tb01501.x.

[5] Ingledew, WJ, Poole, RK (**1984**), The respiratory chains of *Escherichia coli*. *Microbiological Reviews*, 48(3):222–271, doi:10.1128/mr.48.3.222-271.1984.

[6] White, D, Drummond, JT, Fuqua, C (**2012**), *The physiology and biochemistry of prokaryotes*. Oxford University Press, New York, ISBN 9780195393040.

[7] Hau, HH, Gralnick, JA (**2007**), Ecology and biotechnology of the genus *Shewanella*. *Annual Review of Microbiology*, 61:237–258, doi:10.1146/annurev.micro.61.080706.093257.

[8] Hunt, KA, Flynn, JM, Naranjo, B, *et al.* (**2010**), Substrate-level phosphorylation is the primary source of energy conservation during anaerobic respiration of *Shewanella oneidensis* strain MR-1. *Journal of Bacteriology*, 192(13):3345–3351, doi:10.1128/JB.00090-10.

[9] Peters, JW, Miller, AF, Jones, AK, *et al.* (**2016**), Electron bifurcation. *Current Opinion in Chemical Biology*, 31:146–152, doi:10.1016/j.cbpa.2016.03.007.

[10] Buckel, W, Thauer, RK (**2018**), Flavin-based electron bifurcation, a new mechanism of biological energy coupling. *Chemical Reviews*, 118(7):3862–3886, doi:10.1021/acs.chemrev.7b00707.

[11] Mitchell, P (**1975**), The protonmotive Q cycle: a general formulation. *FEBS letters*, 59(2):137–139, doi:10.1016/0014-5793(75)80359-0.

[12] Li, F, Hinderberger, J, Seedorf, H, *et al.* (**2008**), Coupled ferredoxin and crotonyl coenzyme A (CoA) reduction with NADH catalyzed by the butyryl-CoA dehydrogenase/Etf complex from *Clostridium kluyveri*. *Journal of Bacteriology*, 190(3):843–850, doi:10.1128/JB.01417-07.

[13] Lovley, DR, Phillips, EJ (**1988**), Novel mode of microbial energy metabolism: organic carbon oxidation coupled to dissimilatory reduction of iron or manganese. *Applied and Environmental Microbiology*, 54(6):1472–1480, doi:10.1128/aem.54.6.1472-1480.1988.

[14] Lovley, DR (**1991**), Dissimilatory Fe(III) and Mn(IV) reduction. *Microbiological Reviews*, 55(2):259–287, doi:10.1128/mr.55.2.259-287.1991.

[15] Nealson, KH, Saffarini, D (**1994**), Iron and manganese in anaerobic respiration: environmental significance, physiology, and regulation. *Annual Review of Microbiology*, 48:311–343, doi:10.1146/annurev.mi.48.100194.001523.

[16] Mehta-Kolte, MG, Bond, DR (**2012**), *Geothrix fermentans* secretes two different redox-active compounds to utilize electron acceptors across a wide range of redox potentials. *Applied and Environmental Microbiology*, 78(19):6987–6995, doi:10.1128/AEM.01460-12.

[17] Marsili, E, Baron, DB, Shikhare, ID, *et al.* (**2008**), *Shewanella* secretes flavins that mediate extracellular electron transfer. *Proceedings of the National Academy of Sciences of the United States of America*, 105(10):3968–3973, doi:10.1073/pnas.0710525105.

[18] Covington, ED, Gelbmann, CB, Kotloski, NJ, *et al.* (**2010**), An essential role for UshA in processing of extracellular flavin electron shuttles by *Shewanella oneidensis*. *Molecular Microbiology*, 78(2):519–532, doi:10.1111/j.1365-2958.2010.07353.x.

[19] Wang, Y, Kern, SE, Newman, DK (**2010**), Endogenous phenazine antibiotics promote anaerobic survival of *Pseudomonas aeruginosa* via extracellular electron transfer. *Journal of Bacteriology*, 192(1):365–369, doi:10.1128/JB.01188-09.

[20] Light, SH, Su, L, Rivera-Lugo, R, *et al.* (**2018**), A flavin-based extracellular electron transfer mechanism in diverse Gram-positive bacteria. *Nature*, 562(7725):140–144, doi:10.1038/s41586-018-0498-z.

[21] Gorby, YA, Yanina, S, McLean, JS, *et al.* (**2006**), Electrically conductive bacterial nanowires produced by *Shewanella oneidensis* strain MR-1 and other microorganisms. *Proceedings of the National Academy of Sciences of the United States of America*, 103(30):11,358–11,363, doi:10.1073/pnas.0604517103.

[22] Subramanian, P, Pirbadian, S, El-Naggar, MY, *et al.* (**2018**), Ultrastructure of *Shewanella oneidensis* MR-1 nanowires revealed by electron cryotomography. *Proceedings of the National Academy of Sciences of the United States of America*, 115(14):E3246–E3255, doi:10.1073/pnas.1718810115.

[23] Wang, F, Gu, Y, O'Brien, JP, *et al.* (**2019**), Structure of microbial nanowires reveals stacked hemes that transport electrons over micrometers. *Cell*, 177(2):361–369.e10, doi:10.1016/j.cell.2019.03.029.

[24] Yalcin, SE, O'Brien, JP, Gu, Y, *et al.* (**2020**), Electric field stimulates production of highly conductive microbial OmcZ nanowires. *Nature Chemical Biology*, 16(10):1136–1142, doi:10.1038/s41589-020-0623-9.

[25] Edwards, MJ, White, GF, Lockwood, CW, *et al.* (**2018**), Structural modeling of an outer membrane electron conduit from a metal-reducing bacterium suggests electron transfer via periplasmic redox partners. *The Journal of Biological Chemistry*, 293(21):8103–8112, doi:10.1074/jbc.RA118.001850.

[26] Edwards, MJ, White, GF, Butt, JN, *et al.* (**2020**), The crystal structure of a biological insulated transmembrane molecular wire. *Cell*, 181(3):665–673.e10, doi:10.1016/j.cell.2020.03.032.

[27] Aklujkar, M, Coppi, MV, Leang, C, *et al.* (**2013**), Proteins involved in electron transfer to Fe(III) and Mn(IV) oxides by *Geobacter sulfurreducens* and *Geobacter uraniireducens*. *Microbiology*, 159(Pt 3):515–535, doi:10.1099/mic.0.064089-0.

[28] Kim, BC, Leang, C, Ding, YHR, *et al.* (**2005**), OmcF, a putative *c*-type monoheme outer membrane cytochrome required for the expression of other outer membrane cytochromes in *Geobacter sulfurreducens*. *Journal of Bacteriology*, 187(13):4505–4513, doi:10.1128/JB.187.13.4505-4513.2005.

[29] Kim, BC, Qian, X, Leang, C, *et al.* (**2006**), Two putative *c*-type multiheme cytochromes required for the expression of OmcB, an outer membrane protein essential for optimal Fe(III) reduction in *Geobacter sulfurreducens*. *Journal of Bacteriology*, 188(8):3138–3142, doi:10.1128/JB.188.8.3138-3142.2006.

[30] Otero, FJ, Chan, CH, Bond, DR (**2018**), Identification of different putative outer membrane electron conduits necessary for Fe(III) citrate, Fe(III) oxide, Mn(IV) oxide, or electrode reduction by *Geobacter sulfurreducens*. *Journal of Bacteriology*, 200(19), doi:10.1128/JB.00347-18.

[31] Myers, CR, Myers, JM (**1997**), Cloning and sequence of *cymA*, a gene encoding a tetraheme cytochrome *c* required for reduction of iron(III), fumarate, and nitrate by *Shewanella putrefaciens* MR-1. *Journal of Bacteriology*, 179(4):1143–1152, doi:10.1128/jb.179.4.1143-1152.1997.

[32] Marritt, SJ, Lowe, TG, Bye, J, *et al.* (**2012**), A functional description of CymA, an electron-transfer hub supporting anaerobic respiratory flexibility in *Shewanella*. *The Biochemical Journal*, 444(3):465–474, doi:10.1042/BJ20120197.

[33] Levar, CE, Chan, CH, Mehta-Kolte, MG, *et al.* (**2014**), An inner membrane cytochrome required only for reduction of high redox potential extracellular electron acceptors. *mBio*, 5(6), doi:10.1128/mBio.02034-14.

[34] Zacharoff, L, Chan, CH, Bond, DR (**2016**), Reduction of low potential electron acceptors requires the CbcL inner membrane cytochrome of *Geobacter sulfurreducens*. *Bioelectrochemistry*, 107:7–13, doi:10.1016/j.bioelechem.2015.08.003.

[35] Joshi, K, Chan, CH, Bond, DR (**2021**), *Geobacter sulfurreducens* inner membrane cytochrome CbcBA controls electron transfer and growth yield near the energetic limit of respiration. *bioRxiv*, doi:10.1101/2021.04.15.440034.

[36] Methé, BA, Nelson, KE, Eisen, JA, *et al.* (**2003**), Genome of *Geobacter sulfurreducens*: Metal reduction in subsurface environments. *Science*, 302(5652):1967–1969, doi:10.1126/science.1088727.

[37] Ding, YHR, Hixson, KK, Giometti, CS, *et al.* (**2006**), The proteome of dissimilatory metal-reducing microorganism *Geobacter sulfurreducens* under various growth conditions. *Biochimica et Biophysica Acta (BBA)-Proteins and Proteomics*, 1764(7):1198–1206, doi:10.1016/j.bbapap.2006.04.017.

[38] Ding, YHR, Hixson, KK, Aklujkar, MA, *et al.* (**2008**), Proteome of *Geobacter sulfurreducens* grown with Fe(III) oxide or Fe(III) citrate as the electron acceptor. *Biochimica et Biophysica Acta (BBA)-Proteins and Proteomics*, 1784(12):1935–1941, doi:10.1016/j.bbapap.2008.06.011.

[39] Caccavo, F, Lonergan, DJ, Lovley, DR, *et al.* (**1994**), *Geobacter sulfurreducens* sp. nov., a hydrogen- and acetate-oxidizing dissimilatory metal-reducing microorganism. *Applied and Environmental Microbiology*, 60(10):3752–3759, doi:10.1128/aem.60.10.3752-3759.1994.

[40] Bond, DR, Lovley, DR (**2003**), Electricity production by *Geobacter sulfurreducens* attached to electrodes. *Applied and Environmental Microbiology*, 69(3):1548–1555, doi:10.1128/aem.69.3.1548-1555.2003.

[41] Levar, CE, Hoffman, CL, Dunshee, AJ, *et al.* (**2017**), Redox potential as a master variable controlling pathways of metal reduction by *Geobacter sulfurreducens*. *The ISME Journal*, 11(3):741–752, doi:10.1038/ismej.2016.146.

[42] Summers, ZM, Fogarty, HE, Leang, C, *et al.* (**2010**), Direct exchange of electrons within aggregates of an evolved syntrophic coculture of anaerobic bacteria. *Science*, 330(6009):1413–1415, doi:10.1126/science.1196526.

[43] Rotaru, AE, Shrestha, PM, Liu, F, *et al.* (**2012**), Interspecies electron transfer via hydrogen and formate rather than direct electrical connections in cocultures of *Pelobacter carbinolicus* and *Geobacter sulfurreducens*. *Applied and Environmental Microbiology*, 78(21):7645–7651, doi:10.1128/AEM.01946-12.

[44] Leang, C, Coppi, MV, Lovley, DR (**2003**), OmcB, a *c*-type polyheme cytochrome, involved in Fe(III) reduction in *Geobacter sulfurreducens*. *Journal of Bacteriology*, 185(7):2096–2103, doi:10.1128/JB.185.7.2096-2103.2003.

[45] Liu, Y, Wang, Z, Liu, J, *et al.* (**2014**), A trans-outer membrane porin-cytochrome protein complex for extracellular electron transfer by *Geobacter sulfurreducens* PCA. *Environmental Microbiology Reports*, 6(6):776–785, doi:10.1111/1758-2229.12204.

[46] Chan, CH, Levar, CE, Jiménez-Otero, F, *et al.* (**2017**), Genome scale mutational analysis of *Geobacter sulfurreducens* reveals distinct molecular mechanisms for respiration and sensing of poised electrodes versus Fe(III) oxides. *Journal of Bacteriology*, 199(19), doi:10.1128/JB.00340-17.

[47] Mehta, T, Coppi, MV, Childers, SE, *et al.* (**2005**), Outer membrane *c*-type cytochromes required for Fe(III) and Mn(IV) oxide reduction in *Geobacter sulfurreducens*. *Applied and Environmental Microbiology*, 71(12):8634–8641, doi:10.1128/AEM.71.12.8634-8641.2005.

[48] Richter, H, Nevin, KP, Jia, H, *et al.* (**2009**), Cyclic voltammetry of biofilms of wild type and mutant *Geobacter sulfurreducens* on fuel cell anodes indicates possible roles of OmcB, OmcZ, type IV pili, and protons in extracellular electron transfer. *Energy & Environmental Science*, 2(5):506, doi:10.1039/b816647a.

[49] Inoue, K, Qian, X, Morgado, L, *et al.* (**2010**), Purification and characterization of OmcZ, an outer-surface, octaheme *c*-type cytochrome essential for optimal current production by *Geobacter sulfurreducens*. *Applied and Environmental Microbiology*, 76(12):3999–4007, doi:10.1128/aem.00027-10.

[50] Qian, X, Mester, T, Morgado, L, *et al.* (**2011**), Biochemical characterization of purified OmcS, a *c*-type cytochrome required for insoluble Fe(III) reduction in *Geobacter*

sulfurreducens. *Biochimica et Biophysica Acta (BBA)-Bioenergetics*, 1807(4):404–412, doi:10.1016/j.bbabio.2011.01.003.

[51] Zacharoff, LA, Morrone, DJ, Bond, DR (**2017**), *Geobacter sulfurreducens* extracellular multiheme cytochrome PgcA facilitates respiration to Fe(III) Oxides but not electrodes. *Frontiers in Microbiology*, 8, doi:10.3389/fmicb.2017.02481.

[52] Lloyd, JR, Leang, C, Hodges Myerson, AL, *et al.* (**2003**), Biochemical and genetic characterization of PpcA, a periplasmic *c*-type cytochrome in *Geobacter sulfurreducens*. *Biochemical Journal*, 369(Pt 1):153–161, doi:10.1042/BJ20020597.

[53] Butler, JE, Young, ND, Lovley, DR (**2010**), Evolution of electron transfer out of the cell: comparative genomics of six *Geobacter* genomes. *BMC Genomics*, 11:40, doi:10.1186/1471-2164-11-40.

[54] Trumpower, BL (**1990**), Cytochrome bc_1 complexes of microorganisms. *Microbiological Reviews*, 54(2):101–129, doi:10.1128/MMBR.54.2.101-129.1990.

[55] Schütz, M, Brugna, M, Lebrun, E, *et al.* (**2000**), Early evolution of cytochrome *bc* complexes. *Journal of Molecular Biology*, 300(4):663–675, doi:10.1006/jmbi.2000.3915.

[56] Mitchell, P (**1976**), Possible molecular mechanisms of the protonmotive function of cytochrome systems. *Journal of Theoretical Biology*, 62(2):327–367, doi:10.1016/0022-5193(76)90124-7.

[57] Martinez, SE, Huang, D, Szczepaniak, A, *et al.* (**1994**), Crystal structure of chloroplast cytochrome *f* reveals a novel cytochrome fold and unexpected heme ligation. *Structure*, 2(2):95–105, doi:10.1016/s0969-2126(00)00012-5.

[58] Zhang, Z, Huang, L, Shulmeister, VM, *et al.* (**1998**), Electron transfer by domain movement in cytochrome bc_1. *Nature*, 392(6677):677–684, doi:10.1038/33612.

[59] Refojo, PN, Teixeira, M, Pereira, MM (**2012**), The Alternative complex III: Properties and possible mechanisms for electron transfer and energy conservation. *Biochimica et Biophysica Acta (BBA)-Bioenergetics*, 1817(10):1852–1859, doi:10.1016/j.bbabio.2012.05.003.

[60] Crofts, AR, Lhee, S, Crofts, SB, *et al.* (**2006**), Proton pumping in the *bc*1 complex: A new gating mechanism that prevents short circuits. *Biochimica et Biophysica Acta (BBA)-Bioenergetics*, 1757(8):1019–1034, doi:10.1016/j.bbabio.2006.02.009.

[61] Baymann, F, Lebrun, E, Brugna, M, *et al.* (**2003**), The redox protein construction kit: pre-last universal common ancestor evolution of energy-conserving enzymes. *Philosophical*

Transactions of the Royal Society of London Series B, Biological Sciences, 358(1429):267–274, doi:10.1098/rstb.2002.1184.

[62] Armon, A, Graur, D, Ben-Tal, N (**2001**), ConSurf: an algorithmic tool for the identification of functional regions in proteins by surface mapping of phylogenetic information. *Journal of Molecular Biology*, 307(1):447–463, doi:10.1006/jmbi.2000.4474.

[63] Krogh, A, Larsson, B, von Heijne, G, *et al.* (**2001**), Predicting transmembrane protein topology with a hidden Markov model: application to complete genomes. *Journal of Molecular Biology*, 305(3):567–580, doi:10.1006/jmbi.2000.4315.

[64] Huerta-Cepas, J, Serra, F, Bork, P (**2016**), ETE3: reconstruction, analysis, and visualization of phylogenomic data. *Molecular Biology and Evolution*, 33(6):1635–1638, doi:10.1093/molbev/msw046.

[65] Gross, R, Simon, J, Lancaster, CR, *et al.* (**1998**), Identification of histidine residues in *Wolinella succinogenes* hydrogenase that are essential for menaquinone reduction by H_2. *Molecular Microbiology*, 30(3):639–646, doi:10.1046/j.1365-2958.1998.01100.x.

[66] Gross, R, Pisa, R, Sänger, M, *et al.* (**2004**), Characterization of the menaquinone reduction site in the diheme cytochrome *b* membrane anchor of *Wolinella succinogenes* NiFe-hydrogenase. *The Journal of Biological Chemistry*, 279(1):274–281, doi:10.1074/jbc.M310610200.

[67] Deppenmeier, U (**2004**), The membrane-bound electron transport system of Methanosarcina species. *Journal of Bioenergetics and Biomembranes*, 36(1):55–64, doi:10.1023/b:jobb.0000019598.64642.97.

[68] Haddock, BA, Jones, CW (**1977**), Bacterial respiration. *Bacteriological Reviews*, 41(1):47–99, doi:10.1128/mmbr.41.1.47-99.1977.

[69] Fischer, WR (**1987**), Standard potentials (E_o) of iron(III) oxides under reducing conditions. *Zeitschrift für Pflanzenernährung und Bodenkunde*, 150(5):286–289, doi:10.1002/jpln.19871500504.

[70] ZoBell, CE (**1946**), Studies on redox potential of marine sediments. *AAPG Bulletin*, 30(4):477–513, doi:10.1306/3d933808-16b1-11d7-8645000102c1865d.

[71] Takai, Y, Kamura, T (**1966**), The mechanism of reduction in waterlogged paddy soil. *Folia Microbiologica*, 11(4):304–313, doi:10.1007/BF02878902.

[72] Bethke, CM, Sanford, RA, Kirk, MF, *et al.* (**2011**), The thermodynamic ladder in geomicrobiology. *American Journal of Science*, 311(3):183–210, doi:10.2475/03.2011.01.

[73] Simon, J, van Spanning, RJM, Richardson, DJ (**2008**), The organisation of proton motive and non-proton motive redox loops in prokaryotic respiratory systems. *Biochimica et Biophysica Acta (BBA)-Bioenergetics*, 1777(12):1480–1490, doi:10.1016/j.bbabio.2008.09.008.

[74] Unden, G, Dünnwald, P (**2008**), The aerobic and anaerobic respiratory chain of *Escherichia coli* and *Salmonella enterica*: enzymes and energetics. *EcoSal Plus*, 3(1), doi:10.1128/ecosalplus.3.2.2.

[75] Thamdrup, B (**2000**), Bacterial manganese and iron reduction in aquatic sediments. In Schink, B (Editor), *Advances in Microbial Ecology*, 41–84, Springer US, ISBN 9781461541875.

[76] Straub, KL, Benz, M, Schink, B (**2001**), Iron metabolism in anoxic environments at near neutral pH. *FEMS Microbiology Ecology*, 34(3):181–186, doi:10.1111/j.1574-6941.2001.tb00768.x.

[77] Cornell, RM, Schwertmann, U (**2006**), *The iron oxides: structure, properties, reactions, occurrences and uses*. Wiley-VCH, ISBN 9783527606443.

[78] Navrotsky, A, Mazeina, L, Majzlan, J (**2008**), Size-driven structural and thermodynamic complexity in iron oxides. *Science*, 319(5870):1635–1638, doi:10.1126/science.1148614.

[79] Lovley, DR, Phillips, EJP (**1988**), Manganese inhibition of microbial iron reduction in anaerobic sediments. *Geomicrobiology Journal*, 6(3-4):145–155, doi:10.1080/01490458809377834.

[80] Lovley, DR, Giovannoni, SJ, White, DC, *et al.* (**1993**), *Geobacter metallireducens* gen. nov. sp. nov., a microorganism capable of coupling the complete oxidation of organic compounds to the reduction of iron and other metals. *Archives of Microbiology*, 159(4):336–344, doi:10.1007/bf00290916.

[81] Anderson, RT, Vrionis, HA, Ortiz-Bernad, I, *et al.* (**2003**), Stimulating the in situ activity of *Geobacter* species to remove uranium from the groundwater of a uranium-contaminated aquifer. *Applied and Environmental Microbiology*, 69(10):5884–5891, doi:10.1128/AEM.69.10.5884-5891.2003.

[82] Rotaru, AE, Shrestha, PM, Liu, F, *et al.* (**2014**), Direct interspecies electron transfer between *Geobacter metallireducens* and *Methanosarcina barkeri*. *Applied and Environmental Microbiology*, 80(15):4599–4605, doi:10.1128/aem.00895-14.

[83] Shelobolina, ES, Coppi, MV, Korenevsky, AA, *et al.* (**2007**), Importance of *c*-type cytochromes for U(VI) reduction by *Geobacter sulfurreducens*. *BMC Microbiology*, 7:16, doi:10.1186/1471-2180-7-16.

[84] Reguera, G, McCarthy, KD, Mehta, T, *et al.* (**2005**), Extracellular electron transfer via microbial nanowires. *Nature*, 435(7045):1098–1101, doi:10.1038/nature03661.

[85] Jahan, MI, Tobe, R, Mihara, H (**2018**), Characterization of a novel porin-like protein, ExtI, from *Geobacter sulfurreducens* and its implication in the reduction of selenite and tellurite. *International Journal of Molecular Sciences*, 19(3):809, doi:10.3390/ijms19030809.

[86] Leang, C, Adams, LA, Chin, KJ, *et al.* (**2005**), Adaptation to disruption of the electron transfer pathway for Fe(III) reduction in *Geobacter sulfurreducens*. *Journal of Bacteriology*, 187(17):5918–5926, doi:10.1128/JB.187.17.5918-5926.2005.

[87] Finkelstein, DA, Tender, LM, Zeikus, JG (**2006**), Effect of electrode potential on electrode-reducing microbiota. *Environmental Science & Technology*, 40(22):6990–6995, doi:10.1021/es061146m.

[88] Logan, BE, Hamelers, B, Rozendal, R, *et al.* (**2006**), Microbial fuel cells: methodology and technology. *Environmental Science & Technology*, 40(17):5181–5192, doi:10.1021/es0605016.

[89] Chan, CH, Levar, CE, Zacharoff, L, *et al.* (**2015**), Scarless genome editing and stable inducible expression vectors for *Geobacter sulfurreducens*. *Applied and Environmental Microbiology*, 81(20):7178–7186, doi:10.1128/AEM.01967-15.

[90] Choi, KH, Mima, T, Casart, Y, *et al.* (**2008**), Genetic tools for select-agent-compliant manipulation of *Burkholderia pseudomallei*. *Applied and Environmental Microbiology*, 74(4):1064–1075, doi:10.1128/AEM.02430-07.

[91] Hallberg, ZF, Chan, CH, Wright, TA, *et al.* (**2019**), Structure and mechanism of a Hypr GGDEF enzyme that activates cGAMP signaling to control extracellular metal respiration. *eLife*, 8:e43,959, doi:10.7554/eLife.43959.

[92] Ferriéres, L, Hémery, G, Nham, T, *et al.* (**2010**), Silent mischief: Bacteriophage Mu insertions contaminate products of *Escherichia coli* random mutagenesis performed using suicidal transposon delivery plasmids mobilized by broad-host-range RP4 conjugative machinery. *Journal of Bacteriology*, 192(24):6418–6427, doi:10.1128/jb.00621-10.

[93] Peters, JM, Koo, BM, Patino, R, *et al.* (**2019**), Enabling genetic analysis of diverse bacteria with Mobile-CRISPRi. *Nature Microbiology*, 4(2):244–250, doi:10.1038/s41564-018-0327-z.

[94] Joshi, K, Kane, AL, Kotloski, NJ, *et al.* (**2019**), Preventing hydrogen disposal increases electrode utilization efficiency by *Shewanella oneidensis*. *Frontiers in Energy Research*, 7, doi:10.3389/fenrg.2019.00095.

[95] Marsili, E, Rollefson, JB, Baron, DB, *et al.* (**2008**), Microbial biofilm voltammetry: direct electrochemical characterization of catalytic electrode-attached biofilms. *Applied and Environmental Microbiology*, 74(23):7329–7337, doi:10.1128/AEM.00177-08.

[96] Lovley, DR, Phillips, EJP (**1987**), Rapid assay for microbially reducible ferric iron in aquatic sediments. *Applied and Environmental Microbiology*, 53(7):1536–1540, doi:10.1128/aem.53.7.1536-1540.1987.

[97] Langmead, B, Salzberg, SL (**2012**), Fast gapped-read alignment with Bowtie2. *Nature Methods*, 9(4):357–359, doi:10.1038/nmeth.1923.

[98] McClure, R, Balasubramanian, D, Sun, Y, *et al.* (**2013**), Computational analysis of bacterial RNA-Seq data. *Nucleic Acids Research*, 41(14):e140, doi:10.1093/nar/gkt444.

[99] Herigstad, B, Hamilton, M, Heersink, J (**2001**), How to optimize the drop plate method for enumerating bacteria. *Journal of Microbiological Methods*, 44(2):121–129, doi:10.1016/s0167-7012(00)00241-4.

[100] Qu, Y, Brown, P, Barbe, JF, *et al.* (**2009**), GSEL version 2, an online genome-wide query system of operon organization and regulatory sequence elements of *Geobacter sulfurreducens*. *Omics : A Journal of Integrative Biology*, 13(5):439–449, doi:10.1089/omi.2009.0081.

[101] Krushkal, J, Leang, C, Barbe, JF, *et al.* (**2009**), Diversity of promoter elements in a *Geobacter sulfurreducens* mutant adapted to disruption in electron transfer. *Functional & Integrative Genomics*, 9(1):15–25, doi:10.1007/s10142-008-0094-7.

[102] Yan, B, Núñez, C, Ueki, T, *et al.* (**2006**), Computational prediction of RpoS and RpoD regulatory sites in *Geobacter sulfurreducens* using sequence and gene expression information. *Gene*, 384:73–95, doi:10.1016/j.gene.2006.06.025.

[103] Holmes, DE, Chaudhuri, SK, Nevin, KP, *et al.* (**2006**), Microarray and genetic analysis of electron transfer to electrodes in *Geobacter sulfurreducens*. *Environmental Microbiology*, 8(10):1805–1815, doi:10.1111/j.1462-2920.2006.01065.x.

[104] Yu, NY, Wagner, JR, Laird, MR, *et al.* (**2010**), PSORTb 3.0: Improved protein subcellular localization prediction with refined localization subcategories and predictive capabilities for all prokaryotes. *Bioinformatics*, 26(13):1608–1615, doi:10.1093/bioinformatics/btq249.

[105] Leang, C, Krushkal, J, Ueki, T, *et al.* (**2009**), Genome-wide analysis of the RpoN regulon in *Geobacter sulfurreducens*. *BMC genomics*, 10:331, doi:10.1186/1471-2164-10-331.

[106] Blum, M, Chang, HY, Chuguransky, S, *et al.* (**2021**), The InterPro protein families and domains database: 20 years on. *Nucleic Acids Research*, 49(D1):D344–D354, doi:10.1093/nar/gkaa977.

[107] Brasca, M, Morandi, S, Lodi, R, *et al.* (**2007**), Redox potential to discriminate among species of lactic acid bacteria. *Journal of Applied Microbiology*, 103(5):1516–1524, doi:10.1111/j.1365-2672.2007.03392.x.

[108] Vukosav, P, Mlakar, M, Tomišić, V (**2012**), Revision of iron(III)–citrate speciation in aqueous solution. Voltammetric and spectrophotometric studies. *Analytica Chimica Acta*, 745:85–91, doi:10.1016/j.aca.2012.07.036.

[109] Adam, FI, Bounds, PL, Kissner, R, *et al.* (**2015**), Redox properties and activity of iron–citrate complexes: Evidence for redox cycling. *Chemical Research in Toxicology*, 28(4):604–614, doi:10.1021/tx500377b.

[110] Königsberger, LC, Königsberger, E, May, PM, *et al.* (**2000**), Complexation of iron(III) and iron(II) by citrate. Implications for iron speciation in blood plasma. *Journal of Inorganic Biochemistry*, 78(3):175–184, doi:10.1016/S0162-0134(99)00222-6.

[111] Baerends, RJ, Smits, WK, de Jong, A, *et al.* (**2004**), Genome2D: a visualization tool for the rapid analysis of bacterial transcriptome data. *Genome Biology*, 5(5):R37, doi:10.1186/gb-2004-5-5-r37.

[112] Ueki, T, Lovley, DR (**2010**), Genome-wide gene regulation of biosynthesis and energy generation by a novel transcriptional repressor in *Geobacter* species. *Nucleic Acids Research*, 38(3):810–821, doi:10.1093/nar/gkp1085.

[113] Yoho, RA, Popat, SC, Torres, CI (**2014**), Dynamic potential-dependent electron transport pathway shifts in anode biofilms of *Geobacter sulfurreducens*. *ChemSusChem*, 7(12):3413–3419, doi:10.1002/cssc.201402589.

[114] Marsili, E, Sun, J, Bond, D (**2010**), Voltammetry and growth physiology of *Geobacter sulfurreducens* biofilms as a function of growth stage and imposed electrode potential. *Electroanalysis*, 22(7-8):865–874, doi:10.1002/elan.200800007.

[115] Bonneville, S, Behrends, T, Van Cappellen, P (**2009**), Solubility and dissimilatory reduction kinetics of iron(III) oxyhydroxides: A linear free energy relationship. *Geochimica et Cosmochimica Acta*, 73(18):5273–5282, doi:10.1016/j.gca.2009.06.006.

[116] Majzlan, J, Navrotsky, A, Schwertmann, U (**2004**), Thermodynamics of iron oxides: Part III. Enthalpies of formation and stability of ferrihydrite ($\sim Fe(OH)_3$), schwertmannite ($\sim FeO(OH)_{\frac{3}{4}}(SO_4)_{\frac{1}{8}}$), and ϵ-Fe_2O_3. *Geochimica et Cosmochimica Acta*, 68(5):1049–1059, doi:10.1016/s0016-7037(03)00371-5.

[117] Majzlan, J (**2012**), Minerals and aqueous species of iron and manganese as reactants and products of microbial metal respiration. In Gescher, J, Kappler, A (Editors), *Microbial Metal Respiration*, 1–28, Springer Berlin Heidelberg, ISBN 9783642328671.

[118] Bekker, M, Vries, Sd, Beek, AT, *et al.* (**2009**), Respiration of *Escherichia coli* can be fully uncoupled via the nonelectrogenic terminal cytochrome *bd*-II oxidase. *Journal of Bacteriology*, 191(17):5510–5517, doi:10.1128/JB.00562-09.

[119] Jormakka, M, Törnroth, S, Byrne, B, *et al.* (**2002**), Molecular basis of proton motive force generation: structure of formate dehydrogenase-N. *Science*, 295(5561):1863–1868, doi:10.1126/science.1068186.

[120] Chadwick, GL, Otero, FJ, Gralnick, JA, *et al.* (**2019**), NanoSIMS imaging reveals metabolic stratification within current-producing biofilms. *Proceedings of the National Academy of Sciences of the United States of America*, 116(41):20,716–20,724, doi:10.1073/pnas.1912498116.

[121] Krige, A, Ramser, K, Sjöblom, M, *et al.* (**2020**), A new approach for evaluating electron transfer dynamics by using *in situ* resonance raman microscopy and chronoamperometry in conjunction with a dynamic model. *Applied Environmental Microbiology*, 86(20):320–327, doi:10.1128/AEM.01535-20.

[122] Lebedev, N, Strycharz-Glaven, SM, Tender, LM (**2014**), Spatially resolved confocal resonant Raman microscopic analysis of anode-grown *Geobacter sulfurreducens* biofilms. *Chemphyschem: A European Journal of Chemical Physics and Physical Chemistry*, 15(2):320–327, doi:10.1002/cphc.201300984.

[123] Snider, RM, Strycharz-Glaven, SM, Tsoi, SD, *et al.* (**2012**), Long-range electron transport in *Geobacter sulfurreducens* biofilms is redox gradient-driven. *Proceedings of the National Academy of Sciences of the United States of America*, 109(38):15,467–15,472, doi:10.1073/pnas.1209829109.

[124] He, X, Chadwick, G, Otero, FJ, *et al.* (**2021**), Spatially resolved electron transport through anode-respiring *Geobacter sulfurreducens* biofilms: controls and constraints. *ChemElectroChem*, 8(10):1747–1758, doi:10.1002/celc.202100111.

[125] Meyer, TE, Kamen, MD (**1982**), New perspectives on *c*-type cytochromes. *Advances in Protein Chemistry*, 35:105–212, doi:10.1016/s0065-3233(08)60469-6.

[126] Scott Mathews, F (**1985**), The structure, function and evolution of cytochromes. *Progress in Biophysics and Molecular Biology*, 45(1):1–56, doi:10.1016/0079-6107(85)90004-5.

[127] Keller, KL, Wall, JD (**2011**), Genetics and molecular biology of the electron flow for sulfate respiration in *Desulfovibrio*. *Frontiers in Microbiology*, 2:135, doi:10.3389/fmicb.2011.00135.

[128] Unden, G, Bongaerts, J (**1997**), Alternative respiratory pathways of *Escherichia coli*: energetics and transcriptional regulation in response to electron acceptors. *Biochimica et Biophysica Acta (BBA)-Bioenergetics*, 1320(3):217–234, doi:10.1016/S0005-2728(97)00034-0.

[129] Smith, PM, Fox, JL, Winge, DR (**2012**), Biogenesis of the cytochrome bc_1 complex and role of assembly factors. *Biochimica et Biophysica Acta*, 1817(2):276–286, doi:10.1016/j.bbabio.2011.11.009.

[130] Berry, EA, Guergova-Kuras, M, Huang, Ls, *et al.* (**2000**), Structure and function of cytochrome *bc* complexes. *Annual Review of Biochemistry*, 69(1):1005–1075, doi:10.1146/annurev.biochem.69.1.1005.

[131] Daldal, F, Thurnauer, MC, Beatty, JT (**2008**), *The purple phototrophic bacteria*. Springer-Netherlands, ISBN 978-1-4020-8815-5.

[132] Vincent, KA, Parkin, A, Lenz, O, *et al.* (**2005**), Electrochemical definitions of O_2 sensitivity and oxidative inactivation in hydrogenases. *Journal of the American Chemical Society*, 127(51):18,179–18,189, doi:10.1021/ja055160v.

[133] Lissolo, T, Pulvin, S, Thomas, D (**1984**), Reactivation of the hydrogenase from *Desulfovibrio gigas* by hydrogen. Influence of redox potential. *The Journal of Biological Chemistry*, 259(19):11,725–11,729, doi:10.1016/S0021-9258(20)71270-6.

[134] Levar, C (**2015**), Redox potential dependent respiration by *Geobacter sulfurreducens*. *Retrieved from the University of Minnesota Digital Conservancy*, URL http://conservancy.umn.edu/handle/11299/192663.

[135] Deatherage, DE, Barrick, JE (**2014**), Identification of mutations in laboratory-evolved microbes from next-generation sequencing data using breseq. In *Methods in Molecular Biology*, 165–188, Springer New York, doi:10.1007/978-1-4939-0554-6-12.

[136] Regenspurg, S, Brand, A, Peiffer, S (**2004**), Formation and stability of schwertmannite in acidic mining lakes. *Geochimica et Cosmochimica Acta*, 68(6):1185–1197, doi:10.1016/j.gca.2003.07.015.

[137] Post, JE (**1999**), Manganese oxide minerals: Crystal structures and economic and environmental significance. *Proceedings of the National Academy of Sciences of the United States of America*, 96(7):3447–3454, doi:10.1073/pnas.96.7.3447.

[138] Berezin, C, Glaser, F, Rosenberg, J, *et al.* (**2004**), ConSeq: the identification of functionally and structurally important residues in protein sequences. *Bioinformatics (Oxford, England)*, 20(8):1322–1324, doi:10.1093/bioinformatics/bth070.

[139] Torres, CI, Marcus, AK, Parameswaran, P, *et al.* (**2008**), Kinetic experiments for evaluating the Nernst-Monod model for anode-respiring bacteria (ARB) in a biofilm anode. *Environmental Science & Technology*, 42(17):6593–6597, doi:10.1021/es800970w.

[140] Beaumont, HJE, Gallie, J, Kost, C, *et al.* (**2009**), Experimental evolution of bet hedging. *Nature*, 462(7269):90–93, doi:10.1038/nature08504.

[141] McCarter, LL, Gomelsky, M (**2015**), Fifty ways to inhibit motility via cyclic di-GMP: the emerging *Pseudomonas aeruginosa* swarming story. *Journal of Bacteriology*, 197(3):406–409, doi:10.1128/JB.02483-14.

[142] Kuchma, SL, Delalez, NJ, Filkins, LM, *et al.* (**2015**), Cyclic di-GMP-mediated repression of swarming motility by *Pseudomonas aeruginosa* PA14 requires the MotAB stator. *Journal of Bacteriology*, 197(3):420–430, doi:10.1128/JB.02130-14.

[143] Holmes, DE, Nicoll, JS, Bond, DR, *et al.* (**2004**), Potential role of a novel psychrotolerant member of the family *Geobacteraceae*, *Geopsychrobacter electrodiphilus* gen. nov., sp. nov., in electricity production by a marine sediment fuel cell. *Applied and Environmental Microbiology*, 70(10):6023–6030, doi:10.1128/AEM.70.10.6023-6030.2004.

[144] Pérez-Rodríguez, I, Choi, JK, Abuyen, K, *et al.* (**2021**), *Geothermobacter hydrogeniphilus* sp. nov., a mesophilic, iron(III)-reducing bacterium from seafloor/subseafloor environments in the Pacific Ocean, and emended description of the genus *Geothermobacter*. *International Journal of Systematic and Evolutionary Microbiology*, 71(4):004,739, doi:10.1099/ijsem.0.004739.

[145] Yadav, P, Antony-Babu, S, Hayes, E, *et al.* (**2021**), Complete genome sequence of *Geobacter* sp. strain FeAm09, a moderately acidophilic soil bacterium. *Microbiology Resource Announcements*, 10(2):e00,979–20, doi:10.1128/MRA.00979-20.

[146] Sun, Y, Benabbas, A, Zeng, W, *et al.* (**2014**), Investigations of heme distortion, low-frequency vibrational excitations, and electron transfer in cytochrome *c*. *Proceedings of the National Academy of Sciences of the United States of America*, 111(18):6570–6575, doi:10.1073/pnas.1322274111.

[147] Kim, DE, Chivian, D, Baker, D (**2004**), Protein structure prediction and analysis using the Robetta server. *Nucleic Acids Research*, 32(suppl2):W526–W531, doi:10.1093/nar/gkh468.

[148] Baek, M, DiMaio, F, Anishchenko, I, *et al.* (**2021**), Accurate prediction of protein structures and interactions using a three-track neural network. *Science*, eabj8754, doi:10.1126/science.abj8754.

[149] Goldet, G, Brandmayr, C, Stripp, ST, *et al.* (**2009**), Electrochemical kinetic investigations of the reactions of [FeFe]-hydrogenases with carbon monoxide and oxygen: comparing the importance of gas tunnels and active-site electronic/redox effects. *Journal of the American Chemical Society*, 131(41):14,979–14,989, doi:10.1021/ja905388j.

[150] Allen, JF (**2003**), The function of genomes in bioenergetic organelles. *Philosophical Transactions of the Royal Society B: Biological Sciences*, 358(1429):19–38, doi:10.1098/rstb.2002.1191.

[151] Allen, JF, Nield, J (**2017**), Redox tuning in photosystem II. *Trends in Plant Science*, 22(2):97–99, doi:10.1016/j.tplants.2016.11.011.

[152] Yokochi, Y, Yoshida, K, Hahn, F, *et al.* (**2021**), Redox regulation of NADP-malate dehydrogenase is vital for land plants under fluctuating light environment. *Proceedings of the National Academy of Sciences of the United States of America*, 118(6):e2016903,118, doi:10.1073/pnas.2016903118.

[153] Costerton, JW, Lewandowski, Z, Caldwell, DE, *et al.* (**1995**), Microbial biofilms. *Annual Review of Microbiology*, 49:711–745, doi:10.1146/annurev.mi.49.100195.003431.

[154] Flemming, HC, Wingender, J, Szewzyk, U, *et al.* (**2016**), Biofilms: an emergent form of bacterial life. *Nature Reviews Microbiology*, 14(9):563–575, doi:10.1038/nrmicro.2016.94.

[155] Stoodley, P, Sauer, K, Davies, DG, *et al.* (**2002**), Biofilms as complex differentiated communities. *Annual Review of Microbiology*, 56:187–209, doi:10.1146/annurev.micro.56.012302.160705.

[156] Donlan, RM, Costerton, JW (**2002**), Biofilms: survival mechanisms of clinically relevant microorganisms. *Clinical Microbiology Reviews*, 15(2):167–193, doi:10.1128/cmr.15.2.167-193.2002.

[157] Lappin-Scott, HM, Costerton, JW (**1989**), Bacterial biofilms and surface fouling. *Biofouling*, 1(4):323–342, doi:10.1080/08927018909378120.

[158] Inaba, T, Hori, T, Aizawa, H, *et al.* (**2017**), Architecture, component, and microbiome of biofilm involved in the fouling of membrane bioreactors. *npj Biofilms and Microbiomes*, 3(1):1–8, doi:10.1038/s41522-016-0010-1.

[159] Halan, B, Buehler, K, Schmid, A (**2012**), Biofilms as living catalysts in continuous chemical syntheses. *Trends in Biotechnology*, 30(9):453–465, doi:10.1016/j.tibtech.2012.05.003.

[160] Singer, SW, Erickson, BK, VerBerkmoes, NC, *et al.* (**2010**), Posttranslational modification and sequence variation of redox-active proteins correlate with biofilm life cycle in natural microbial communities. *The ISME Journal*, 4(11):1398–1409, doi:10.1038/ismej.2010.64.

[161] Ehrlich, HL, Newman, DK (Editors) (**2008**), *Geomicrobiology*. 5th ed., CRC Press, ISBN 9780429116544.

[162] Stewart, PS, Franklin, MJ (**2008**), Physiological heterogeneity in biofilms. *Nature Reviews Microbiology*, 6(3):199–210, doi:10.1038/nrmicro1838.

[163] Quejigo, JR, Korth, B, Kuchenbuch, A, *et al.* (**2021**), Redox potential heterogeneity in fixed bed electrodes leads to microbial stratification and inhomogeneous performance. *ChemSusChem*, (14):1155–1165, doi:10.1002/cssc.202002611.

[164] de Beer, D, Stoodley, P, Roe, F, *et al.* (**1994**), Effects of biofilm structures on oxygen distribution and mass transport. *Biotechnology and Bioengineering*, 43(11):1131–1138, doi:10.1002/bit.260431118.

[165] Xu, KD, Stewart, PS, Xia, F, *et al.* (**1998**), Spatial physiological heterogeneity in *Pseudomonas aeruginosa* biofilm is determined by oxygen availability. *Applied and Environmental Microbiology*, 64(10):4035–4039, doi:10.1128/AEM.64.10.4035-4039.1998.

[166] Kiely, PD, Call, DF, Yates, MD, *et al.* (**2010**), Anodic biofilms in microbial fuel cells harbor low numbers of higher-power-producing bacteria than abundant genera. *Applied Microbiology and Biotechnology*, 88(1):371–380, doi:10.1007/s00253-010-2757-2.

[167] Yates, MD, Kiely, PD, Call, DF, *et al.* (**2012**), Convergent development of anodic bacterial communities in microbial fuel cells. *The ISME Journal*, 6(11):2002–2013, doi:10.1038/ismej.2012.42.

[168] Tejedor-Sanz, S, Fernández-Labrador, P, Hart, S, *et al.* (**2018**), *Geobacter* dominates the inner layers of a stratified biofilm on a fluidized anode during brewery wastewater treatment. *Frontiers in Microbiology*, 9, doi:10.3389/fmicb.2018.00378.

[169] Lovley, DR, Phillips, EJP, Gorby, YA, *et al.* (**1991**), Microbial reduction of uranium. *Nature*, 350(6317):413–416, doi:10.1038/350413a0.

[170] Atkinson, JT, Campbell, IJ, Thomas, EE, *et al.* (**2019**), Metalloprotein switches that display chemical-dependent electron transfer in cells. *Nature Chemical Biology*, 15(2):189–195, doi:10.1038/s41589-018-0192-3.

[171] Franks, AE, Nevin, KP, Jia, H, *et al.* (**2009**), Novel strategy for three-dimensional real-time imaging of microbial fuel cell communities: monitoring the inhibitory effects of proton accumulation within the anode biofilm. *Energy & Environmental Science*, 2(1):113–119, doi:10.1039/B816445B.

[172] Franks, AE, Nevin, KP, Glaven, RH, *et al.* (**2010**), Microtoming coupled to microarray analysis to evaluate the spatial metabolic status of *Geobacter sulfurreducens* biofilms. *The ISME Journal*, 4(4):509–519, doi:10.1038/ismej.2009.137.

[173] Liu, Y, Kim, H, Franklin, R, *et al.* (**2010**), Gold line array electrodes increase substrate affinity and current density of electricity-producing *G. sulfurreducens* biofilms. *Energy & Environmental Science*, 3(11):1782–1788, doi:10.1039/C0EE00242A.

[174] Kato Marcus, A, Torres, CI, Rittmann, BE (**2007**), Conduction-based modeling of the biofilm anode of a microbial fuel cell. *Biotechnology and Bioengineering*, 98(6):1171–1182, doi:10.1002/bit.21533.

[175] Liu, Y, Kim, H, Franklin, RR, *et al.* (**2011**), Linking spectral and electrochemical analysis to monitor *c*-type cytochrome redox status in *Geobacter sulfurreducens* biofilms. *ChemPhysChem*, 12(12):2235–2241, doi:10.1002/cphc.201100246.

[176] Liu, Y, Bond, DR (**2012**), Long-distance electron transfer by *G. sulfurreducens* biofilms results in accumulation of reduced *c*-type cytochromes. *ChemSusChem*, 5(6):1047–1053, doi:10.1002/cssc.201100734.

[177] Babauta, JT, Beasley, CA, Beyenal, H (**2014**), Investigation of electron transfer by *Geobacter sulfurreducens* biofilms by using an electrochemical quartz crystal microbalance. *ChemElectroChem*, 1(11):2007–2016, doi:10.1002/celc.201402127.

[178] Kees, ED, Levar, CE, Miller, SP, *et al.* (**2021**), Survival of the first rather than the fittest in a *Shewanella* electrode biofilm. *Communications Biology*, 4(1):1–9, doi:10.1038/s42003-021-02040-1.

[179] Simon, R, Priefer, U, Pühler, A (**1983**), A broad host range mobilization system for *in vivo* genetic engineering: transposon mutagenesis in gram negative bacteria. *Bio/Technology*, 1(9):784–791, doi:10.1038/nbt1183-784.

[180] Nakamura, Y, Gojobori, T, Ikemura, T (**2000**), Codon usage tabulated from international DNA sequence databases: status for the year 2000. *Nucleic Acids Research*, 28(1):292, doi:10.1093/nar/28.1.292.

[181] Puigbò, P, Guzmán, E, Romeu, A, *et al.* (**2007**), OPTIMIZER: a web server for optimizing the codon usage of DNA sequences. *Nucleic Acids Research*, 35(2):W126–131, doi:10.1093/nar/gkm219.

[182] Eshaghi, M, Sun, G, Grüter, A, *et al.* (**2015**), Rational structure-based design of bright GFP-based complexes with tunable dimerization. *Angewandte Chemie International Edition*, 54(47):13,952–13,956, doi:10.1002/anie.201506686.

[183] Bindels, DS, Haarbosch, L, van Weeren, L, *et al.* (**2017**), mScarlet: a bright monomeric red fluorescent protein for cellular imaging. *Nature Methods*, 14(1):53–56, doi:10.1038/nmeth.4074.

[184] Schindelin, J, Arganda-Carreras, I, Frise, E, *et al.* (**2012**), Fiji: an open-source platform for biological-image analysis. *Nature Methods*, 9(7):676–682, doi:10.1038/nmeth.2019.

[185] Malvankar, NS, Tuominen, MT, Lovley, DR (**2012**), Biofilm conductivity is a decisive variable for high-current-density *Geobacter sulfurreducens* microbial fuel cells. *Energy & Environmental Science*, 5(2):5790–5797, doi:10.1039/C2EE03388G.

[186] Barondeau, DP, Putnam, CD, Kassmann, CJ, *et al.* (**2003**), Mechanism and energetics of green fluorescent protein chromophore synthesis revealed by trapped intermediate structures. *Proceedings of the National Academy of Sciences of the United States of America*, 100(21):12,111–12,116, doi:10.1073/pnas.2133463100.

[187] Ma, Y, Sun, Q, Smith, SC (**2017**), The mechanism of oxidation in chromophore maturation of wild-type green fluorescent protein: a theoretical study. *Physical Chemistry Chemical Physics*, 19(20):12,942–12,952, doi:10.1039/C6CP07983K.

[188] Zhang, X, Prévoteau, A, Louro, RO, *et al.* (**2018**), Periodic polarization of electroactive biofilms increases current density and charge carriers concentration while modifying biofilm structure. *Biosensors & Bioelectronics*, 121:183–191, doi:10.1016/j.bios.2018.08.045.

[189] Liu, P, Hao, W, Mohamed, A, *et al.* (**2021**), Spatial variation of electrical conductance in electrochemically active biofilm growing on interdigitated microelectrode array. *Journal of Power Sources*, 491:229,615, doi:10.1016/j.jpowsour.2021.229615.

[190] Lebedev, N, Stroud, RM, Yates, MD, *et al.* (**2019**), Spatially resolved chemical analysis of *Geobacter sulfurreducens* cell surface. *ACS Nano*, 13(4):4834–4842, doi:10.1021/acsnano.9b02032.

[191] O'Toole, G, Kaplan, HB, Kolter, R (**2000**), Biofilm formation as microbial development. *Annual Review of Microbiology*, 54:49–79, doi:10.1146/annurev.micro.54.1.49.

[192] Evans, CR, Kempes, CP, Price-Whelan, A, *et al.* (**2020**), Metabolic heterogeneity and cross-feeding in bacterial multicellular systems. *Trends in Microbiology*, 28(9):732–743, doi:10.1016/j.tim.2020.03.008.

[193] Wessel, AK, Arshad, TA, Fitzpatrick, M, *et al.* (**2014**), Oxygen limitation within a bacterial aggregate. *mBio*, 5(2):e00,992–14, doi:10.1128/mBio.00992-14.

[194] Ramsing, NB, Kühl, M, Jørgensen, BB (**1993**), Distribution of sulfate-reducing bacteria, O_2, and H_2S in photosynthetic biofilms determined by oligonucleotide probes and microelectrodes. *Applied and Environmental Microbiology*, 59(11):3840–3849, doi:10.1128/aem.59.11.3840-3849.1993.

[195] Vanderkooi, JM, Erecińska, M (**1975**), Cytochrome *c* interaction with membranes. Absorption and emission spectra and binding characteristics of iron-free cytochrome *c*. *European Journal of Biochemistry*, 60(1):199–207, doi:10.1111/j.1432-1033.1975.tb20992.x.

[196] Strottmann, JM, Stellwagen, A, Bryant, C, *et al.* (**1984**), Spectral studies of horse heart porphyrin cytochrome *c*. *The Journal of Biological Chemistry*, 259(11):6931–6936, doi:10.1016/S0021-9258(17)39817-4.

[197] Bevis, BJ, Glick, BS (**2002**), Rapidly maturing variants of the Discosoma red fluorescent protein (DsRed). *Nature Biotechnology*, 20(1):83–87, doi:10.1038/nbt0102-83.

[198] Pédelacq, JD, Cabantous, S, Tran, T, *et al.* (**2006**), Engineering and characterization of a superfolder green fluorescent protein. *Nature Biotechnology*, 24(1):79–88, doi:10.1038/nbt1172.

[199] Valbuena, FM, Fitzgerald, I, Strack, RL, *et al.* (**2020**), A photostable monomeric superfolder green fluorescent protein. *Traffic (Copenhagen, Denmark)*, 21(8):534–544, doi:10.1111/tra.12737.

[200] Robuschi, L, Tomba, JP, Schrott, GD, *et al.* (**2012**), Spectroscopic slicing to reveal internal redox gradients in electricity-producing biofilms. *Angewandte Chemie International Edition*, 52(3):925–928, doi:10.1002/anie.201205440.

[201] Sosa Alfaro, V, Campeciño, J, Tracy, M, *et al.* (**2021**), Elucidating electron storage and distribution within the pentaheme scaffold of cytochrome *c* nitrite reductase (NrfA). *Biochemistry*, 60(23):1853–1867, doi:10.1021/acs.biochem.0c00977.